

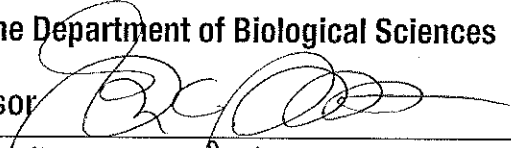
# Thesis

Submitted in partial fulfillment of the requirements for the degree of Ph.D. in Biological Sciences

Title Unbiased, high-throughput electron microscopy analysis of experience-dependent synaptic plasticity

Presented by Santosh Chandrasekaran

Accepted by the Department of Biological Sciences

Major Professor 

Date 1-21-15

Department Head John Woolford

Date 2-17-15

Approved by the MCS College Council

Dean Fredrick J. Milman

Date 2/17/15

**Unbiased, high-throughput electron microscopy  
analysis of experience-dependent synaptic changes**

Santosh Chandrasekaran

Submitted in partial fulfillment of the requirements  
for the degree of Doctor of Philosophy

Department of Biological Sciences  
Carnegie Mellon University  
Pittsburgh, PA 15213

**Thesis Committee Members**

Dr. Alison Barth, Advisor  
Dr. Nathan Urban, Co-advisor  
Dr. Carl Olson  
Dr. Marlene Cohen  
Dr. Ziv Bar-Joseph  
Dr. Stanislaw Glazewski

## Abstract

Neocortical circuits can adapt to changes in sensory input by modifying the strength or number of synapses. These changes have been well-characterized electrophysiologically in primary somatosensory (barrel) cortex of rodents across different ages and with different patterns of whisker stimulation. Previous work from our lab has identified layer-specific critical periods for synaptic potentiation after selective whisker experience (SWE), where all but one row of facial whiskers has been removed. Although whole-cell patch-clamp recording methods enable a mechanistic understanding of how synaptic plasticity can occur in vivo, they are painstakingly slow, typically focus on a small number of observed events, and are focused on a single pathway or restricted anatomical area. For example, most studies of plasticity in barrel cortex have focused on analyses of experience-dependent synaptic changes in layer 4 and layer 2/3, at a single time point, but it is unclear whether such changes are limited to these layers, or whether they persist over long time periods.

Here we employ an established electron-microscopic technique that selectively intensifies synaptic contacts, in combination with unbiased, automated synapse detection, to broadly explore experience-dependent changes in synaptic size and density across many neocortical layers, regions, and time periods in a high-throughput fashion. To validate the method, we focused on imaging synaptic contacts at time points surrounding the critical period for strengthening of excitatory synapses in mouse barrel cortex, and compared these to electrophysiological analyses that show a doubling of synaptic events targeting layer 2/3 pyramidal neurons following SWE. We found that the pattern of occurrence of synapses across the cortical layers is significantly different following SWE. Also, an increase in length was

observed specifically in layer 3 synapses. Furthermore, we uncovered potential bidirectional plasticity in L6 synapses depending on the developmental state of circuit and a potential critical period onset for L5A synapse at PND 18.

The high resolution imaging and unbiased synapse detection has enabled us to potentially tease apart synaptic changes that occur in a laminar specific fashion. This high-throughput method will facilitate analysis of experience-dependent changes in synaptic density by age, sensory experience, genotype, pharmacological treatments or behavioral training, and will enable classification of synaptic structure to identify key parameters that can be changed by these variables.

## Acknowledgements

This has been a long and twisting journey for me. But, all through the way I learnt a lot and enjoyed the experiences. It is only now I realize what a great scientific community I have been a part of here at Carnegie Mellon University and the Center for Neural Basis of Cognition.

Firstly, I would like to thank my advisor(s). Dr. Nathan Urban and Dr. Alison Barth have been extremely supportive and encouraging throughout. They have been both extremely patient with me on a lot of occasions and never gave up. It has been a real pleasure working on the projects I took up during my stay in the lab. Thank you both for being so approachable and enthusiastic about whatever it was I wanted to talk about with you.

A special thanks to my committee members Dr. Carl Olson, Dr. Marlene Cohen, Dr. Ziv Bar-Joseph and Dr. Stanislaw Glazewski. They have been the perfect balance of being supportive and being critical. It has helped me learn to make sense of the data and present as coherently as possible. I would like to thank Dr. Justin Crowley as well for letting me enter into neuroscience. It saddens me that things did not work out but it was great fun while it lasted.

A big thanks to Saket Navlakha for being patient with my questions and helping me understand machine learning. I would like to thank profusely Joseph Suhan for having struggled with me as we tried to get the experiments working.

A special thanks to the close friends in Pittsburgh that helped in every which way. Thanks to David Whitney for helping me with everything, right from getting my driver's license, teaching me how to ski, all the way to teaching my animal surgery. Thanks to Jineta Banerjee for being such a great friend. I will miss our evening coffee sessions. Thanks to Prasannakumar

Muthukumar for being a great friend over the years. Thanks to my classmates in the Department of Biological Science, Mark Deblois, Cassandra Priddy and Alys Cheatle. Thank you for making me feel welcome in the country and Pittsburgh.

Thanks to the members of the Barth Lab – Jing Wen, Joanna Urban-Ciecko, Nick Audette, Dylan McCreary, Urban Lab – Krishnan Padmanabhan, Rick Gerkin, Ken Hovis, Sonya Giridhar, Anne Marie Oswald, Shreejoy Tripathy, Shawn Burton, Matthew Geramita, Yi yi and Crowley Lab – Corey Flynn and David Whitney. A special thanks to Sonya Giridhar for teaching me how to patch neurons and being a really great, fun, Tamil-speaking baymate. I would also like to thank Greg Larocca, Joanne Steinmiller, Jennifer Dry-Henich and Megumi Matsushita. Without you, none of this would have been possible.

A special thanks to Mithila Agnihotri for being a close friend through the years and Rashmi Jejurikar for all the reminders that helped me meet my personal deadlines.

Lastly, I would like to thank my parents for letting me come so far away from home and standing by me all through way. Without your love, motivation, encouragement and support this would not have been possible.

# Table of Contents

<b>1. <a href="#">Introduction</a></b> .....	<b>1</b>
1.1 <a href="#">The importance of characterizing synaptic changes</a> .....	1
<a href="#">Synaptic plasticity in development</a> .....	2
<a href="#">Synaptic plasticity in learning</a> .....	4
<a href="#">Synaptic plasticity in neurological disorders</a> .....	6
1.2 <a href="#">Techniques for studying synaptic changes</a> .....	8
<a href="#">In vitro electrophysiological recordings</a> .....	8
<a href="#">In vivo imaging of dynamics of dendritic spines</a> .....	9
<a href="#">Array tomography</a> .....	10
<a href="#">Electron microscopy</a> .....	11
1.3 <a href="#">Choice of rodent barrel cortex as model system</a> .....	12
1.4 <a href="#">Experience-dependent synaptic plasticity</a> .....	16
<a href="#">Narrow focus and diversity in experimental design of previous studies</a> .....	16
<a href="#">Barrel cortex as a model for experience-dependent plasticity</a> .....	17
<a href="#">Need for an unbiased high-throughput technique to study synaptic plasticity</a> .....	19
1.4 <a href="#">Critical Period Plasticity</a> .....	20
<a href="#">Layer-specific critical periods</a> .....	21
<a href="#">Progression of critical period onsets through cortical layers</a> .....	22
<a href="#">Role of inhibitory circuitry – Onset of critical period</a> .....	24
<b>2. <a href="#">Animal-to-animal variation in absolute synapse density in a layer-specific manner</a></b> .....	<b>25</b>
2.1 <a href="#">Introduction</a> .....	25
<a href="#">Assessment of the performance of the semi-automated synapse detection from EPTA stained tissue</a> .....	27
<a href="#">Variability in synapse density measurements</a> .....	28

2.2	<a href="#">Methods</a> .....	32
2.3	<a href="#">Results</a> .....	38
	<a href="#">Laminar-specific effect on variability observed in automated EPTA-stained synapse density measurements</a> .....	38
	<a href="#">Automated detection of synapses provides similar results as manual curation</a> .....	41
	<a href="#">Dense imaging of EPTA-stained tissue provides reliable estimation of underlying synapse density</a> .....	41
	<a href="#">Staining contrast does not contribute significantly to synapse density variability</a> .....	44
	<a href="#">Differences across batches does not completely address the observed variability</a> .....	46
	<a href="#">Within-animal normalization of mean synapse density is most effective in reducing observed variability</a> .....	49
	<a href="#">Conventional EM images underestimate synapse density counts</a> .....	51
	<a href="#">Conventional EM images show more intra-animal variability than images of EPTA-stained tissue</a> .....	54
	<a href="#">EPTA images potentially detect smaller synapses more effectively</a> .....	56
2.4	<a href="#">Discussion</a> .....	58
3.	<b><a href="#">Layer-specific changes in synaptic density and lengths following altered whisker experience</a></b> .....	<b>64</b>
3.1	<a href="#">Introduction</a> .....	64
3.2	<a href="#">Methods</a> .....	67
3.3	<a href="#">Results</a> .....	71
	<a href="#">24hr SRE gives rise to layer-specific changes in synapse density</a> .....	71
	<a href="#">Global distribution of synapses across the cortical layers undergoes change following 24h SRE</a> .....	73
	<a href="#">Correlation in synapse density between adjacent layers is stronger after 24h SRE</a> .....	77
	<a href="#">Synapses in L3 are significantly longer following 24h SRE</a> .....	78
3.4	<a href="#">Discussion</a> .....	81
4.	<b><a href="#">Layer-specific critical periods for synaptic plasticity in the infragranular layers</a></b> .....	<b>85</b>
4.1	<a href="#">Introduction</a> .....	85
	<a href="#">Layer-specific critical periods</a> .....	85
	<a href="#">Progression of critical period onsets through cortical layers</a> .....	85

4.2	<a href="#">Methods</a>	88
4.3	<a href="#">Results</a>	92
	<a href="#">Synapse density increases in superficial layers from P14 to P18</a>	92
	<a href="#">24hr single row experience at PND 17 results in changes in synapse density in L6</a>	94
	<a href="#">Synapses in L5A are significantly longer after 24h SRE in PND 18 animals</a>	96
4.4	<a href="#">Discussion</a>	99
5.	<a href="#">Discussion</a>	106
	<a href="#">Unbiased high-throughput analysis of synaptic plasticity</a>	106
	<a href="#">Future endeavors</a>	108
	<a href="#">Potential applications of the technique</a>	110
<b>Appendix A. <a href="#">Average synapse density in unit volume of cortex</a></b>		<b>112</b>
<b>Appendix B. <a href="#">Inter-animal variability</a></b>		<b>114</b>
<b>Appendix C. <a href="#">Increase in mEPSC frequency in L2 pyramidal neurons following 24h SRE</a></b>		<b>115</b>
<b>Appendix D. <a href="#">Time course of synaptic plasticity</a></b>		<b>118</b>
<b>Appendix E. <a href="#">Synapse density measurements</a></b>		<b>124</b>

# Chapter 1

## 1. Introduction

### 1.1 The importance of characterizing synaptic changes

Neurons communicate through synapses in order to receive and process incoming input and ultimately, determine the behavior of the organism. A neuronal circuit can be roughly defined as a group of interconnected neurons, usually localized in a spatially restricted manner, and are involved in processing a specific input. Depending upon changes in the inputs, due to development or learning experiences, these circuits actively modify the properties of these synapses, like strength and number of synapses. Through such synaptic modifications, the neuronal circuits can tailor their outputs in response to the stimulus received.

Synaptic modifications have been observed and characterized in various subcortical as well as cortical circuits. During development of an organism, synaptic plasticity occurs extensively as neurons are incorporated into newly forming circuits. New connections are formed and lost at a high rate early in development, as observed by *in vivo* imaging of dendritic spine dynamics (Holtmaat A. J. et al., 2005). In case of the sensory cortices, as the neuronal circuits develop, they often go through a short phase, known as the critical period (CP), during which they are highly responsive, and exhibit heightened levels of synaptic plasticity in response

to the nature of the external stimulus (Hensch, 2005). Plasticity of synapses is not restricted to younger animals, as was previously thought. The adult brain retains remarkable ability to both modify the strength of synapses and also form or remove synapses in response to altered sensory experience (Holtmaat A. et al., 2006; Hofer et al., 2009) or under conditions of learning (Xu et al., 2009; Lai et al., 2012). Given that synaptic plasticity is so essential for the normal development, functioning and adaptability of the neuronal circuits, it is not surprising that defects in the mechanisms regulating synaptic plasticity often involved in neurological disorders.

### **Synaptic plasticity in development**

In the cortical circuits, it has been a common observation among various animals, like rodents (Micheva and Beaulieu, 1996; De Felipe et al., 1997), macaques (Rakic et al., 1986; Bourgeois and Rakic, 1993) and humans (Huttenlocher and de Courten, 1987; Huttenlocher and Dabholkar, 1997) that early in development, synapse density increases rapidly, reaching a maximum soon after birth, followed by a prolonged phase of synaptic pruning wherein almost 40% of the synapses are lost to reach adult levels of synapse density. This has been observed in multiple regions of the brain, but with each region following a slightly different timeline of development (Huttenlocher and Dabholkar, 1997) with sensory cortices often reaching an adult-like state earlier than other areas, like the prefrontal cortex. Moreover, within the same region, the different cortical layers show slight differences in the maximal synapse density reached and the synapse density reached when the animal reaches adulthood. While the superficial layers (L1, L2, and L3) and the granular layer (L4) of the cortex reach very high synapse densities, the infragranular layers (L5A and L5B) register slightly lower maximal synapse densities (Micheva and Beaulieu, 1996; Huttenlocher and Dabholkar, 1997) and L6 shows the least increase

(Huttenlocher and Dabholkar, 1997). This difference in synaptic density across the cortical layers is maintained into adulthood.

Studies that observed *in vivo* dynamics of spines located on the apical dendrites of L2/3 and L5 neurons observed that there are more spines in younger animals, the minority of which are persistent for more than a week. In adult animals, the overall spine density is lower and the majority of spines are persistent (Holtmaat A. J. et al., 2005). Since dendritic spines are an indicator of the presence of excitatory synapses (Knott et al., 2006), these studies provide a dynamic picture which suggests that, as the cortical circuit is developing, new synapses are formed and lost, along with an exuberant production of synapses early in development forming less precise connections. In older animals, synapses are more stable, and over a prolonged phase of synaptic pruning targets, presumably, lesser used synapses that are not critical for the proper functioning of the cortical circuit are lost.

During this early developmental phase, cortical circuits also exhibit a CP wherein they can undertake rapid synaptic modifications in response to alterations in sensory experience. This has been extensively studied in sensory cortices, but it has been observed in higher cognitive functions such as language acquisition in humans, and song learning in song birds. Again, the different brain regions can exhibit their own uniquely-timed critical periods, for example, the onset of CP for TC synapses in the rodent somatosensory cortex occurs right after birth (Fox, 1992; Crair and Malenka, 1995) while in the visual cortex it does not occur until the fourth postnatal week (Gordon and Stryker, 1996). Moreover, in the somatosensory cortex, each class of synapse has been observed to have its own unique CP onset and offset (Wen and Barth, 2011).

These layer-specific differences in development and experience-dependent synaptic plasticity suggest that, it is imperative to simultaneously study the changes that are occurring throughout the cortical column, in order to understand the functioning of the whole cortical circuit.

### **Synaptic plasticity in learning**

Synaptic plasticity also underlies the acquisition of new tasks and their subsequent consolidation. It was shown that L2/3-L2/3 synapses exhibit long-term potentiation (LTP) in rats that were trained to perform a forelimb reach-and-grasp task (Rioult-Pedotti et al., 2000) and as long as the animal retained the task performance, the synapses maintained their strength of connections (Rioult-Pedotti et al., 2007) even when training was discontinued. By way of *in vivo* imaging of dendritic spines, it has been established that spine dynamics are correlated with learning. A similar reach-and-grasp motor task (Xu et al., 2009) or a rotarod training (Yang et al., 2009) in mice resulted in rapid onset (within hours) of extensive spine formation on the apical dendrites of L5 neurons. Following the initial burst of spine formation, spine elimination was observed as well, which reduced the spine density back to levels observed in untrained animals. However, synapse elimination did not eliminate all newly formed synapses and some of them persisted even after training was discontinued (Xu et al., 2009). Mice that had undergone training previously, when tested again after a month of no training, retained the same performance levels and did not exhibit heightened levels of spine formation again. But, extensive spine formation was observed when the same animals were trained on a different task or when naïve age-matched animals were trained on the same task and heightened levels of spine

formation was observed (Xu et al., 2009; Yang et al., 2009). This suggests that the synapses that were associated with spines that persisted after the initial training session encoded the skill that was learned, and their persistence resulted in the retention of the skill.

Similar observations of a novel experience leaving an anatomical trace, which enable the circuit to rapidly adapt upon reintroduction of the same experience later in life, has been observed in the visual cortex of adult mice following monocular deprivation (Hofer et al., 2009) and in the auditory cortex of mice after fear conditioning (Moczulska et al., 2013) in the form of persistent spines on the apical dendrites of L5 neurons, and in the optic tectum of barn owls after abnormal association between their auditory and visual maps in the form of persistent axonal projections (Linkenhoker et al., 2005).

A more direct proof of synapses being the structural representation of newly formed memories was provided by a recent study that subjected mice to a fear-conditioning learning paradigm in which the animal is trained to associate an auditory cue with a foot shock, followed by a fear extinction paradigm which involved repeated presentation of the auditory cue without the foot shock (Lai et al., 2012) which lead the animals to lose the association previously established. These experiments showed that, in the frontal association areas, fear extinction formed spines in close vicinity to, and oriented in the same direction as those spines that were eliminated during fear conditioning. This proves that certain individual synapses were associated with a specific memory, and their loss erases the memory. Meanwhile, the same fear conditioning training leads to spine formation in the auditory cortices of mice (Moczulska et al., 2013).

It is worth pointing out that while these individual studies provide an excellent picture of the turnover of dendritic spines, and consequently synapses, during learning, they are concentrated on only a single region of the cortex or specific set of spines, namely the spines on the apical dendrites of L5 neurons. One of the studies did characterize the changes, if any, occurring on the basal dendrites of L5 and L6 neurons in response to learning (Yang et al., 2009) they did not include L1 (Letzkus et al., 2011) and L2/3 synapses (Rioult-Pedotti et al., 2000; Rioult-Pedotti et al., 2007) in their study both of which are known to be involved in learning.

### **Synaptic plasticity in neurological disorders**

A number of proteins associated with synapses have been implicated in intellectual disability, autism spectrum disorders or schizophrenia (Penzes et al., 2011; Caroni et al., 2012). A large body of work has established that dysregulation of synaptic structure and function is involved in a number of neuropsychiatric disorders (Penzes et al., 2011).

*Autism Spectrum Disorders (ASD)* – ASD is a family of neurological disorders commonly characterized by behavioral deficits that include sociobehavioral, cognitive, linguistic, and perceptuomotor abnormalities (Rapin, 1997). Recent work has uncovered a defining characteristic of autistic brains, that is, having a higher number of spines than age-matched normal brains. This was established by way of spine counts obtained from Golgi-impregnated postmortem human brains (Hutsler and Zhang, 2010). Patients of Fragile X syndrome (FXS) (Irwin et al., 2001), a form of mental retardation closely associated with autism, and mouse models of FXS (Galvez and Greenough, 2005; McKinney et al., 2005) exhibit a similar phenotype of high density of spines. Mouse models of other syndromes that are comorbid with

autism, like Rett syndrome caused by the deletion of MeCP2 gene, exhibit higher synapse density but reduced number of functional synapses (Chao et al., 2007) and Angelman syndrome, caused by the lack of the maternal Ube3a allele, exhibit impaired plasticity and altered spine density (Yashiro et al., 2009). Recently, mouse models have been generated that involve mutation of proteins that have been directly linked to ASDs, like the Shank proteins, a scaffolding protein localized to the post synaptic densities in excitatory synapses. Although these mouse models exhibit behavioral phenotypes that are characteristic of autism, their synaptic characteristics have not been studied extensively (Yoo et al., 2014).

*Schizophrenia* – Post-mortem brains from schizophrenic patients revealed decreased spine density as compared to normal individuals (Glantz and Lewis, 2000). Surprisingly, this decrease in spine density was restricted to layer 3 pyramidal neurons in both prefrontal cortex (Glantz and Lewis, 2000; Kolluri et al., 2005) and in the auditory cortex (Sweet et al., 2009). Transgenic mouse models for schizophrenia show that the onset of reduction of spine density and behavioral deficits occurs at adolescence (Cahill et al., 2009) which matches with the fact that onset of symptoms of schizophrenia also occurs at adolescence in humans.

*Alzheimer's disease (AD)* – Although AD is primarily characterized as a neurodegenerative disease, recent work has revealed that synaptic deficits might underlie the earliest symptoms of AD (Selkoe, 2002; Arendt, 2009).

Synaptic changes have been implicated in many other disorders like stress (Kim and Diamond, 2002) as well. Again, most of the characterization of synaptic pathology in these diseases has been done in a piecemeal fashion with different research groups focusing on specific areas, neurons or class of synapses. To obtain a holistic picture of the synaptic pathology that is

brought about by any disorder, synaptic properties would need to be characterized over a wide area, such as throughout the cortical column. Moreover, most of the studies focus on the changes happening in the excitatory synapses. It has been shown that the inhibitory circuit is affected as well. For instance, inhibitory synaptic strength is increased in one transgenic mouse model for autism (Tabuchi et al., 2007).

## **1.2 Techniques for studying synaptic changes**

Researchers have been investigating synaptic changes using a variety of techniques. Some of them allow very high spatial resolution, of the order of a few nanometers for electron microscopy or a few microns for *in vivo* imaging of dendritic spines allowing researchers to study single synapses. Other techniques like electrophysiological recordings enable the analysis of specific synaptic pathways at the level of circuits. Here we shall review these techniques briefly and bring forth their limitations which, to an extent, can be addressed by the technique used in the work.

### ***In vitro* electrophysiological recordings**

Researchers have employed *in vitro* electrophysiological recordings extensively to study synaptic properties of neuronal circuits over the years. The greatest advantage of this technique is that it allows targeted investigation of specific connections in a neuronal circuit, like isolating the L4-L2/3 synaptic connections (Clem and Barth, 2006; Wen and Barth, 2011). By careful dissections of the brain, the connections that the investigators are interested in can be preserved

for the most part. This, in turn, enables the technique to be unrestricted by anatomical considerations. Moreover, employing genetic, morphological, anatomical and electrophysiological markers investigators can ensure the precise targeting of specific cell-types or excitatory, inhibitory or neuromodulatory inputs. Pharmacological interventions further help isolate the specific receptors and channels that are involved in any synaptic changes under investigation. Thus, this technique is able to provide an unequivocal functional marker of synapses.

On the other hand, performing electrophysiological recordings is extremely labor-intensive, time consuming and requires extensive training. It is biased towards the strongest inputs as they are easier to detect. While it provides the ability to detect some real-time changes like LTP (Crair and Malenka, 1995) and LTD (Bender et al., 2006), long-term changes cannot be studied using this technique. Finally, neither the acquisition of data nor the subsequent analysis has any degree of automation making it extremely time-consuming.

### ***In vivo* imaging of dynamics of dendritic spines**

Recent introduction of two-photon microscopy (Yuste and Denk, 1995) has enabled the study of dendritic spines *in vivo* (Trachtenberg et al., 2002; Holtmaat A. et al., 2006). Since it has been established that spines are a good marker for synapses (Knott et al., 2006), this is a powerful technique allowing long-term imaging of the same synapses and study their dynamics. Thus, using this technique, a lot of understanding has been gained about long-term synaptic dynamics that occur in the same animal in response to altered sensory experience, learning or

disease (Holtmaat A. and Svoboda, 2009; Fu and Zuo, 2011; Caroni et al., 2012; Chen C. C. et al., 2014).

On the other hand, due to the scattering of light by biological tissue, researchers are limited to studying the spines situated only in the superficial layers of the cortex. Furthermore, dendritic spines are markers of only excitatory spines. Thus, this technique does not provide any information about the synaptic dynamics of inhibitory synapses that are predominantly found on the dendritic shafts or soma of neurons. Again, neither the acquisition of data nor the subsequent analysis has any degree of automation making it extremely time-consuming.

### **Array tomography**

The recently developed technique of array tomography (Micheva and Smith, 2007) enables detailed study of molecular composition of synapses over wide areas of the brain. This technique straddles a good range of scale providing information about synapses at circuit-level. Combining this and the subsequent step of ultrastructural reconstructions provides a complete set of structural, anatomical and functional information about the synapses in the neuronal circuit.

Unfortunately, this is a hugely complex problem and current state-of-the-art computational techniques are still struggling to process and analyze these large amounts of data efficiently.

## **Electron microscopy**

Electron microscopy has been used for a long time to study synapses. It is regarded as the “gold standard” for characterizing synapses. Traditionally, synapses were counted manually (Micheva and Beaulieu, 1996; De Felipe et al., 1997) and hence, it was extremely time consuming.

Recent technological advances have enabled techniques like serial section electron microscopy to provide highly detailed three-dimensional structural information about neuronal circuits (Mishchenko et al., 2010; Briggman and Bock, 2012). Although the data acquisition and subsequent processing is automated to a large degree, substantial human intervention is still required (Chklovskii et al., 2010) for the segmentation of images and subsequent identification of various structures, like synapses, dendritic spines, and axonal boutons, in them. Any algorithm to be designed for automated synapse detection in such series of images has to be able to isolate synapses from the rest of the membranous structures (Kreshuk et al., 2011; Morales et al., 2011; Helmstaedter, 2013; Kreshuk et al., 2014). Moreover, dense volumetric reconstructions of entire circuits is an enormous task (Helmstaedter, 2013). Again, these volumetric techniques are limited in their spatial coverage and more importantly, present only a static picture of the neuronal circuit. The limited coverage of these techniques prevents researchers from characterizing synaptic changes that are occurring throughout the neuronal circuit.

Thus, some of the major requirements that need to be addressed are that the technique should be unbiased and unrestricted to any anatomical consideration, resolve both excitatory and inhibitory synapses, provide a quantitative analysis and provide the opportunity for automating both data acquisition and the subsequent analysis. We employed ethanolic phosphotungstic acid

staining of synapses with a machine-learning algorithm that helped automatically detect and characterize synapses in the tissue. This enabled us to perform unbiased high-throughput analysis of synaptic changes in the cortical circuit in response to altered sensory experience.

### **1.3 Choice of rodent barrel cortex as model system**

To test the feasibility of our technique in successfully characterizing synaptic changes in a neuronal circuit, we chose the mouse barrel cortex as our model cortical circuit to study. Primary somatosensory cortex (S1) in rodents has a substantial area devoted to processing the inputs from the whiskers on the snout of the animal. This area in S1 is termed the barrel cortex owing to the cytoarchitectonic barrel-like structures observed in L4 by Nissl-staining (Woolsey and Van der Loos, 1970). It was subsequently discovered that the cortical column delineated by a L4 barrel, termed the barrel column, preferentially received and processed tactile information from an individual whisker, with each whisker have its own barrel column in the barrel cortex (Simons, 1978, 1985) giving rise to a one-to-one correspondence. The ability to anatomically identify the neuronal circuit that processes information received from a given whisker makes the barrel cortex an excellent model to study development, sensory processing and experience-dependent plasticity of cortical circuits.

Sensory information from the whiskers is first transmitted to primary sensory neurons located in the trigeminal ganglion by way of an array of sensory nerve endings that innervate the whisker follicle. These sensory neurons transmit the information to clusters of neurons in the principal sensory nucleus of the trigeminal nerve (PrV) in the brain stem. These cells form topographical clusters named barrellettes (Bates and Killackey, 1985), with information from

each whisker being restricted to an individual cluster (Veinante and Deschenes, 1999). Next, the axons of these trigeminal nucleus neurons, cross the midline, and transmit the information to anatomically segregated clusters of neurons, called barreloids, in the ventral posteromedial (VPM) nucleus in the thalamus (Killackey and Fleming, 1985). Subsequently, the axons of VPM neurons innervate the barrels in L4 of the somatosensory cortex. Throughout this circuit, called the lemniscal pathway, the sensory information from each whisker is transmitted to the cortex in a segregated fashion.

But, in addition to this, a parallel circuit brings broad-field multi-whisker sensory information to the cortex as well. This circuit, called the paralemniscal pathway, originates from the neurons in the rostral section of the interpolar spinal trigeminal nucleus (SpV) (Veinante et al., 2000), which lies posterior to the PrV. This nucleus does not show any anatomical clustering of neurons and the neurons show multi-whisker responses (Veinante and Deschenes, 1999). These neurons transmit the information to the posteromedial thalamic nucleus (POm), which again, does not show any topographical segregation of neurons. Subsequently, axons of the POm neurons reach the barrel cortex carrying multi-whisker information (Diamond et al., 1992). While the VPM axons preferentially innervate L4, L5B and L6A, the POm axons innervate L1 and L5A preferentially (Lu and Lin, 1993; Bureau et al., 2006; Wimmer et al., 2010b). But, almost all the cortical layers receive some amount of thalamic input from either VPM (Petreanu et al., 2009) or POm.

The intracortical circuit of the barrel cortex has been extensively characterized (Schubert et al., 2007; Lefort et al., 2009; Feldmeyer, 2012). In broad strokes, L4 spine stellate neurons primarily send their axons up to L2/3 and they remain confined to the barrel column. L4 neurons are also connected with each other extensively (Feldmeyer et al., 1999; Lefort et al., 2009).

In addition to L4 inputs, L3 neurons preferentially receive some thalamic input from VPM (Petreanu et al., 2009; Meyer et al., 2010; Oberlaender et al., 2012a) and there is extensive interconnectivity between L2/3 neurons. While both L4-L2/3 synapses (Feldmeyer et al., 2002) and L2/3-L2/3 synapses (Feldmeyer et al., 2006) are localized to the basal dendrites of L2/3 neurons, they occupy largely non-overlapping segments (Petreanu et al., 2009). L2/3 neurons also receive long range inputs from other cortical layers like motor cortex contralateral somatosensory cortex, motor cortex and secondary somatosensory cortex via their apical dendrites (Petreanu et al., 2009). Recently, it was established that a subset of L2 neurons receive POM input representing multi-whisker information (Jouhanneau et al., 2014) presumably through the POM axons that innervate L1. L2/3 neurons also project to other cortical areas (Aronoff et al., 2010) and to L5B within their home column (Feldmeyer et al., 2006; Broser et al., 2008; Bruno et al., 2009). Both L2 and L3 pyramidal neurons, send their axons beyond the boundaries of the barrel column (Adesnik and Scanziani, 2010). Thus, L2/3 neurons exhibit both within-column and inter-column connectivity and are able to integrate information from multiple whiskers.

In addition to the subset of L2 neurons, L5A neurons are in a position to integrate the information borne by the lemniscal and paralemniscal pathways as they receive direct POM input and indirect VPM input via L4 (Feldmeyer et al., 2005) and L3 neurons (Lefort et al., 2009). L5A neurons also exhibit a high rate of interconnectivity both within-barrel and across-barrels. L5B neurons receive inputs from virtually all the cortical layers with the exception of L6 (Lefort et al., 2009). The localization of each of these connections has been characterized as well. While L2/3-L5B and L4-L5B synapse target the basal dendrites, VPM-L5B synapses, in addition to the basal dendrites, target the entire apical dendrite which traverses through L4 and L2/3. L2/3-L5B

synapses are located on the oblique apical dendrites as well. Finally, long range connections from other cortical areas target the apical tuft and basal dendrites (Petreanu et al., 2009). While L5A neuronal predominantly axons project up through the cortical column and arborize in L2/3, axons of L5B neurons arborize in L5B itself, both going beyond their home column (Oberlaender et al., 2011). L5 is designated as the output layer of the barrel cortex. While L5A neurons send long-range projections to the contralateral side of cortex, primary motor cortex, the secondary somatosensory cortex and the striatum, L5B neurons project to subcortical targets including the superior colliculus, pontine and trigeminal nuclei or spinal cord.

Lastly, L6 is designated as the layer that sends feedback to the thalamus via corticothalamic (CT) connections. But, CT-projecting neurons constitute only half the excitatory neuron population of L6 with the rest of the neurons forming corticocortical (CC) connections (Zhang and Deschenes, 1997). While VPM-projecting CT neurons are localized to the top part of L6, those that project to both VPM and POm are restricted to the deeper regions of L6 (Zhang and Deschenes, 1997) and CC neurons are equally distributed throughout L6. CC neuronal axons project extensively in L6 covering a large part of the barrel field (Pichon et al., 2012).

In addition to these excitatory connections in the barrel cortex, there exists a complex network of inhibitory connections involving intra-laminar as well as inter-laminar connections. Synaptic plasticity has been shown to affect both inhibitory and excitatory synapses, with the former often preceding the latter.

## **1.4 Experience-dependent synaptic plasticity**

Experience-dependent synaptic plasticity has been studied extensively in the sensory cortices. This is primarily due to the fact that the stimulus to the system can be modified in a precisely controlled fashion, like depriving visual stimulus to only one of the eyes by monocular deprivation (MD) or, depriving or sparing selective somatosensory stimulus by trimming or sparing of whiskers.

### **Narrow focus and diversity in experimental design of previous studies**

A rich body of literature has provided a wealth of information about synaptic plasticity, with each study focusing on a specific set of synapses, say L4-L2/3 or a specific set of dendritic spines, say, those on the apical dendrites of L5 neurons. The differences among these studies in experimental design, like the age of the animals studied, the nature of the sensory manipulation, and the length of sensory manipulation prevents researchers from obtaining a holistic picture about the synaptic changes occurring in different parts of the circuit in response to the same sensory manipulation. For example, experience-dependent synaptic plasticity in the rodent barrel cortex has been studied with various forms of sensory manipulations like trimming of one or two whisker rows for 40 days starting at birth (Simons and Land, 1987), sparing a pair of whiskers for 24h (Diamond et al., 1994), sparing of a single whisker for at least 21 days (Fox, 1992; Glazewski and Fox, 1996) or for 24h (Clem and Barth, 2006; Benedetti et al., 2009; Wen and Barth, 2011), deprivation of a single row of whiskers (Allen et al., 2003; Bender et al., 2006; Jacob et al., 2012) or chessboard deprivation for 7 days (Wallace H. and Fox, 1999a, b) being employed.

## **Barrel cortex as a model for experience-dependent plasticity**

The rodent barrel cortex has been repeatedly used as the model system to study experience-dependent synaptic plasticity. This is primarily due to the fact that sensory input from each whisker is received by neurons localized in specific regions called ‘barrels’ in layer 4 of the cortex (Woolsey and Van der Loos, 1970) and processed in the cortical column defined by the barrel. Such segregated inputs enable examining the effects of specifically targeted modifications to the circuit. These localized neuron distributions are readily identifiable regions which allows easy targeting of the necessary circuitry to study synaptic changes. Finally, the incoming stimuli can be easily modified by trimming or removing the whiskers, a simple, non-invasive procedure.

Using any one of the numerous whisker manipulation paradigms, different studies have concentrated on the experience-dependent modifications occurring in a few chosen synaptic pathways in cortical circuit. Long-lasting selective whisker deprivation, initiated before PND 4, resulted in increase in responsiveness of neurons in L4 to the stimulation of the spared whiskers (Fox, 1992). This was temporally coincident with, and hence attributed to, the synapses made by thalamocortical (TC) axons onto layer 4 neurons undergoing robust experience-dependent strengthening, initially thought to be limited to only a specific developmental time window in early postnatal life (Crair and Malenka, 1995). But, more recent studies have observed extensive remodeling in TC axonal arbors (Oberlaender et al., 2012b; Yu et al., 2012) and TC synapses (Wimmer et al., 2010a) upon sensory deprivation even in adult animals.

Other studies observed an increase in responsiveness in L2/3 neurons to the spared whisker to both inter-barrel inputs (Diamond et al., 1994; Glazewski and Fox, 1996) and intra-barrel inputs (Glazewski et al., 2007; Benedetti et al., 2009) in young (P13-16) and juvenile

(P35) animals. Previous work from our group discovered that rapid (within 24hr) potentiation of L4-L2/3 synapses and L2/3-L2/3 (Clem and Barth, 2006; Clem et al., 2008; Wen and Barth, 2011) upon removal of all but the principal whisker, occurred only in the second postnatal week. With a longer duration of spared whisker experience in older animals, pairs of L2/3 neurons in the spared whisker barrel column show strengthened connectivity (Cheetham et al., 2007) and these were found to be accompanied by corresponding structural changes, that is, enlargement of the synapses involved (Cheetham et al., 2014). On the other hand, the connectivity between neighboring layer 2/3 pyramidal neurons in the deprived column and the axonal arborization of layer 2/3 inputs from the non-deprived to the deprived column decreased (Cheetham et al., 2007; Broser et al., 2008; Bruno et al., 2009). Similar studies looking at the plasticity of L2/3-L5 synapses, revealed target cell-type specific changes. Removal of a single row of whiskers for 10 days, starting at PND 30, weakened the synapses made by L2/3 axons onto L5B regular spiking (RS) cells in the deprived whisker barrel column while those onto L5B intrinsic bursting (IB) cells remain unchanged (Jacob et al., 2012). But, it has not been explored whether these L2/3-L5 synapses can undergo experience-dependent changes at the same developmental time point as when the TC-L4, L4-L2/3 and L2/3-L2/3 synaptic changes were studied.

In addition to just changes in synaptic strength, long-term imaging of dendritic spines also reveal gain, loss and increased stabilization (Zuo et al., 2005) of spines in response to altered sensory experience. Experience-dependent plasticity is not limited to excitatory synapses. Inhibitory synapses also undergo experience-dependent modification (Gaiarsa et al., 2002). Inhibitory synapse density increased in L4 upon persistent whisker stimulation (Knott et al., 2002) and decreased upon whisker deprivation (Micheva and Beaulieu, 1995), including a critical period during which inhibitory synapses exhibit heightened plasticity (Jiao et al., 2006).

Inhibitory inputs to L2/3 pyramidal neurons exhibit a source layer-specific change following altered sensory experience in adult animals (Katzel and Miesenbock, 2014).

### **Need for an unbiased high-throughput technique to study synaptic plasticity**

Taken together, it is evident that gaining a complete picture of how the cortical circuit responds to changes in sensory experience is extremely difficult by this “piecemeal” experimental approach. While there has been a push in the field to develop high-throughput techniques to map the connectivity of neural circuits at both the mesoscale level using light microscopy (Osten and Margrie, 2013) and at the microscale level using serial section electron microscopy (Briggman and Bock, 2012), these volumetric techniques present only a static picture of the neuronal circuit.

We set about to test the feasibility of a high-throughput technique to study synaptic plasticity, we using an automated synapse detection and characterization technique developed in our lab to study experience-dependent synaptic changes occurring throughout the cortical column in the mouse barrel cortex. Ethanolic phosphotungstic acid (EPTA) was used to selectively stain synapses and subsequently, a machine-learning algorithm was able to detect and characterize the stained synapses. We were interested in utilizing this tool to uncover previously unknown loci of plasticity and generate novel hypotheses regarding experience-dependent synaptic plasticity. By virtue of the high-throughput nature of the technique, we were able to uncover laminar-specific experience-dependent changes in synapse density and length in the spared whisker barrel column after 24h of sparing the ‘D’ whisker row.

## 1.5 Critical Period Plasticity

It has been a common observation that neuronal circuits in the cortex can undergo extensive plasticity in response to short periods of altered sensory experience in early development. This time period is often termed the “Critical Period”. Although plasticity is observed in adult animals, it often takes prolonged exposure to altered stimulus (Sawtell et al., 2003; Sato and Stryker, 2008; Benedetti et al., 2009). Moreover, the changes observed as a result of plasticity in adult animals are often reversible, that is, restoration of normal sensory experience reverts the cortical circuit into its previous untouched state (Prusky and Douglas, 2003). On the other hand, critical period plasticity results in long-lasting, sometimes irreversible changes (LeVay et al., 1980; Prusky and Douglas, 2003). The classic experimental evidence for critical period plasticity was obtained by monocular deprivation (MD) experiments in kittens (Hubel and Wiesel, 1970) wherein it was established that the shift in the response of neurons to the undeprived eye was maximal if the deprivation was done during the second month after birth. Since then, the phenomenon of critical period has been characterized in the visual cortex of monkeys (Horton, 1997), ferrets (Issa et al., 1999) and mice (Gordon and Stryker, 1996) and also in other sensory cortices, namely the somatosensory cortex (Fox, 1992) and auditory cortex (de Villers-Sidani et al., 2007) of rodents.

Synaptic changes are the primary factors responsible for such extensive changes in neuronal responses (Feldman, 2009; Espinosa and Stryker, 2012). These include the synaptic plasticity mechanisms of long-term potentiation (LTP) of the spared inputs, weakening of the deprived inputs through NMDAR-mediated long-term depression (LTD) or by mechanisms involving pre-synaptic changes mediated by endocannabinoid receptors, like CB1, or homeostatic scaling of the synapses. These synaptic modifications involve pre- and post-synaptic

elements depending upon the class of synapses, cortical layer or developmental time point. Thus, the study of critical period plasticity has helped uncover the complex interplay between different mechanisms of synaptic plasticity at different synapses in the cortical circuit.

### **Layer-specific critical periods**

In the barrel cortex, it was observed that TC synapses, up till PND 7, undergo NMDAR-mediated strengthening (Crair and Malenka, 1995) or weakening (Feldman et al., 1998) in response to *in vitro* pairing protocols to induce LTP or LTD respectively. Genulocortical synapses in L4 of mice V1 can undergo *in vitro* LTP (Kirkwood et al., 1995) and also could undergo LTD and exhibit internalization of AMPARs even with just 24hrs of MD at the age P21-25 (Heynen et al., 2003). These time periods for rapid synaptic changes match with that during which L4 neuronal response show experience-dependent changes to whisker deprivation (Fox, 1992), and to deprivation of visual input to one eye (Gordon and Stryker, 1996). Also, genulocortical (or TC) axonal arbors of the deprived eye are able to undergo substantial pruning only if MD is started during the CP in mice (Antonini et al., 1999). Structural changes in TC axons were evident even with just 3 days of MD, like rapid reduction in number and size of TC axonal boutons (Coleman et al., 2010), and rapid pruning of TC axons serving the deprived eye in kittens (Antonini and Stryker, 1993). Thus, major structural and synaptic changes seem to underlie the changes observed in neuronal responses to altered sensory experience at this early developmental time point.

Supragranular layers also show rapid plasticity with their own distinct critical period. Map plasticity is extensive in L2/3 with just 24h of MD (Trachtenberg et al., 2000). Dendritic

spines on L2/3 apical dendrites show extensive motility following 2-3 days MD (Oray et al., 2004) or reduced motility following whisker deprivation (Lendvai et al., 2000). Previous work from our lab has characterized a critical period for rapid experience-dependent strengthening of synapses targeting L2/3 pyramidal neurons in the mouse barrel cortex (Clem and Barth, 2006; Wen and Barth, 2011). After 24h of single whisker experience (SWE), L4-L2/3 and L2/3-L2/3 show increase in strength. While the CP for this L4-L2/3 strengthening spans the ages P12-14, the CP of L2/3-L2/3 synaptic strengthening spans the ages P13-16 (Wen and Barth, 2011).

### **Progression of critical period onsets through cortical layers**

Interestingly, the progression of CPs for each cortical layer closely follows the developmental timeline of cortical circuits. For instance, thalamocortical circuits exhibit critical period very early in postnatal development (Crair and Malenka, 1995; Kirkwood et al., 1995), followed by L4-L2/3 synapses and then the recurrent excitatory connections in L2/3 (Wen and Barth, 2011) which matches the timeline of maturation of receptive fields of neurons in S1 (Stern et al., 2001). Layer 4 cells of the rat barrel cortex respond to whisker stimulation reliably at P12, compared with layer 2/3 cells that respond to whisker stimulation only at P14 (Stern et al., 2001). Thus, the earlier maturation of L4 neuronal responses to sensory stimulation may facilitate an earlier CP for L4-L2/3 synapses. Although a similar trend of the timeline of maturation of visual-evoked responses in rodent V1 (Fagiolini et al., 1994), matching the critical periods is observed in the visual cortex, layer-specific CPs have not been reported.

While layer-specific CPs have been well-characterized in L4 and L2/3, little is known if other cortical layers exhibit a critical period for synaptic plasticity. Following MD around the

critical period in mice, L5 apical dendrites show extensive spine motility (Oray et al., 2004) but only localized to the supragranular and infragranular layers, not in the granular layer. But, L5 apical dendritic spines were observed to be motile even in adult animals with short periods of MD (Hofer et al., 2009) or whisker deprivation (Holtmaat A. et al., 2006). Also, L2/3-L5B synapses can undergo plasticity after prolonged whisker deprivation (Jacob et al., 2012) in P30 mice. The ability to shift their responsiveness to the undeprived eye has been observed to linger in L5 and L6 neurons to a much later developmental time point (Daw et al., 1992), though these were longer (3 month) deprivations. This raises the question – does the sequential progression of P onsets, as observed in L4, L4-L2/3 and L2/3-L2/3 synapses, reach L5 synapses after L2/3 synapses? A systematic exploration of whether a CP, as characterized by rapid changes, exists for L2/3-L5 or recurrent L5-L5 synapses has not been carried out. Even less is known about synapses targeting L6 neurons. Although, several studies have established that TC synapses in L6 do not undergo plasticity (Wang et al., 2013; Crocker-Buque et al., 2014), the development, maturation and plasticity of L6-L6 synapses is largely uncharacterized.

We employed our automated synapse detection technique to test, in an unbiased fashion, whether infragranular cortical layers exhibit a CP, possibly at a slightly later developmental time point. Our analysis revealed that L5A synapses in the spared barrel column do show a rapid increase in size, and thus, strength of synapses, in response to just 24hrs of SRE starting at age PND 17. Since this change was not observed when the same manipulation was carried out an earlier age, it suggests that the L5A synapses do exhibit an onset of a phase for synaptic plasticity and that it is later than that for L2/3 synapses. Also, L6 synapses in the spared barrel column showed an increase in synaptic density. This shows that cortical circuits can modify synaptic strengths and numbers independently in response to altered sensory experience.

## **Role of inhibitory circuitry – Onset of Critical Period**

Critical period plasticity is not restricted to excitatory synapses. In the visual cortex, the maturation of inhibitory circuits has emerged as the most important phenomenon that determines the onset of the critical period. Accelerated maturity of the inhibitory circuits as characterized by an increase in both number of inhibitory interneurons, and amplitude of inhibitory synaptic input received by excitatory neurons, was observed by overexpression of BDNF in transgenic rats. These animals exhibited a precocious onset and closure of the critical period for OD plasticity (Huang et al., 1999). Furthermore, administration of GABA agonists, rescued OD plasticity in mice with a genetic inactivation of the GABA-synthesizing enzyme glutamic acid decarboxylase (GAD65) resulting in low levels of GABA (Hensch et al., 1998), and induced a precocious CP in wild-type animals (Fagiolini and Hensch, 2000). It was further discovered that, the  $\alpha 1$  subunit of the GABA-A receptor was required for OD plasticity (Fagiolini et al., 2004). Since these receptors are enriched in the synapses formed by parvalbumin (PV) – expressing basket cells (Fagiolini et al., 2004), it suggests this class of interneurons plays a crucial role in regulating CP onset. Recent electrophysiological observations show that, it is only during the critical period does MD reduce the inhibition mediated by PV neurons and this disinhibition of excitatory neurons is critical for their shift in response to the undeprived eye (Kuhlman et al., 2013).

Ultrastructural analysis showed inhibitory synaptic density significantly increase and reaches adult levels by P16 in the rat somatosensory cortex (Micheva and Beaulieu, 1996), which matches the age range when L2/3 neurons exhibit their critical period (Wen and Barth, 2011). Thus, the role played by the maturation of inhibitory circuitry in determining the critical period onset could extend to other cortical layers.

## Chapter 2

# Animal-to-animal variation in absolute synapse density in a layer-specific manner

### 2.1 Introduction

Numerous techniques, like electrophysiological recordings (Clem and Barth, 2006), *in vivo* imaging of dendritic spines (Trachtenberg et al., 2002; Knott et al., 2006), electron microscopy (Knott et al., 2002) and array tomography (Kay et al., 2013) enable researchers to study synaptic changes. But, these techniques are limited in their coverage of a given network of neurons or a neuronal circuit. For example, electrophysiological recordings from pairs or a few neurons at a time is time consuming and labor intensive which limits researchers to studying only few chosen pathways of any given neuronal circuit. *In vivo* imaging limits the researchers to a spatially localized region. Recent technological advances have enabled techniques like serial section electron microscopy to provide highly detailed structural information about neuronal circuits (Mishchenko et al., 2010; Briggman and Bock, 2012). Although the data acquisition and subsequent processing is automated to a large degree, substantial human intervention is still

required (Chklovskii et al., 2010) for the segmentation of images and subsequent identification of various structures, like synapses, dendritic spines, and axonal boutons, in them. Any algorithm to be designed for automated synapse detection in such series of images has to be able to isolate synapses from the rest of the membranous structures (Kreshuk et al., 2011; Morales et al., 2011; Helmstaedter, 2013; Kreshuk et al., 2014). Again, these volumetric techniques are limited in their spatial coverage and more importantly, present only a static picture of the neuronal circuit. The limited coverage of these techniques prevents researchers from characterizing synaptic changes that are occurring throughout the neuronal circuit.

Thus, it would be highly advantageous to utilize a technique that can characterize the changes occurring in the neuronal circuit in an unbiased manner, that is, not limited to a spatial region or a specific branch of the neuronal circuit. To achieve this, the technique would need to be able to acquire information over a large spatial area. Automation would enable rapid processing of such large datasets and enable characterization of synaptic changes occurring across multiple conditions, like developmental time points, altered sensory experiences, and disease.

We used a machine-learning algorithm, previously developed in our lab (Navlakha et al., 2013), to automatically detect synapses in transmission electron microscopy (TEM) images of the mouse somatosensory cortex. To enable automated detection by the algorithm, we used ethanolic phosphotungstic acid (EPTA) to selectively stain synapses in the cortical tissue (Bloom and Aghajanian, 1966, 1968). EPTA binds to basic proteins found in the synapses and selectively renders them electron-dense (Quintarelli et al., 1971a; Quintarelli et al., 1971b).

## **Assessment of the performance of the semi-automated synapse detection from EPTA stained tissue**

Prior to this technique being utilized to investigate a biological question about synapses and their associated changes, careful assessment of its accuracy and reproducibility must be carried out. That is, determining if this technique gives a reliable estimate of the synaptic properties being investigated, like number and length of synapses and also determining how robust is the technique to any variations that might arise due to batch-to-batch differences in sample preparation, possible developmental differences across litters of animals or efficiency of the EPTA staining.

Here we used this technique to measure synaptic properties, like synapse density and length of synapses, in mouse somatosensory barrel cortex. Specifically, we focused our analysis on the anatomically defined ‘D’ row barrel column. Given that we could accurately identify this specific region repeatedly across all animals, we expected to observe minimal variation in synapse properties that might arise from imaging anatomically different areas of the brain in different animals.

However, we observed a substantial amount of variability across animals, specifically in the synapse density measurements we obtained from the ‘D’ row barrels. For example, in layer 3, the synapse density showed a 4-fold range (mean synapse density = 4.72 synapses/image; standard deviation, S.D. = 1.65 synapses/image). Thus, we carried out a detailed analysis to determine the sources of this variability across animals.

## Variability in synapse density measurements

A common feature of techniques that enable the study of morphological features of synapses, like electron microscopy, is that they provide a very high spatial resolution, on the order of tens of nanometers. As the cortical circuit typically spans a few hundred microns (Helmstaedter, 2013), assessing synaptic features at this scale can lead to biased estimates due to local inhomogeneities in the tissue. For instance, in layer 4 there is a higher density of cells towards centers of the barrel hollows than the outer regions which could lead to variations in synapse density measurements (Meyer et al., 2013). This can typically be countered by averaging the measurements acquired over a wide area. On the other hand, even if data acquisition for performing such extensive sampling might be possible, the subsequent processing and analysis of data is often labor intensive and time consuming. Imaging techniques like electron microscopy can be used to quantify a range of synaptic features, like synapse density, synapse type frequency, and synaptic size distribution. Estimating the density of synapses is probably the most straightforward among all the synaptic properties that can be evaluated by ultrastructural studies as it involves merely detecting of synapses and no further morphological characterizations, like length or type of synapse. Thus, we primarily used synapse density as the parameter to test the reliability of our technique.

For conventional electron microscopy it has been estimated that, in the cortex, 10-15 non-contiguous images ( $35\mu\text{m}^2$  each) are sufficient to provide an adequate estimate of the synaptic density in any cortical layer (Granger et al., 1995; DeFelipe et al., 1999b). This was ascertained by observing the decrease in variance in the mean synapse density measure obtained as a function of increasing number of images used. The 95% confidence intervals around the mean narrowed down further only marginally with addition of more images, once 10-15 non-

contiguous images had been used to obtain the mean synapse density. This suggested that a reliable estimate of the true synapse density has been achieved.

Others have reported that even with extensive sampling, synaptic density measurements can show substantial variability (Table 2.1) across individuals. In a study that used array tomography to estimate synapse density, the authors observed 20% variability (coefficient of variation, 0.2) in layer 2/3 in adult human cortex between samples from the same individual as well as across individuals (Kay et al., 2013). Some conventional EM studies show similar variability in synapse density across animals in the rodent somatosensory cortex (Micheva and Beaulieu, 1996; De Felipe et al., 1997; Landers et al., 2011). But, other studies have shown remarkably little animal-to-animal variability both in rat barrel cortex (Knott et al., 2002) and in the density of synapses in conventional EM images (Peters et al., 2008) and EPTA-stained synapses (Uemura, 1980) in the macaque prefrontal cortex.

**Table 2.1: Summary of mean and standard deviation of synapse density in cortical tissue reported by different groups**

Study	Animal	Age	'n'	Brain region	Lamina	Mean synapse density (x 10 <sup>8</sup> /mm <sup>3</sup> )	S.D.	C.V.
Micheva and Beaulieu, 1996	Rat	PND 15	3	Somatosensory Cortex	Supra-granular layers	4.86	0.95	0.20
De Felipe, et.al., 1997	Mouse	PND 11	2	Somatosensory Cortex	Layer 2/3	7.97	2.36	0.29
Landers, et.al., 2008	Mouse	Adult	4	Somatosensory Cortex	Layer 4	14.21	1.7	0.12
Knott et.al., 2002	Mouse	Adult	6	Somatosensory Cortex	Layer 4	6.0	0.2	0.03
Peters, et.al., 2008	Macaque	5-10 years	5	Prefrontal cortex	Layer 2/3	5.95	0.29	0.05
Uemura, 1980	Macaque	7-12 years	3	Prefrontal Cortex	Upper third	8.5	0.6	0.07

n = Number of animals used; S.D. = Standard deviation, and C.V. = Coefficient of variation

These studies differed in the ages of the animals and in the technique used to observe the synapses. The studies reported the variance in synapse density observed among animals in terms of the standard deviation (SD). As compared to the SD, the coefficient of variation (CV), being a ratio of the standard deviation to the mean, gives an unbiased estimate of the variability in a dataset and can be used to compare variability across different datasets. Thus, we computed the CV from the reported mean and standard deviation of synapse densities from each study, to gauge the magnitude of animal-to-animal variability observed in these diverse studies.

It is difficult to explain the differences in variability reported by these different studies. Low variability in macaque studies suggests a species-specific effect on synapse density variability while higher variability in young rodents suggests a developmental-specific effect. Minor experimental differences, like accurate reporting of the age of the animals depending how they were birth-dated, sample preparation and criteria employed for detecting synapses in the images, all can contribute to the variability reported.

Individual animals could truly differ from each other in terms of the absolute number of synapses their cortical circuits have, and it might be a biological attribute subject to the animal's development and experiences. To determine whether the variability observed in our synapse density measurements was primarily due to technical factors or biological factors, we carefully tested the contribution of various potential sources of variability, like accuracy of the detection algorithm, variations that might exist among different animal litters and the level of contrast of the staining.

In this study, we evaluated the animal-to-animal variability we observed in mean synaptic density in an anatomically identified region of the mouse somatosensory cortex. We show that

our automated synapse detection algorithm performs at par with human experts suggesting that the automated detection algorithm is not the source of variability. Next, we test whether we obtained a large enough dataset to reliably estimate synapse densities. Using linear regression analysis, we tested if the staining contrast determined the number of synapse detected in a given sample or if batch-to-batch variations in EPTA staining chemistry affected the synapse detection. Additionally, we also determined if minor developmental variations, that might exist across litters or individual animals affected the synapse density measurements obtained. To address the question whether EPTA staining itself is the source of variability, we compared the synapse density measurements obtained from our technique against those obtained by the gold standard, i.e., conventional EM imaging. We show that our technique gives more consistent results within an animal and also appears to detect smaller synapses more effectively. Taken together, these results suggest that the animal-to-animal variability in synapse density is indeed a biological phenomenon and may be dependent on the developmental state of the neuronal circuit.

## 2.2 Methods

**Animals:** Animals from litters of wildtype C57bl6 (Harlan origin, raised in CMU colony) mice were birth-dated by daily cage checks. At postnatal day 13 and 17 (P13 and P17) they were divided into two groups, a control group and a “single row experience” (SRE) group, where all but the D-row whiskers were plucked gently from the right side of the animal face. All contralateral whiskers were fully removed from SRE animals (Wen et al., 2013). Both control and SRE-treated animals were subjected to a brief period (<1 min) isofluorane anaesthesia on the day of SRE treatment. Twenty-four hours later, the animals were euthanized by decapitation, their brains dissected out and immersion-fixed in ice-cold 2.5% glutaraldehyde (Electron Microscopy Sciences (EMS), Hatfield PA) in 0.1M phosphate buffer (PB). After 24h of glutaraldehyde fixation at 4°C, brains were transferred to PB with 30% sucrose solution until they equilibrated, and then stored at 4°C until sectioning.

**Tissue preparation:** To preserve the order of barrel column rows (A-E), brains were cut 45° to the midline (Fig. 2.1A) for cryostat sectioning (Finnerty et al., 1999). Sections were cut at 50 µm thickness and stored in PB. The A-E row of barrels was visualized by mitochondrial (cytochrome oxidase) staining (Land and Simons, 1985), and sections where the ‘D’ row could be unambiguously identified (Fig. 2.1 B) as the second-most medial barrel of five distinct barrels in the specimen were selected for manual tissue dissection using a razor blade (Fig. 2.1 C). In only two to three 50 µm-thick sections were all rows unambiguously present; specimens without 5 clear barrels present were excluded from further analysis. Because barrels within the posterior-medial barrel subfield are larger, ranging from 150-300 µm in diameter, visualization of a clear cytochrome oxidase signal in the second-most medial barrels likely indicated that the section was from the middle of the D barrel. Dissected columns were typically 200-300 µm wide and

spanned the pial surface to the white matter, and only one column per animal was quantitated. Where results from the EPTA method were compared to traditional EM staining, adjacent sections from the same animal were examined.

**Electron Microscopy tissue preparation:** Tissue was prepared for imaging by a transmission electron microscope (TEM), a Hitachi H7100, in a series of steps. For ethanolic phosphotungstic acid (EPTA) staining of synapses (Bloom and Aghajanian, 1966, 1968), the selected 50 $\mu$ m section was washed three times in distilled water (5 min each, no shaking), followed by incubation in 0.02% NaOH in water for 10 minutes (no shaking). The tissue was dehydrated with an ascending series of ethanol baths (25%, 50%, 70%, 80%, 90%, and 100%). A 1% phosphotungstic acid (PTA; Ladd Research, Williston VT) solution was prepared in 100% EtOH. A critical step for this solution was the addition of a tiny amount of water, via a 95% ethanol solution (7  $\mu$ l/1000  $\mu$ l of PTA). The dehydrated tissue was moved into the PTA solution and incubated at room temperature, shaking, for 1 h. PTA was washed from the sample with two changes of 100% ethanol. Fourth, propylene oxide (PO) (EMS) was used as a transitional solvent (the first change of PO was on ice), and then the specimen was infiltrated with Spurr (Ted Pella) embedding resin, which was polymerized at 60° C for 48h. Finally, 100nm sections were cut using a diamond knife (Delaware Diamond Knife) on an Ultracut-E ultramicrotome (Riechert-Jung), and were picked up using single slot copper grids (EMS).

For conventional EM imaging, the 50 $\mu$ m thick slice was initially exposed to osmium tetroxide (OsO<sub>4</sub>) and lead citrate. Then, the tissue was taken through same procedure as described above with the exception of the exposure to EPTA.

**Tissue shrinkage:** We found that, there was substantial amount of shrinkage of the tissue after it was cut from the resin block and mounted onto the copper grid for imaging. The amount of

shrinkage was determined by comparing the separation between fiduciary landmarks, namely the pia and an angular cut manually made underneath layer 6, under the TEM versus when the tissue is in the resin. Once cut and mounted, the sections measured only 70-80% of their length as when embedded in the resin. This was remarkably consistent across all our samples. Subsequently, we adjusted the previously reported depths of each layer as measured from the pia (Lefort et al., 2009) with the shrinkage factor we determined.

**Image Acquisition:** The specimen was observed using a TEM and images were taken digitally using a Kodak Megaplug 1.6i camera. The electron beam was scanned across each cortical layer parallel to the pial surface and images were obtained in a continuous fashion (Fig. 2.1 C). The electron beam was positioned for each image such that there was no overlap between images of adjacent areas of the cortex. On average, the image centers were separated by a distance of 8-10 $\mu$ m. In order to ensure that the images were indeed obtained from the designated cortical layer, the acquisition of images was done at the following depths, as measured from the pia, for the respective cortical layers, L1 - 50 $\mu$ m, L2 - 125 $\mu$ m, L3 - 325 $\mu$ m, L4 - 500 $\mu$ m, L5A - 600 $\mu$ m, L5B - 725 $\mu$ m and L6 - 900 $\mu$ m. Depending upon the shrinkage determined for each individual tissue section, these depths were adjusted accordingly. We obtained about 100 images (an example image from layer 2 is shown in Fig. 2.1 D) per cortical layer with each image capturing 4.31 $\mu$ m X 4.31 $\mu$ m region of the cortex.

**Image Analysis:** The analysis of all the images was carried out using custom-written software in MATLAB. Firstly, the contrast of each image was enhanced and then subsequently, each image was binarized based on a manually determined threshold. Following this, connected segments were computed in each image and were filtered based on their size (min. area - 5.5 X 10<sup>3</sup> nm<sup>2</sup> and max. area - 66 X 10<sup>3</sup> nm<sup>2</sup>). Each connected segment and its surrounding area as bounded by a

square patch of side 125 pixels (~500nm) is used for subsequent classification. A machine learning algorithm that employs support vector machines (SVM) was used to classify the connected segments as synapses based on texture- and shape-based features (Navlakha et al., 2013). The classifier was first trained using 1,665 positive (synapses; Fig. 2.1 E) and 10,441 negative (non-synapses) examples. In order to account for sample-to-sample variability in staining contrast, a testing dataset that included both synapses as well as non-synapses was generated from 10% of images for each layer in each animal. All synapses within this image subset were identified manually. The performance of the classifier was evaluated on the testing image set. A classification threshold of 50% correct recall (where exactly 50% of manually-identified synapses were labeled correctly by the classifier) was chosen for the subsequent analysis of all images obtained for that particular layer in a given animal.

$\text{Recall} = \text{TP} / (\text{TP} + \text{FN})$ , where TP = True Positives, and FN = False Negatives

In cases where the classifier performed at very high levels (correctly identifying 95% of synapses), we found an unacceptably high level of false positives, i.e., objects that were not synapses; thus, a threshold of 50% recall was established to compromise between accurate detection of synapses without inaccurate classification of non-synapses.

For synapse density, we scaled the measured density by the precision that the classifier exhibited at 50% recall. For all other measurements, we used only samples that had >75% precision.

$\text{Precision} = \text{TP} / (\text{TP} + \text{FP})$ , where TP = True Positives, and FP = False Positives

The lengths of synapses were obtained when the connected segments were calculated for each image.

**Sources of variability:** We chose to test the following sources of variability –

1. **Animal identity** – Each animal was uniquely identified.
2. **Litter identity** – Each animal belonged to one of six litters.
3. **Image quality** – Each synapse density measurement was associated with a parameter that estimated the average image quality for that sample. We used the range of histogram of the image to estimate the quality of the image. The range of the image histogram for each image is obtained after assigning the maximum and minimum values as the highest and lowest pixel values respectively that were observed in at least 0.01% of pixels. Since our images constituted of 1024 X 1016 pixels, 0.01% translates to roughly 100 pixels.

**Linear Regression:** Potential sources of variability were tested using linear regression models. The parameters that were chosen to be tested as potential sources of variability were – individual animal identity, litter identity, and image quality as measured by the range of the image histogram. The linear regression models were of the form  $Y = \alpha + \beta X$  where  $Y$  is the dataset of synapse density measurements and  $X$  is any one of the potential sources of variability. The parameters were also tested in different additive combinations ( $Y = \alpha + \beta_1 X_1 + \beta_2 X_2$ ). Interactions between the chosen parameters could not be tested, possibly due to insufficient spread of data.

The  $R^2$  value obtained for these linear models of regression was used as a measure to estimate how much of the variability in synapse density measurements was explained by any individual parameter or combination of parameters. To estimate the  $R^2$  value, a 90% jackknifing approach was used wherein the entire dataset was resampled (without replacement) and only 90% of the dataset was used in the linear regression models. This was repeated 500 times and the mean and standard deviation of  $R^2$  was determined.

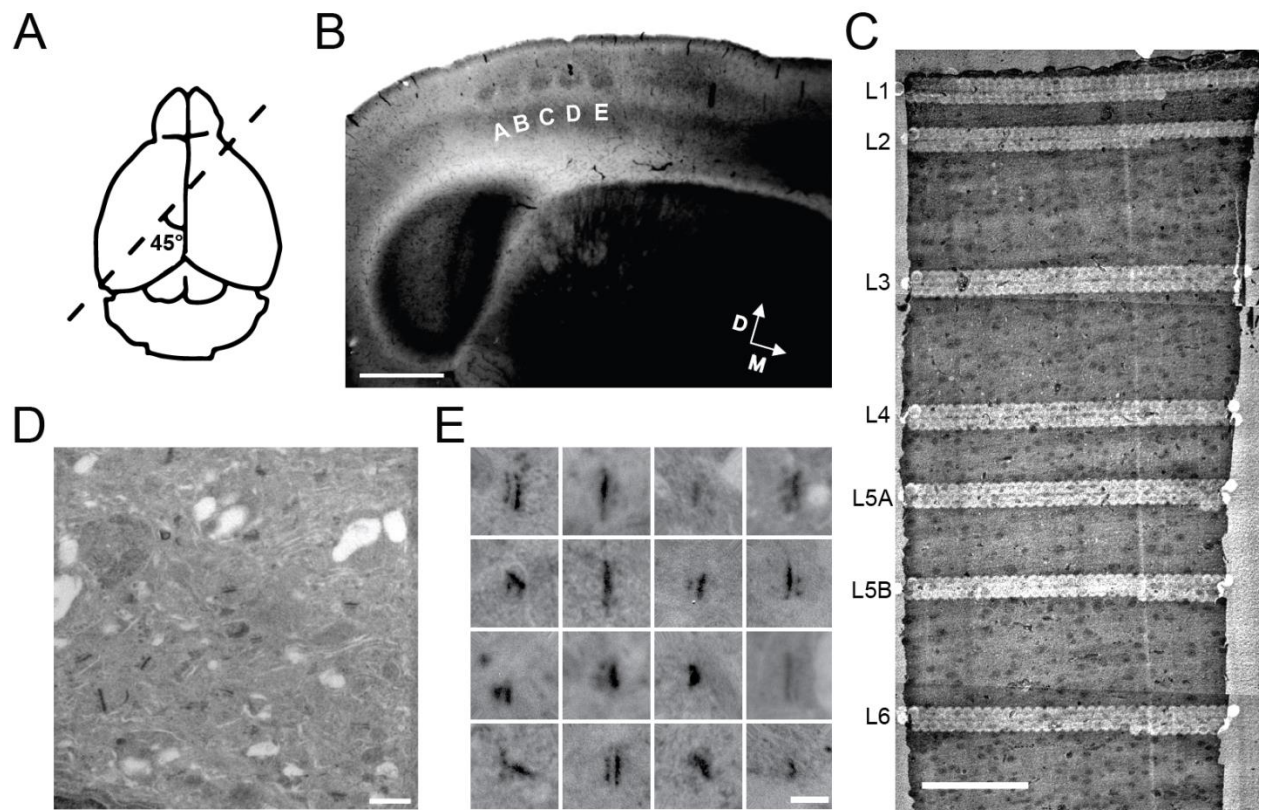


**Figure 2.1: Pipeline of tissue preparation and imaging.**

- A. A schematic showing the angle at which the brain is initially cut to obtain slices in which the 5 barrel rows can be visualized.
- B. An example cytochrome oxidase stained tissue showing the 5 barrel rows. – Scale bar – 1mm.
- C. An example tissue that has been imaged under the TEM. Scale bar - 100 $\mu$ m.
- D. An example image as obtained from the TEM. Scale bar – 500nm.
- E. A mosaic showing a few examples of synapses that have been manually chosen to constitute the training set. Scale bar – 200 nm.

## 2.3 Results

### Laminar-specific effect on variability observed in automated EPTA-stained synapse density measurements

In this study, we measured synapse density in the ‘D’ barrel column in 14 day old mice (PND 14). We utilized a machine-learning algorithm to automatically detect EPTA-stained synapses in TEM images (Fig. 2.2 A). We obtained the synaptic density for a given layer as estimated by the algorithm after it processed all of the images. We subsequently adjusted for the precision of the algorithm for that particular sample and the 50% recall. The mean synapse density was observed to be remarkably consistent across the different cortical layers (Fig. 2.2 B). However, one of the most striking characteristics of our EPTA-stained synapse density measurements is the high-degree of variability that existed across animals (Fig. 2.2 C). Substantial variability was observed in all cortical layers but the superficial layers tended to show slightly higher variability (ranging from 2.08-8.04 synapses/image in layer 3; mean S.D. for L2-4 = 0.72) than the infragranular layers (ranging from 4.26-5.59 synapses/image in layer 5A; mean S.D. for L5A-L6 = 0.38).

We used coefficient of variation (CV), the ratio of SD to the mean, as a measure to quantify variability. We computed the CV of synapse density measurement for each layer by a bootstrapping procedure as described below. For each layer, we generated a set of synapse density measurements, by sampling, with replacement, from the original set that constituted of synapse density measurements obtained from the different animals used. For each sampled set, we computed the CV. Following 200 iterations of this sampling procedure, we obtained the mean

and SD of the CV for that cortical layer (Fig. 2.2 D). An advantage of this procedure is that it gives an estimate of the CV with minimal bias from any outliers.

As expected from the SD, layers 2, 3 and 4 have a high CV while layers 5A, 5B and 6 have a slightly lower CV. Layer 1 shows the same amount of variability as layer 5B or 6. This suggests a potential lamina-specific effect on the range of mean synapse density across animals. If the variability observed was a property of our protocol of automated detection of EPTA-stained synapses, one would expect similar amount of variability irrespective of cortical layers. The lamina-specific difference in variability suggests that this is not the case.

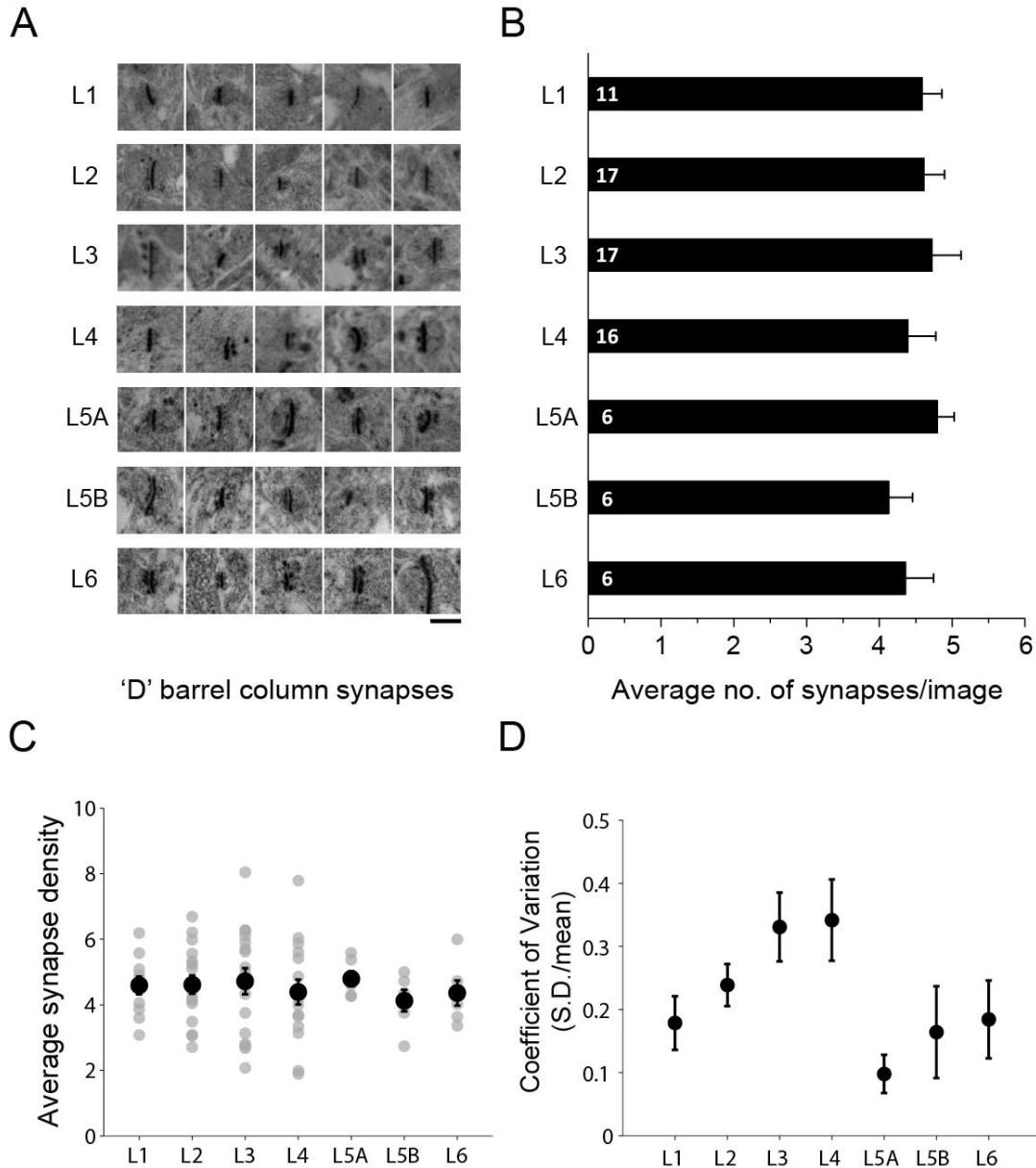


**Figure 2.2: Laminar-specific differences in variability in synapse density in P14 mice.**

A. Mosaic showing example synapses from each cortical layer. Scale bar – 200nm.

B. Mean synapse density obtained for each cortical layer. Numbers within bars indicate *n*.

C. Plot shows the inter-animal variability in synapse density measurements for each cortical layer. Grey dots represent average synapse density from each individual animal for that cortical layer. Black dots represent mean synapse density for each cortical layer determined across all animals. Error bars represent standard error of mean (SEM).

D. Plot shows the CV of synapse density in each cortical layer. Black dots represent mean CV after 200 iterations of a bootstrap sampling of synapse density measurements. Error bars represent SD of CV.

### **Automated detection of synapses provides similar results as manual curation.**

We sought out to determine the accuracy and robustness of the automated detection of synapses. To evaluate the level of accuracy of the algorithm, we compared its performance to a human expert. Once we used the algorithm to label the synapses in a set of images (Fig. 2.3 A), we manually labeled all the synapses in 10% of the images and obtained an estimate of the synaptic density for the same sample (Fig. 2.3 B shows the same image as in Fig. 2.3 A, but with manual identification of synapses). Comparing the manual estimates of synapse density against those obtained from the algorithm across multiple samples revealed a high degree of correlation ( $r \geq 0.70$ ;  $p < 0.01$ ; Fig. 2.3 C). Similar levels of correlation were observed for all cortical layers. These results indicate that the algorithm is able to perform on par with human experts in estimating the synaptic density in any given sample.

### **Dense imaging of EPTA-stained tissue provides reliable estimation of underlying synapse density.**

Next, we wanted to ascertain whether we were acquiring a large enough dataset to be able to counter local inhomogeneities in the tissue while estimating the synapse density. Acquiring a large enough dataset is necessary to be able to make a reliable estimate of synapse density for a given sample. One way to test this is to randomly divide all the images obtained from a sample into groups and determine how much do these groups vary in their estimates of synapse density.

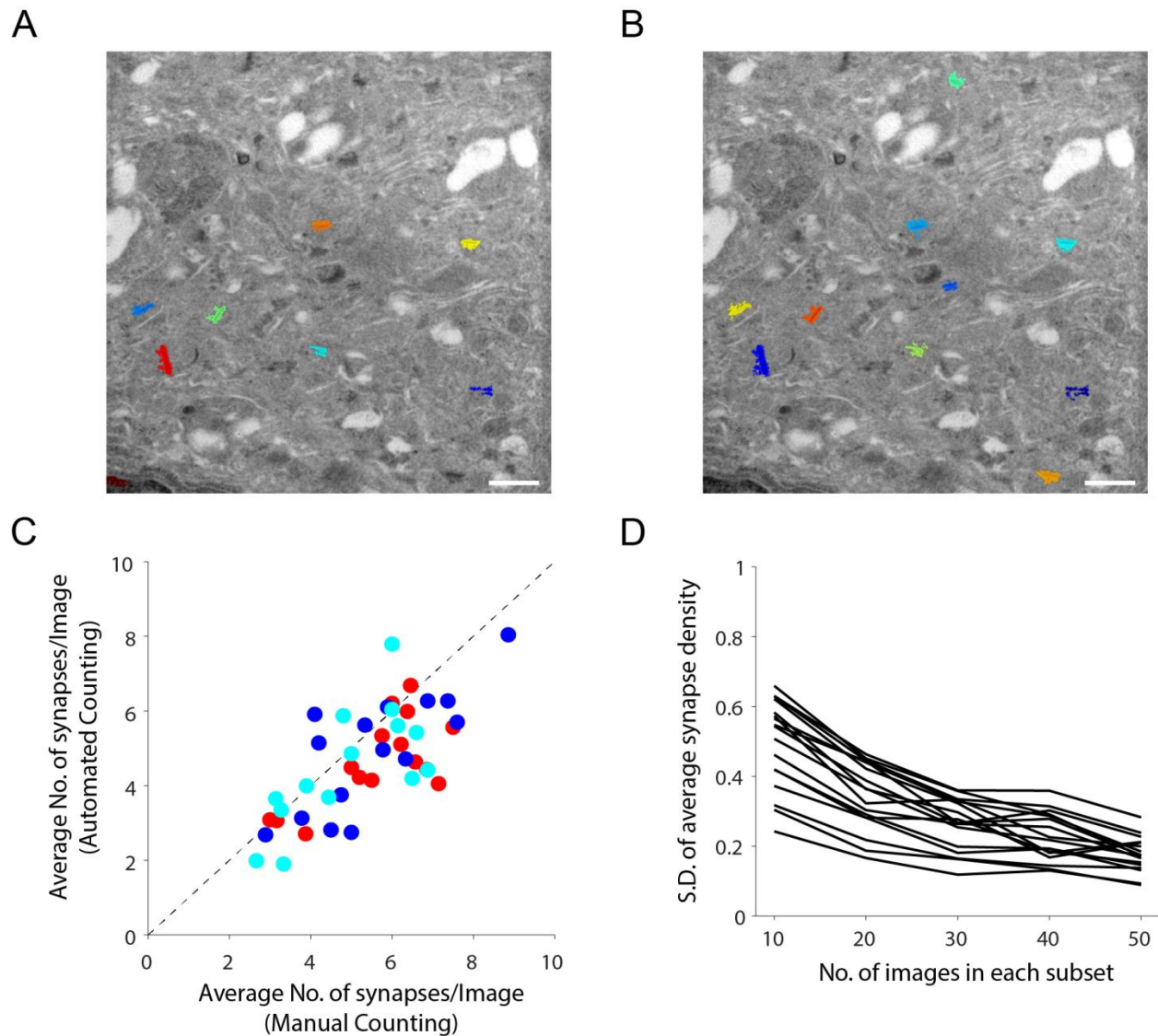


**Figure 2.3: Images of EPTA-stained synapses provide a reliable estimate of the true synaptic density and the automated detection performs at par with manual curation.**

- An example image of EPTA-stained synapses. Synapses detected by the automated algorithm are colored.
- Same image as in A. Synapses detected manually are colored.
- Comparison of synaptic density obtained from the algorithm against manual labelling for layers 2 (red), 3 (blue) and 4 (cyan). Pearson's correlation coefficient ( $r$ ) is 0.70 for layer 2;  $p < 0.01$ , 0.77 for layer 3;  $p < 0.01$  and 0.70 for layer 4;  $p < 0.01$ .
- Images were pooled randomly into subsets of varying sizes. SD in mean synaptic density among the subsets decreased as the size of subsets increased. Plot shows this variation for cortical layer 2. Each line represents an individual animal.

The variance between groups of images is expected to decrease as the number of images in each group is increased, as local tissue inhomogeneities contribute less effectively to the mean synapse density. Thus, a high level of variability between groups of images would indicate low level of reliability of the synapse density measurement. The minimum number of images required for obtaining a reliable estimate of synapse density would be the number of images that constitute a group when the variance in synapse density between groups reaches a minimum value.

We carried out the above test in the following manner – we initially obtained roughly 100 non-overlapping images in a given cortical layer from a single animal. The images were separated by a distance of 8-10 $\mu$ m to avoid repeated counting of synapses located at the image borders. Following automated detection and counting of synapses from each image, the images were randomly divided up into multiple groups. The mean synapse density was calculated for each of these groups of images. As expected, the standard deviation of the mean synapse density between groups decreased as the number of images in each subset was increased. The standard deviation reached a minimum value of about 0.3 when each subset contained around 30-40 images (Fig. 2.3 D). A similar trend was observed in all animals for all cortical layers.

It is worth pointing out that this set of minimum number of images cannot be contiguous and need to be evenly spaced apart to be able to provide a reliable estimate of the synapse density. Since the groups were assigned images in a random fashion, this set of 30-40 images contains, on average, every third image from the larger pool of 100 images. As the initial separation between images was 8-10 $\mu$ m, we can determine that the average distance between the 30-40 images that can provide a reliable synapse density measurement needs to be 25-30 $\mu$ m (distance between every third images).

Thus, 30-40 images obtained 25-30 $\mu$ m from each other can provide a reliable estimate of the synaptic density of a particular cortical layer. Given that, we obtained around 100 images per cortical layer, our estimates of synapse density are highly reliable.

### **Staining contrast does not contribute significantly to synapse density variability**

To detect synapses, our machine-learning algorithm utilized the contrast generated between synapses and the rest of tissue by virtue of the EPTA staining (Navlakha et al., 2013). We reasoned that, differences in staining contrast between tissues could lead to differences in the number of synapses detected. That is, higher contrast in staining of some tissue could lead to easier detection, and thus, artificially higher number of synapses as compared to tissue in which staining contrast was low.

We used the range of pixel values spanned by the image pixels to estimate the staining contrast. This was done based on the hypothesis that pixels from images with higher staining contrast would span a larger range of values. We computed the range as the difference between the minimum and maximum pixel values that were observed in at least 0.01% of pixels. Fig. 2.4 A and B show an example of an image from layer 2 with low and high contrast of staining respectively. Manual enhancement of the contrast reveals stained synapses in both images (Fig. 2.4 C and D). The distribution pixel values reveals that the image with lower contrast has a much narrower range (Fig. 2.4 E; grey histogram) than the image with higher staining contrast (Fig. 2.4 E; black histogram). We determined the average range of the pixel values across the nearly images obtained for each cortical layer. We observed that there was only a very weak level of correlation between the average range of histogram and the synapse density measured (Fig. 2.4 F;  $r = -0.2$  for layer 2). This trend was observed for all cortical layers. This clearly shows that

staining contrast, as represented by the image range histogram does not determine the number of synapses detected in a sample.

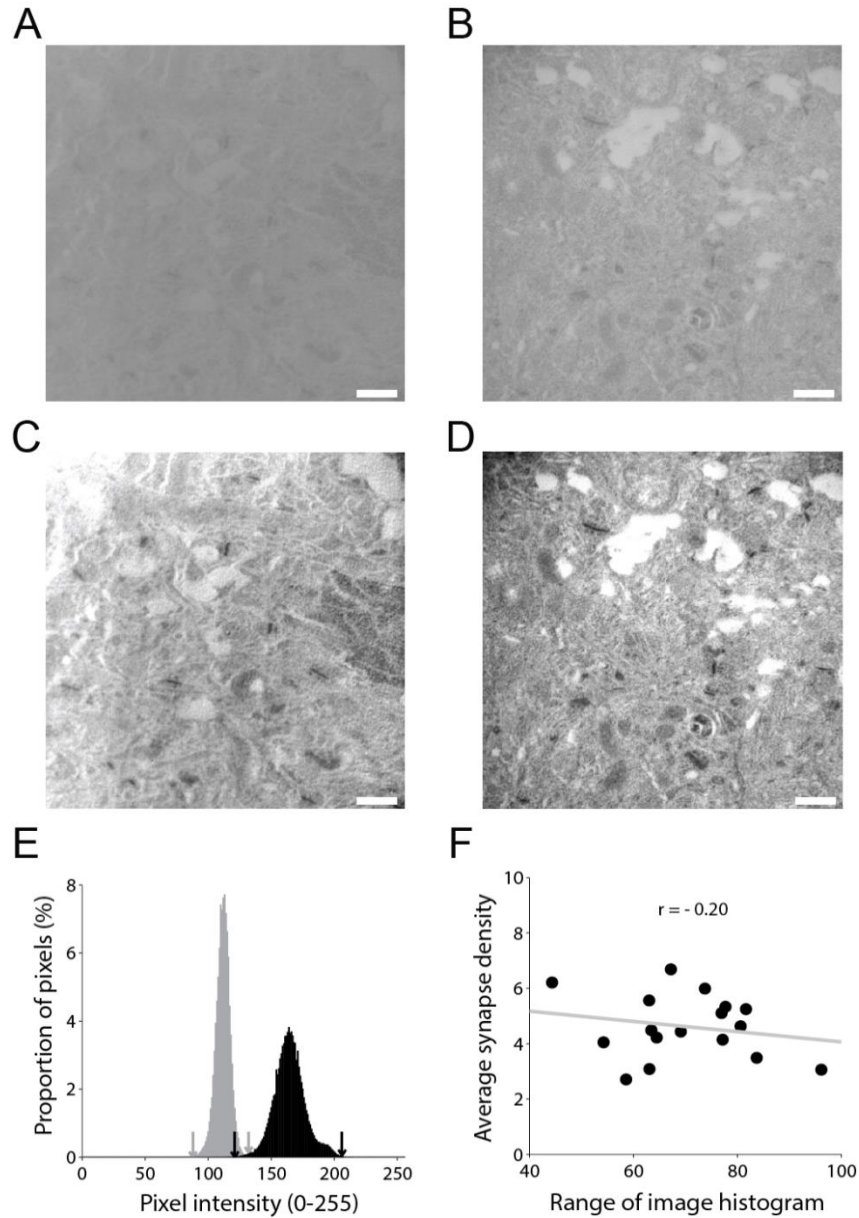


**Figure 2.4: Staining contrast does not affect synapse detection.**

- A. An example raw image that had a low range of pixel intensity.
- B. An example raw image with high range of pixel intensity.
- C. Same image as in A, with manually adjusted contrast to show synapses
- D. Same image as in B, with manual adjustment of contrast
- E. Plot of histogram of pixel intensities of images in A (low range; gray) and in B (high range; black)
- F. Plot showing almost no correlation between synapse density determined in an image and the range of pixel intensity for that image ( $r = -0.20$ , n.s.)

### **Differences across batches does not completely address the observed variability**

Our experimental design was such that, cortical tissue from animals that belonged to the same litter underwent processing and staining together as a single batch. The individual batches differed primarily in two main factors. The first one was the ethanolic EPTA staining solution itself, which was freshly prepared for each batch of tissue. Inconsistencies in the staining solution between aliquots could lead to differences in the EPTA staining contrast among the different batches. This, in turn, could result in easier detection and hence, higher number of synapses in some batches as compared to others. The second major factor potential differences between litters of animals due to their development and experiences in the home cage. Our recording of the birth of a litter of mice could be delayed from the actual time of birth by 24-36hrs. Variations in maternal care have been shown to affect synaptogenesis in the pups (Liu et al., 2000). Moreover, the size of the litters also affect the growth (Rodel et al., 2008) and brain development (Dobbing, 1964; Rocha-de-Melo et al., 2006) of the pups. Thus, we explored the potential existence of systematic differences between these different batches of tissue.

Grouping synapse density measurements from animals belonging to the same litter revealed that some litters tended to have higher synapse density than others. Fig. 2.4 A shows such litter-to-litter variation in synapse density as observed in layer 3. A similar but less pronounced trend was observed in other cortical layers. Unlike in layer 4, where differential neuron densities between barrel centers and periphery introduce local inhomogeneities, layer 3 has a more uniform distribution of neurons. Thus, this variation is unlikely to be due to differences in the anatomical region imaged.

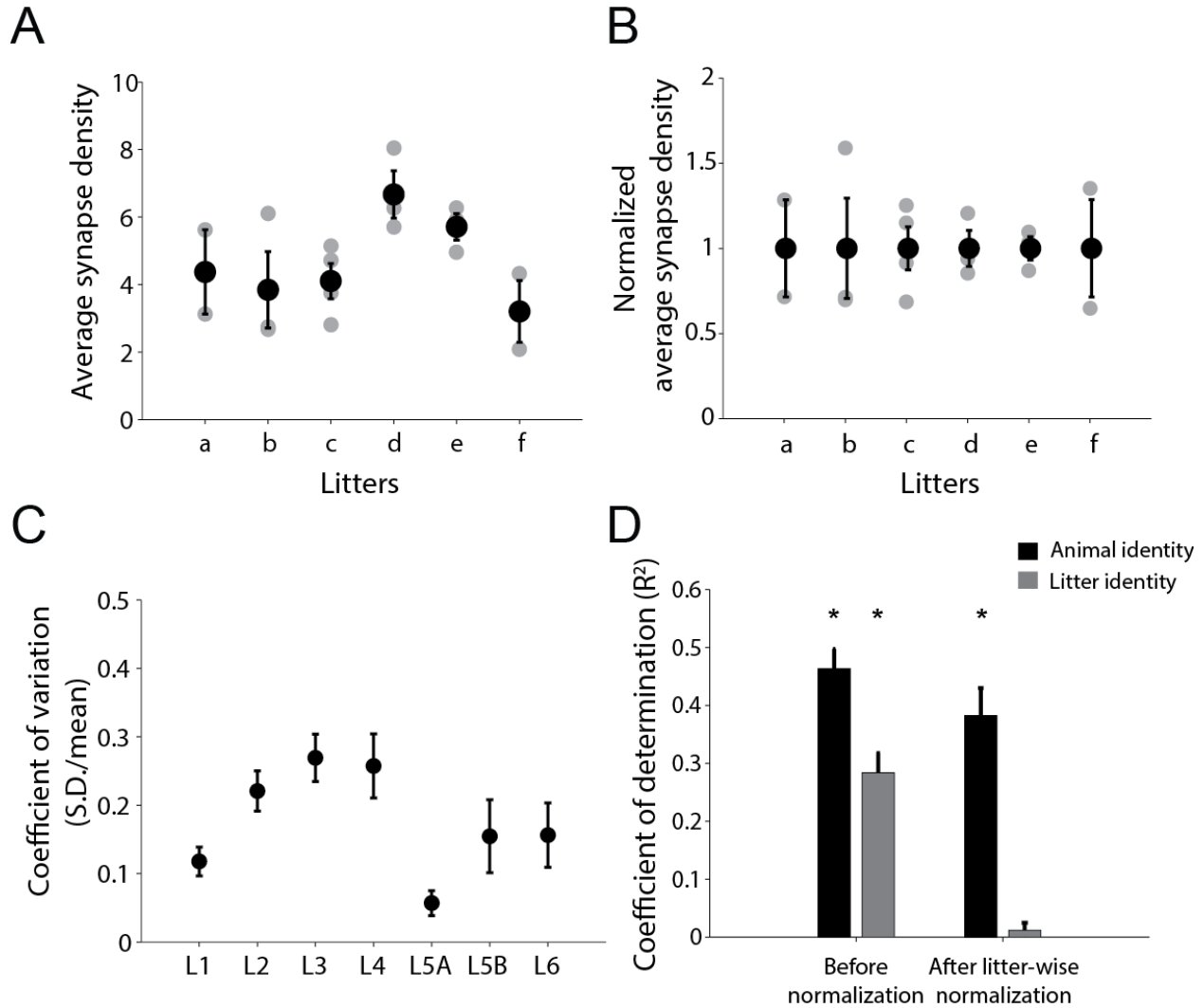


**Figure 2.5: Normalizing to litter average does not remove all animal-to-animal variability**

- A. Average synapse densities for each control animal grouped by litters (a – f) for layer 3. Error bars indicate SEM.
- B. Plot showing the litter-grouped synapse densities normalized to the litter means.
- C. Plot shows the CV of synapse density in each cortical layer after normalizing to the litter means.
- D. Plot shows the coefficient of determination ( $R^2$ ) for animal and litter identity before and after litter-wise normalization. After litter-wise normalization, litter identity does not contribute to the residual variability ( $R^2 = 0.01$ ) while animal identity still explains a lot of the residual variability ( $R^2 = 0.39$ ). \* indicates  $p < 0.05$  for linear regression fit for that parameter. Error bars indicate SD.

We used linear regression to determine the contribution of this litter-to-litter variation to overall synapse density variability and compared it to variability across animals taken individually. When determining the contribution of litter identity to overall variability, the linear regression model basically tested for a statistically significant trend among the mean synapse densities obtained from each litter. In case of determining the contribution of animal identity, the models tested for trends across mean synapse densities obtained from each individual animal. We found that both animal identity and litter identity significantly contributed to overall variability (Fig. 2.5 D, left; animal identity, mean  $R^2 = 0.47$ ; litter identity, mean  $R^2 = 0.29$ ). Since litter identity had a contributed significantly to overall variability, it is not surprising that animal identity also had a significant contribution. To tease apart contribution of animal identity and litter identity, we normalized the synapse density measured by the litter mean (Fig. 2.5 B). This was done individually across all layers. This normalization resulted in a modest reduction of the CV of synapse density across all layers (compare Fig, 2.5 C with Fig. 2.2 D) suggesting a reduction in overall variability. Following this normalization procedure, we observed that litter identity no longer explained any of the remaining variability (Fig.2.5 D, right). Interestingly, animal identity still contributed significantly to the residual variability. This suggests that animal-to-animal variability was not merely due to litter based differences and that there exists substantial variability even among littermates.

## **Within-animal normalization of mean synapse density is most effective in reducing observed variability**

In order to address this animal-to-animal variability, we carried out within-animal normalization of synapse density. We tried normalizing all the layer-specific density measurements in any given animal to the synapse density for a particular layer. The aim was to choose a normalizing factor that would represent the underlying cause for the variability observed across animals. We hypothesized that slight differences in sensory experiences in the home cage between animals might give rise to this animal-to-animal variability in synapse density.

It has been shown that layer 4 synapses undergo changes in response to altered sensory experiences at an early age (PND 7-8) and then stabilize by the age of PND 14, the age at which we carried out this study. We hypothesized that the synapse density in layer 4 would be most representative of the state of the cortical circuit of an animal given its sensory experiences since birth. Thus, normalizing to synapse densities of layer 4 should abolish animal-to-animal variability arising due to differential sensory experiences the individual animals have had during their lifetime. On the other hand, inhomogeneities between barrel centers and periphery in cell soma distribution could lead to differences in synapse densities measured across animals. Thus, we also tested normalization to L1 synapse density measurements as this layer is expected to be more homogeneous in its distribution of synapses. Synapses in layers 2 and 3 are amenable to changes in response to sensory experiences in the timeframe of PND 12-14. Thus, we reasoned that, synapse densities in these layers are more representative of the current state of the cortical circuit in a given animal. Thus, we also tested the effect of normalizing to synapse densities in layers 2 and 3.

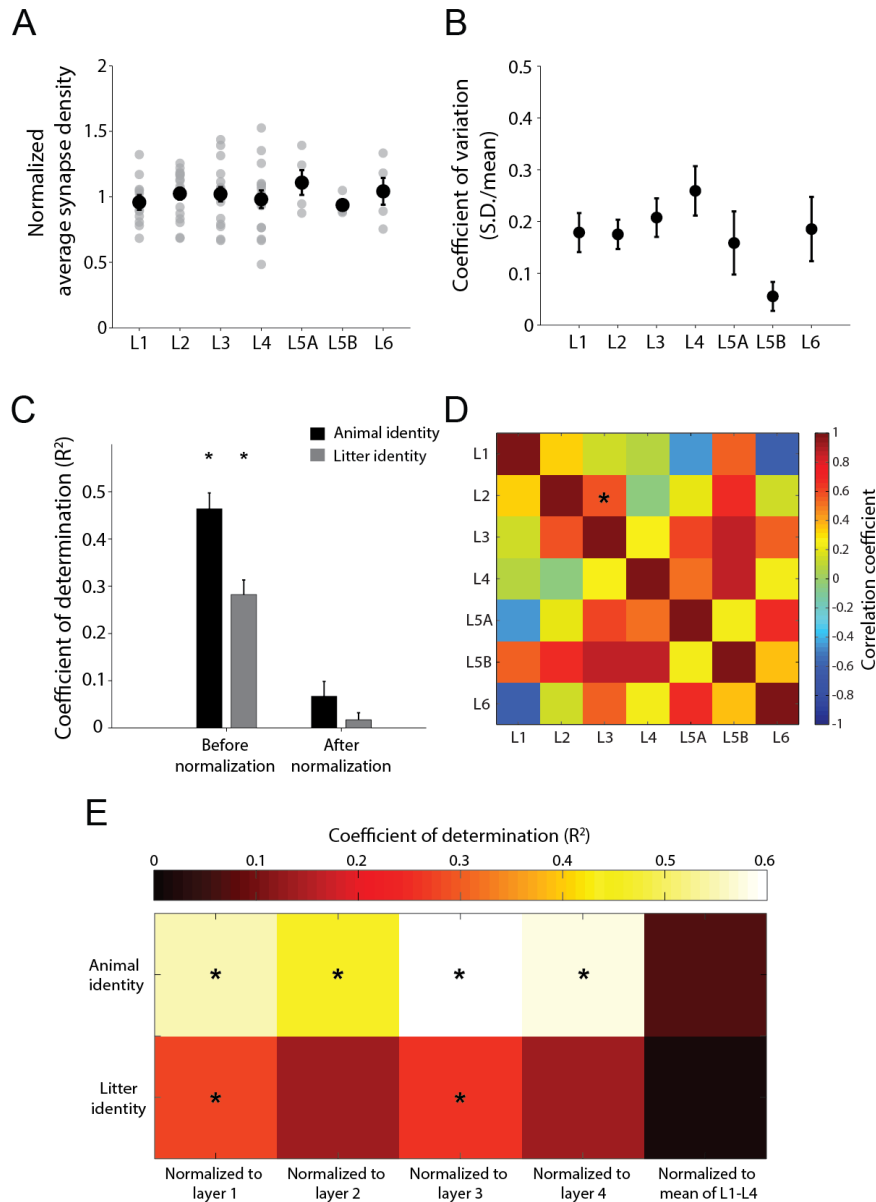


**Figure 2.6 Within-animal normalization is most effective in reducing inter-animal variability**

- A. Scatter plot showing variability in synapse density measurements following normalizing to the mean synapse density determined across L1 through 4 for each animal.
- B. CV of synapse density following this normalization. Error bars indicate SD.
- C. Plot shows the coefficient of determination ( $R^2$ ) for animal and litter identity before and after normalization. After normalizing to mean of L1-4, neither animal identity nor litter identity contribute to the residual variability (animal identity, mean  $R^2 = 0.07$ ; litter identity, mean  $R^2 = 0.02$ ). \* indicates  $p < 0.05$  for linear regression fit for that parameter. Error bars indicate SD.
- D. Correlation coefficient for all pairs of layers shows little correlation in synapse density between layers.
- E.  $R^2$  for animal and litter identity following each normalization procedure. \* indicates  $p < 0.05$  for linear regression fit for that parameter.

In all of these cases, animal identity continued to significantly explain the residual variability (Fig. 2.6 E). This suggests that there is no trend in mean synapse density measurements that transcended layers. That is, if an animal has high synaptic density in, say, layer 2, it does not necessarily suggest the synaptic density in layer 4 will also be similarly high. In other words, correlation of synapse density across cortical layers is very low (Fig. 2.6 D). Finally, we chose the mean synapse density across layers 1 through 4 as the normalizing factor. Normalizing all the layer-specific density measurements in any given animal by the mean synapse density determined across L1 through L4 removes the animal-to-animal variability, as signified by the low  $R^2$  value (Fig. 2.6 A-C).

### **Conventional EM images underestimate synapse density counts**

The next question we wanted to answer was whether the efficiency of the EPTA staining of synapses itself was variable across samples. Previous studies using conventional EM approaches to stain and detect synapses that matched our study closely in the ages of the animals used, report a CV of 0.2-0.3 (Micheva and Beaulieu, 1996; DeFelipe et al., 1999b), which is in line with the CV we observed in our EPTA synapse density measurements. But, other EM studies have reported substantially lower variability; a CV of around 0.05. To rule out the effect of technical differences among these studies, like experimental design, criteria for detecting synapses, we carried out our own synapse density measurements on samples prepared by the conventional EM approach. For this, out of all the tissue used for EPTA staining, we chose tissue from five animals for preparation using the conventional EM approach of uranyl acetate and lead citrate staining (Fig. 2.7 A). The five animals were chosen such that they represented the spread of the data, that is, they included animals that exhibited high, low and medium level of synapse

density. Following this, we manually labeled synapses in the conventional EM images (Fig. 2.7 B and C) and the resultant synapse density numbers were compared against the automated counts from the animal-matched EPTA-stained samples (Fig 2.7 E and F). Surprisingly, we found that we consistently underestimated the synapse density by using conventional EM images as compared to the EPTA-stained images (Fig 2.8 A) in all the cortical layers we imaged. This suggests that given the higher background in conventional EM images, the manual labeling might be missing some synapses.

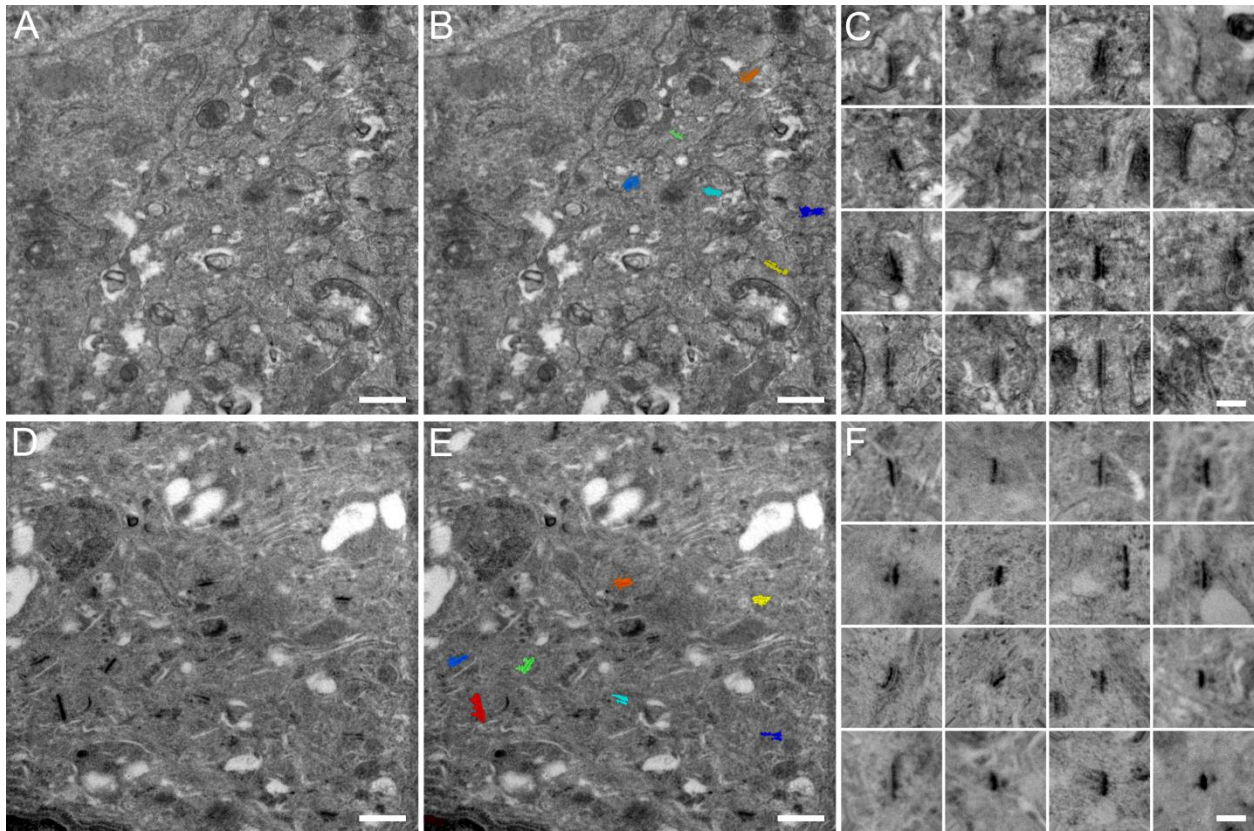


**Figure 2.7: Example images of synapses if tissue was exposed to conventional EM or EPTA staining.**

- A. An example TEM image after osmification and uranyl acetate staining. Scale bar – 500nm
- B. Same image as in A. Synapses manually labelled are colored. Scale bar – 500nm
- C. A few example synapses detected from conventional EM images. Scale bar – 200nm
- D. An example image after EPTA staining. Scale bar – 500nm
- E. Same image as in A. Synapses detected by the algorithm are colored. Scale bar – 500nm
- F. A few example EPTA-stained synapses. Scale bar – 200nm

## **Conventional EM images show more intra-animal variability than images of EPTA-stained tissue**

Here, we imaged a single 100nm thick slice per animal in order to estimate the synapse density. Although we determined that we acquired a large enough dataset (around 100 images per cortical layer) to reliably estimate the synapse density in any given slice, we cannot say that this dataset accounted for inhomogeneities in the tissue and/or staining across the thickness of the slice. Thus, we asked the question – Do we see consistent synapse density measurements throughout the thickness of the tissue by both EPTA and conventional EM approaches? To answer this question, we proceeded to image an additional 100nm slice from the same tissue that was used previously. Synapses reach a maximum length of around 1.5 $\mu$ m. Thus, to avoid repeated counting of any synapse that might appear in both slices, we ensured that the new slice and the previously imaged slice were separated by at least 4-5 $\mu$ m. Following this, we compared the numbers obtained from these two slices that originated from the same 50 $\mu$ m coronal slice from a given animal. We observed that in conventional EM images, there was substantial variability between the two slices from the same animal. This within-animal variability was similar in magnitude to the inter-animal variability as suggested by the low correlation coefficient ( $r = 0.06$ ; Fig. 2.8 B). On the other hand, within-animal variability was much smaller in EPTA-stained images than inter-animal variability (Fig. 2.8 C). To quantify the within- and inter- animal variability, we computed the mean absolute differences. All pairwise differences were computed among the density measurements from either the within- or inter-animal cohorts. We found that EPTA-stained images show substantially lower within-animal variability than conventional EM images. Also, within-animal variability in EPTA stained images is lower than inter-animal variability. On the other hand, conventional EM images have a similar level of within-and inter-animal variability.

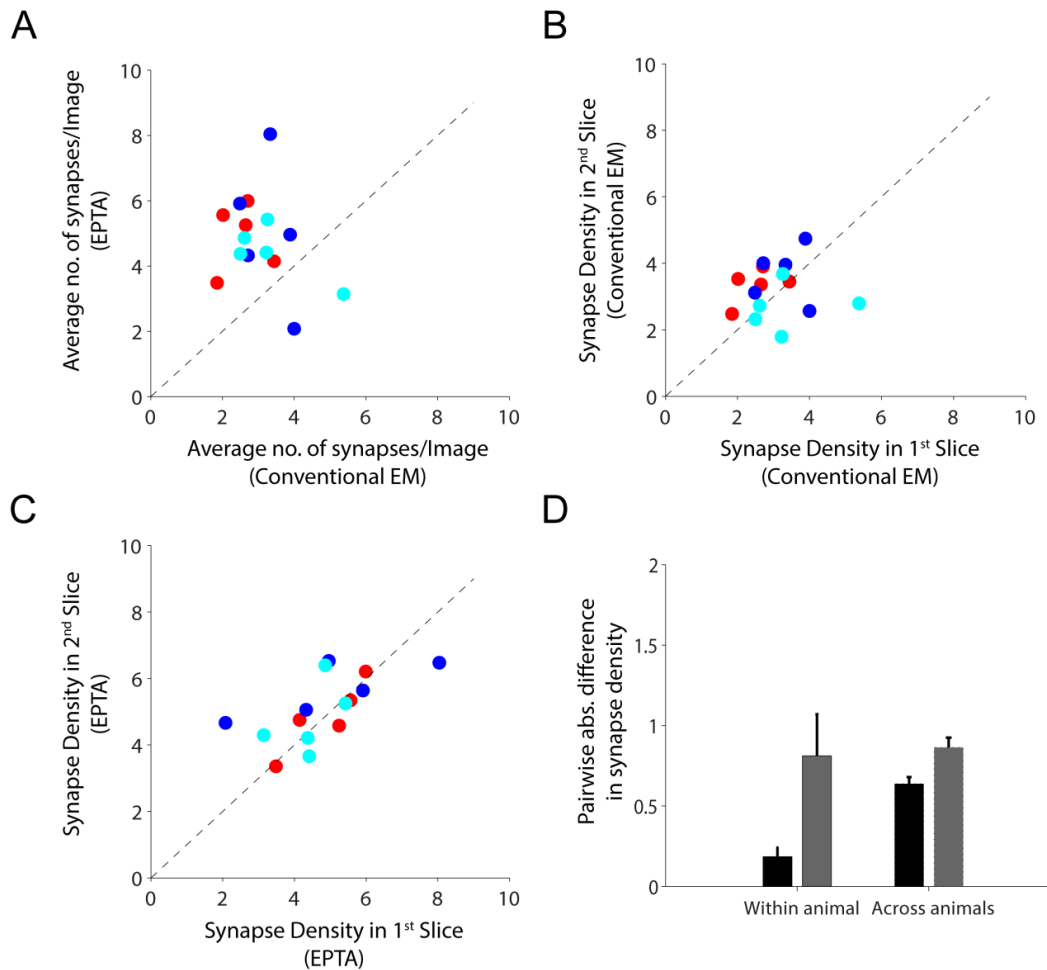


**Figure 2.8: Conventional EM images underestimate synapse density and also show higher within-animal variability.**

- A. Synapse density measurements obtained from EPTA images as compared to conventional EM images for layers 2 (red), 3 (blue) and 4 (cyan) from the same 5 animals. Pearson's correlation coefficient ( $r$ ) = -0.33; n.s.
- B. Scatter plot showing variability in synaptic density calculated in 2 slices obtained from the same animal (4-5  $\mu\text{m}$  apart) for conventional EM images. Dots represent data from 5 animals for layers 2 (red), 3 (blue) and 4 (cyan) from the same 5 animals.  $r = 0.06$ ; n.s.
- C. Scatter plot showing variability in synaptic density estimated in 2 slices obtained from the same animal (4-5  $\mu\text{m}$  apart) for EPTA images. Dots represent data from 5 animals for layers 2 (red), 3 (blue) and 4 (cyan) from the same 5 animals.  $r = 0.64$ ; n.s.
- D. Within-animal variability is estimated from the magnitude of the difference in synapse density obtained in the 2 slices from the same animal. Mean of absolute values of all possible pairwise differences of synapse density obtained from different animals estimates the across-animal variability. Bars show mean values for EPTA (black) and conventional EM images (grey) for cortical layer 2. Error bars represent SEM.

### **EPTA images potentially detect smaller synapses more effectively**

Given that conventional EM images consistently exhibited lower synapse density as compared to EPTA-stained images, we hypothesized that manual labeling in conventional EM images was systematically missing a subset of synapses. Since it is difficult to identify morphological features of a synapse when it is of a smaller size, the higher background in the conventional EM images could preferentially lead to the missing of smaller synapses.

To test this hypothesis, we compared the lengths of synapses reported by these two procedures. We found that conventional EM images reported a significant higher mean length of synapses as compared to EPTA synapses in all layers that were imaged ( $p < 0.05$ , one-way ANOVA and post-hoc t-test with Bonferroni correction; Fig. 2.9 C). This suggests that smaller synapses are under-represented among the synapses manually detected in conventional EM images. We confirmed this by looking at the cumulative histogram distributions of synapse lengths. The cumulative distribution curves provide an estimate about the composition of the synapse population. For a population of synapses which have a higher proportion of smaller synapses, the curve would rise faster and be limited to the left half of the graph. On the other hand, for population with higher proportion of longer synapses, the curve would rise much slower and exhibit a rightward shift in the graph. In support of our hypothesis, we observed that the cumulative distribution curves for conventional EM images were significantly shifted towards the right ( $p < < 0.01$ , K-S test; Fig. 2.9 D, E and F) suggesting that this population of synapses had a lower proportion of smaller synapses.

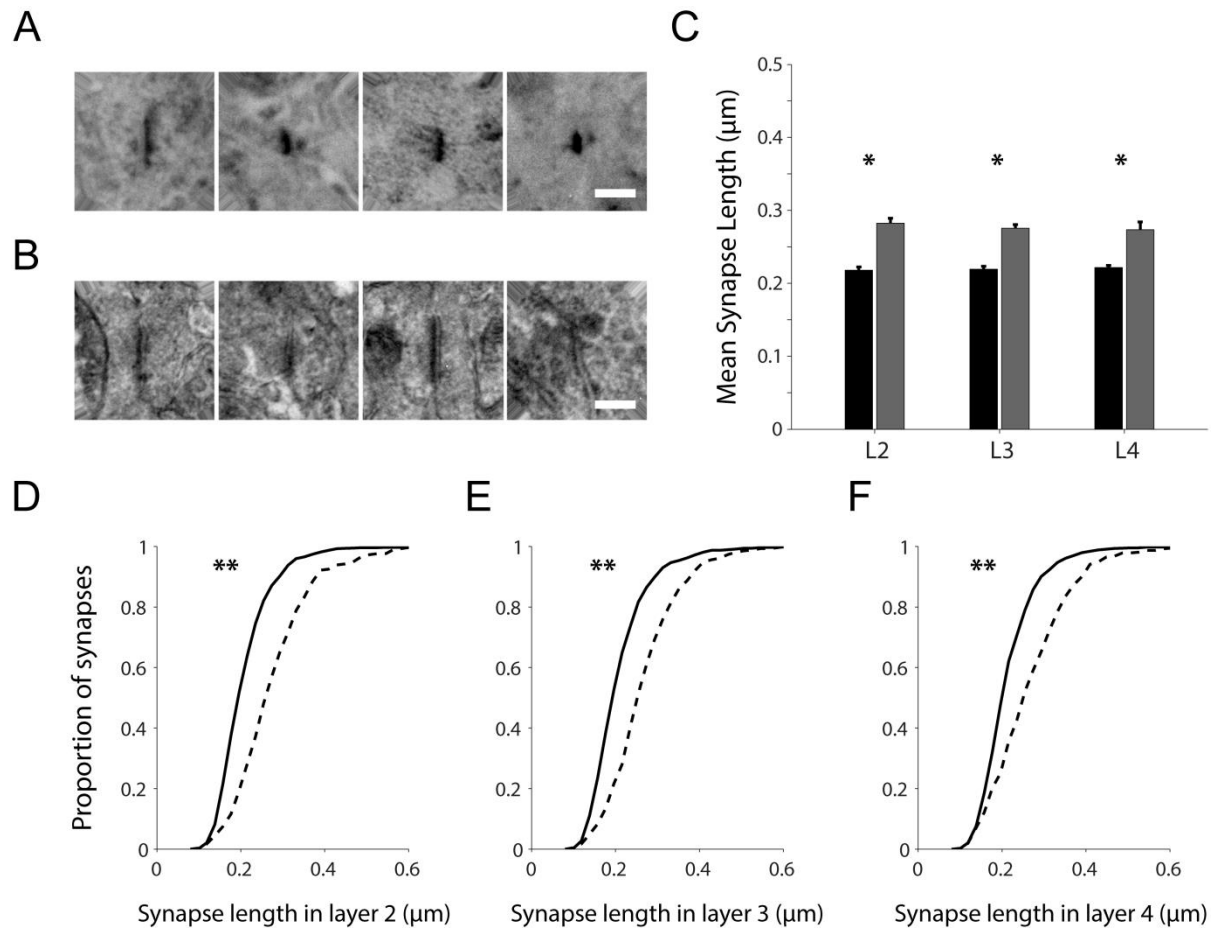


**Figure 2.9: Synapse detection in EPTA images makes detection of smaller synapses more efficient.**

A. Example images of synapses stained by EPTA. Scale bar – 200nm.

B. Example images of synapses after conventional EM procedures. Scale bar – 200nm.

C. Mean synapse length of synapses detected in EPTA (black) and conventional EM images (grey). Error bars represent SEM. \* $p < 0.05$ , one-way ANOVA and post-hoc t-test

D., E. and F. Cumulative histograms of synapse size in cortical layers 2, 3 and 4 respectively for synapses detected in EPTA images (solid line) and conventional EM images (dotted line).\*\* $p < < 0.01$ , Kolmogorov-Smirnov test

## 2.4 Discussion

In this study, we employed EPTA staining to selectively highlight synapses in TEM images and subsequently used a machine-learning algorithm to identify these synapses in an automated fashion. The synapse density measurements obtained from an anatomically distinct region of the mouse somatosensory cortex showed substantial inter-animal variability. Firstly, we established that the synapse density measurements obtained by the automated synapse detection algorithm matched those obtained with manual identification of synapses. We also systematically established that our synapse density measurements were obtained from a large enough collection of images that ensured adequate sampling of the tissue. Moreover, we showed that the contrast between the stained synapses and the background tissue, which could vary across samples, did not determine the number of synapses detected in a given sample.

Subsequently, we determined that although there was a variation across different batches of tissue, normalization to the mean synapse density obtained for each batch of tissue did not account for all the variability observed. Only within-animal normalization accounted for all the variability observed in synapse density measurements.

Finally, to establish that the inter-animal differences in synapse density were not due to variability in EPTA staining efficiency, we used conventional EM to measure synapse density from a subset of animals. We observed that, conventional EM consistently provided lower estimates of synapse density than EPTA. Also, within an animal, repeated measurements of synapse density from two different tissue sections yielded more consistent results for EPTA images than conventional EM. On the other hand, conventional EM images showed lower synapse density variability across animals. Comparing the population of synapses detected in

EPTA and conventional EM images, we observed that synapses detected from conventional EM images were enriched with longer synapses.

Taken together, these observations suggest that our technique of automated detection of EPTA stained synapses provided a highly reliable estimate of synapse density for a given tissue and that the inter-animal variability is most likely due to an underlying biological factor rather than an artifact introduced by the technique.

### **High-throughput technique enabled generation of dataset of a robust size**

Previous studies characterizing synaptic changes, especially utilizing EM, have been limited to a handful of animals. This is due to the fact that synapse detection and characterization is time-consuming process. The automated nature of our technique enabled us to estimate synaptic properties in tissue obtained from >6 animals for each cortical layer while other studies were restricted to 2 or 3 animals per group. Consequently, the synaptic properties are much more robustly characterized.

### **Comparing level of sampling with previous studies**

Previous attempts to determine the minimum number of electron micrographs required for adequate sampling have arrived at numbers ranging from 10 to 15 non-contiguous micrographs (Granger et al., 1995; DeFelipe et al., 1999b). It should be pointed out that, in those studies, each micrograph sampled an area of  $\sim 35\mu\text{m}^2$  while the images we obtained sampled an area of  $\sim 18\mu\text{m}^2$ . Thus, while these studies reported requiring only half as many images as our study, their individual images sampled twice as much area as the images in the current work. Collectively, similar amounts of the tissue required to be imaged to obtain a reliable estimate of the underlying synapse density. Combined with the fact that the algorithm closely matched human performance

in reporting synapse density, we believe that we were accurately estimating the underlying synapse density for a given cortical layer, at least in the slice being imaged.

### **Possible biological factors responsible for inter-animal variability**

It was interesting to note that supragranular layers exhibited a higher CV, and thus, more variability than infragranular layers. We used animals that were 14 days old (PND 14). It has been well-documented by previous studies that at this time point major synaptic changes can occur in response to sensory experience in the supragranular layers (Clem et al., 2008; Wen and Barth, 2011). We cannot control for small differences in experience that may exist even among littermates, like litter size that can affect growth (Rodel et al., 2008) and brain development (Dobbing, 1964; Rocha-de-Melo et al., 2006), or that nature of maternal care that affects synaptogenesis (Liu et al., 2000). Combined with the fact that our recording of a birth of a litter can be off by at least a day, it is plausible that we have animals that are at slightly different stages of development. This might be the major underlying source of the observed variability.

It has been shown that human males show higher synaptic density than females (Alonso-Nanclares et al., 2008). Thus, the sex of the animal is another potential source of variability. But, the lack of a bimodal distribution in our synapse density measurements suggests that the gender of the animal does not contribute significantly to the spread of the data.

Among the parameters that we thought were best candidates as sources of variability, only animal identity showed a significant contribution. This existed even when the data were controlled for litter identity. This further corroborates the hypothesis that the variability might be due to slight variations in development among animals.

It was surprising to note that normalizing to any single cortical layer did not abolish animal-to-animal variability. This suggests that there is very little correlation in synapse density across cortical layers. It would be interesting if this can be perturbed by either developmental processes, learning paradigm or altered sensory experience.

### **Animal-to-animal variability in other neural circuits**

*Caenorhabditis elegans*, a nematode containing 302 neurons, is the only organism for which the connectivity map of its nervous system has been mapped in its entirety (White J. G. et al., 1986). With such a stereotypical nervous system that is highly conserved between animals, it has been observed to exhibit some variations in its connectivity. One of the most comprehensive comparisons of the *C.elegans* neuronal connectivity map showed that only 75% of all connected pairs of neurons were connected reproducibly across animals (Durbin, 1987). Moreover, the reproducibility of the synapses between a pair of neurons depended upon the number of synapses between the given pair. That is, a pair of neurons that were connected by only 1 or 2 synapses tended to exhibit more variability between individual animals and vice versa.

The pyloric circuit of the stomatogastric ganglion (STG) of the crab *Cancer borealis* has approximately 26 neurons that are unambiguously identifiable. The circuit generates motor rhythms that control the contractions of the pylorus, part of the crab's stomach. Each (STG) has two PD neurons, 1 LP neuron, 1 DG neuron and 4 GM neurons. These neurons show considerable animal-to-animal variability in their basic electrophysiological properties (Grashow et al., 2010). Since each of these identified neuron types have a specific function, such variability could affect the functional output of the STG circuit. But, by modulating the various ion channel conductances and the strength of synaptic connections, these neurons can tune themselves such

that the circuit achieves the appropriate rhythmic behavior (Prinz et al., 2004; Goaillard et al., 2009; Grashow et al., 2010).

Thus, even simple neuronal circuits exhibit substantial amount of animal-to-animal variability in its connectivity and functioning.

### **Comparing conventional EM and EPTA**

Finally, we compared the procedure of EPTA-staining of synapses against conventional EM approaches in estimating the synapse density. It was incredibly surprising that the conventional EM images resulted in consistently lower synapse density estimates. A scan through previous work revealed that a similar comparison done for synapse density measurements for the macaque frontal cortex. EPTA staining (Uemura, 1980) resulted in synapse counts that were 40-60% higher than conventional EM approaches (Peters et al., 2008). This was similar to the level of difference we observed in our comparisons of the two approaches. We hypothesized that the high background in conventional EM images made it difficult synapses, especially the smaller synapses. Comparing the mean synapse length and the synapse length distributions between the two approaches confirmed this hypothesis. Smaller synapses were apparently being missed by conventional EM images. But, we cannot rule out the scenario that the small-sized structures detected from the EPTA images are not synapses to begin with. To exclude this, we will have to carry out immunoEM experiments where we immunohistochemically label synaptic structures that can then be identified in EPTA-stained images (Hildebrandt et al., 2011).

Another surprising observation we made was that EPTA-stained images generated remarkably consistent counts for any given animal even though the inter-animal variability was

quite high. On the other hand, conventional EM images generated similar amount of variability in both intra- and inter-animal synapse density counts. Given our current hypothesis that conventional EM images are missing smaller synapses, the high inter-animal variability among EPTA-stained images might be due to these subset of synapses. This will be answered by carefully dissecting out the variability in synapse numbers across animals by synapse-size.

Combining all the results reported here, we can conclude that EPTA-stained images produce remarkably low intra-animal variability in estimating synapse density; animal identity is the best candidate that explains most of the observed variability, and that the algorithm for automated detection of synapses performs as well as human experts. This also suggests that the variability observed is representative of true animal-to-animal variability and that is indeed a biological phenomenon.

# Chapter 3

## Layer-specific changes in synaptic density and lengths following altered whisker experience

### 3.1 Introduction

The collective body of work involved in characterizing experience-dependent plasticity in the barrel cortex has been essentially piecemeal in nature with each study focusing on a specific set of synapses, say L4-L2/3 (Bender et al., 2006; Clem and Barth, 2006; Wen and Barth, 2011) or a specific set of dendritic spines, say, those on the apical dendrites of L5 (Trachtenberg et al., 2002; Holtmaat A. et al., 2006) or L2/3 neurons (Lendvai et al., 2000; Kuhlman et al., 2014). But, the differences among these studies in experimental design, like the age of the animals studied, the nature of the sensory manipulation, and the length of sensory manipulation prevents researchers from obtaining a holistic picture about the synaptic changes occurring in different parts of the circuit in response to the same sensory manipulation.

We were interested in characterizing the synaptic changes that could be happening throughout the neuronal circuit present in cortical column in response to the same sensory

manipulation. Our lab has used a single whisker/row preparation, wherein all the whiskers from the both sides of the snout are removed except the 'D1' or 'D' row of whiskers, effectively to uncover rapid experience dependent plasticity in L2/3 synapses during development. We coupled this sensory manipulation with our unbiased and high-throughput technique to characterize synaptic properties to capture the experience-dependent synaptic plasticity that could be occurring throughout the cortical column.

Extensive work from our lab has established that L4-L2/3 synapses can undergo rapid experience-dependent potentiation (Clem and Barth, 2006; Clem et al., 2008; Wen and Barth, 2011) during the ages PND 12-14. It was established that this strengthening involves postsynaptic NMDAR-dependent AMPAR trafficking to the synapses (Bender et al., 2006; Clem and Barth, 2006) resulting in increased activity in L2/3 neurons (Glazewski et al., 2007; Benedetti et al., 2009). However, it is unclear if this strengthening of L4-L2/3 synapses is the only synaptic change occurring in the entire cortical column following 24h SRE at this age, or even if strengthening of existing synapses is the only change occurring in L2/3. Other studies have shown that sensory deprivation can lead to loss of synapses in L2/3 neurons (Lendvai et al., 2000; Cheetham et al., 2007; Bruno et al., 2009), sparing of a pair of whiskers (Diamond et al., 1994) or two adjacent rows of whiskers, results in the decreased spread of activity into the deprived barrel columns following spared whisker stimulation (Wallace D. J. and Sakmann, 2008) and decrease in axonal arborization of L2/3 inputs from the non-deprived to the deprived column (Broser et al., 2008; Bruno et al., 2009). But, this contradicts the observation that there was increased spread of activity following spared whisker stimulation into deprived columns during single whisker sparing (Glazewski and Fox, 1996). Thus, the experience-dependent map plasticity observed is highly dependent on the whisker trimming paradigm employed.

Similar studies looking at the plasticity of L2/3-L5 synapses, revealed target cell-type specific changes. Single-row whisker deprivation starting at PND 30, weakened the synapses made by L2/3 axons onto L5B regular spiking (RS) cells in the deprived whisker barrel column while those onto L5B intrinsic bursting (IB) cells remain unchanged (Jacob et al., 2012). Due to use of different altered sensory experience paradigms, it is unknown whether L2/3-L5 synapses undergo similar changes at the earlier developmental time point as when the TC-L4, L4-L2/3 and L2/3-L2/3 synaptic changes were studied. Moreover, these synaptic pathways have a specific window in the developmental time period, termed “critical period” wherein they are capable of rapid and extensive experience-dependent synaptic plasticity. But, it is unknown whether other synaptic pathways like L2/3-L5 or those targeting L6 also exhibit such a critical period.

Inhibitory synapses also undergo experience-dependent modification (Gaiarsa et al., 2002). Inhibitory synapse density increased in L4 upon persistent whisker stimulation (Knott et al., 2002) and decreased upon whisker deprivation (Micheva and Beaulieu, 1995), including a critical period during which they exhibit heightened plasticity (Jiao et al., 2006). Inhibitory inputs to L2/3 pyramidal neurons exhibit a source layer-specific change following altered sensory experience in adult animals (Katzel and Miesenbock, 2014). In fact, it has been shown that inhibitory plasticity is necessary for the onset of experience-dependent plasticity of excitatory synapses (Chen J. L. et al., 2012; Gambino and Holtmaat, 2012; van Versendaal et al., 2012).

Thus, to characterize the synaptic changes occurring in the entire cortical column, we automated synapse detection and characterization following 24hr SRE in P14 mice.

## 3.2 Methods

**Whisker experience and animal preparation:** Litters of wildtype C57bl6 (Harlan) mice aged PND 13 were divided into two groups, namely the control group and the single row experience (SRE) group. For the SRE group, all the whiskers were plucked gently from the snout of the animal except the 'D' row on the right side. At postnatal day (PND) 14, the animals were euthanized, their brains dissected out and drop-fixed in 2.5% Glutaraldehyde (Electron Microscopy Sciences; EMS) in 0.1M Phosphate Buffer. After 24h of glutaraldehyde fixations, brains were transferred to 30% sucrose solution. The brains were kept in this solution until they were sectioned.

**Tissue preparation:** Brains stored in 30% sucrose solution were cut at 45° to the midline (Fig. 2.1A) and mounted on the cryostat (Finnerty et al., 1999). 50µm-thick sections were cut and stored in 0.1M phosphate buffer. The presence of barrels was verified by mitochondrial (cytochrome oxidase) staining. The slices in which the 'D' barrel could be identified unambiguously (Fig. 2.1 B) were selected for dissecting out the column (Fig. 2.1 C).

**Electron Microscopy tissue preparation:** Tissue was prepared for transmission electron microscopy (TEM, Hitachi H7100) in a series of steps.

For EPTA staining of synapses, the 50µm thick slice, chosen in the previous step, was washed with three changes (5 minutes each) of distilled water, followed by incubation in 0.02% NaOH for 10 minutes. Second, the tissue was dehydrated with an ascending series of EtOH (25%, 50%, 70%, 80%, 90%, and 100%), followed by fixation with 1% phosphotungstic acid (PTA) (Ladd) in 100% EtOH. Third, a small amount, 7µl, of 95% ethanol, was added to each 1000µl of PTA stain used, and the PTA was washed from the sample with two changes of 100%

ethanol. Fourth, propylene oxide (PO) (EMS) was used as a transitional solvent (the first change of PO was on ice), and then the specimen was infiltrated with Spurr (Ted Pella) embedding resin, which was polymerized at 60° C for 48h. Finally, 100nm sections were cut using a diamond knife (Delaware Diamond Knife) on an Ultracut-E ultramicrotome (Riechert-Jung), and were picked up using single slot copper grids (EMS).

For conventional EM imaging, the 50µm thick slice was initially exposed to osmium tetroxide (OsO<sub>4</sub>) and lead citrate. Then, the tissue was taken through same procedure as described above with the exception of the exposure to EPTA.

**Tissue shrinkage:** We found that, there was substantial amount of shrinkage of the tissue after it was cut from the resin block and mounted onto the copper grid for imaging. The amount of shrinkage was determined by comparing the separation between fiduciary landmarks, namely the pia and an angular cut manually made underneath layer 6, under the TEM versus when the tissue is in the resin. Once cut and mounted, the sections measured only 70-80% of their length as when embedded in the resin. This was remarkably consistent across all our samples. Subsequently, we adjusted the previously reported depths of each layer as measured from the pia (Lefort et al., 2009) with the shrinkage factor we determined.

**Image Acquisition:** The specimen was observed using a TEM and images were taken digitally using a Kodak Megaplug 1.6i camera. The electron beam was scanned across each cortical layer parallel to the pial surface and images were obtained in a continuous fashion (Fig. 2.1 C). The electron beam was positioned for each image such that there was no overlap between images of adjacent areas of the cortex. In order to ensure that the images were indeed obtained from the designated cortical layer, the acquisition of images was done at the following depths, as measured from the pia, for the respective cortical layers, L1 - 50µm, L2 - 125µm, L3 - 325µm,

L4 - 500 $\mu\text{m}$ , L5A - 600 $\mu\text{m}$ , L5B - 725 $\mu\text{m}$  and L6 - 900 $\mu\text{m}$ . Depending upon the shrinkage determined for each individual tissue section, these depths were adjusted accordingly. We obtained about 100 images (an example image from layer 2 is shown in Fig. 2.1 D) per cortical layer with each image capturing 4.31 $\mu\text{m}$  X 4.31 $\mu\text{m}$  region of the cortex.

**Image Analysis:** The analysis of all the images was carried out using custom-written software in MATLAB. Firstly, the contrast of each image was enhanced and then subsequently, each image was binarized based on a manually determined threshold. Following this, connected segments were computed in each image and were filtered based on their size (min. area - 5.5 X 10<sup>3</sup> nm<sup>2</sup> and max. area - 66 X 10<sup>3</sup> nm<sup>2</sup>). Each connected segment and its surrounding area as bounded by a square patch of side 125 pixels (~500nm) is used for subsequent classification. A machine learning algorithm that employs support vector machines (SVM) was used to classify the connected segments as synapses based on texture- and shape-based features (Navlakha et al., 2013). The classifier was first trained using 1,665 positive (synapses; Fig. 2.1 E) and 10,441 negative (non-synapses) examples. In order to provide a quantitative estimate for sample variability, a testing dataset that included both synapses as well as non-synapses was generated from 10% of images for each layer in each animal. All synapses within this image subset were identified manually. The performance of the classifier was evaluated on the testing image set. A classification threshold of 50% correct recall (where exactly 50% of manually-identified synapses were labeled correctly by the classifier) was chosen for the subsequent analysis of all images obtained for that particular layer in a given animal. In cases where the classifier performed at very high levels (correctly identifying 95% of synapses), we found an unacceptably high level of false positives, i.e., objects that were not synapses; thus, a threshold of 50% recall

was established to compromise between accurate detection of synapses without inaccurate classification of non-synapses.

For synapse density, we scaled the measured density by the precision that the classifier exhibited at 50% recall. For all other measurements, we used only samples that had >75% precision. The lengths of synapses were obtained when the connected segments were calculated for each image.

**Linear regression analysis:** Linear regression models of the form,  $Y = \beta_0 + \beta_1 X_1 + \beta_2 X_2 + \beta_3 (X_1 * X_2)$ , where Y represented the synapse density measurements,  $X_1$  represented the cortical layers ( $X_1 = 1$  through 7 for layers 1, 2, 3, 4, 5A, 5B and 6 respectively) and  $X_2$  represented the state of whisker experience with control animals signified by  $X_2 = 0$ , and spared whisker animals signified by  $X_2 = 1$  were fitted to the data to determine whether the term  $(X_1 * X_2)$ , which signified interaction between layers and the nature of sensory experience, contributed to the significantly.

### 3.3 Results

#### 24hr SRE gives rise to layer-specific changes in synapse density

We subjected C57 mice aged PND 13 to bilateral whisker deprivation, except the ‘D’ row on the right side. Littermates of whisker-deprived mice were subjected to sham-deprivation and used as control animals. Mice remained in their home cage for 24h after whisker deprivation after which they were euthanized and their brain fixed in 2.5% glutaraldehyde (Fig. 3.1 A). We dissected out the ‘D’ barrel column and estimated synaptic properties from about 100 TEM images obtained from each cortical layer. No gross differences in the morphology of synapses were observed between control and the experimental group of animals (Fig. 3.1 B and D).

We first characterized the changes in synapse density that occurred in response to the altered sensory experience. We found that there was a layer-specific change in synapse density after 24h SRE. While layers 2 and 3 showed a slight increase of around 20% and 10% respectively, layer 6 showed a strong decrease in synapse density of around 35% as compared to control animals (Fig. 3.1 C). It is worth pointing out that the synapse density measurements took into consideration all of the synapses that were localized in any given layer, and did not differentiate based on the source or target cell type. For example, the synaptic population found in L3 comprises of L4-L3 synapses (Feldmeyer et al., 2002), within-column (Feldmeyer et al., 2006) and inter-column L3-L3 synapses and synapses that are made onto L5 apical dendrites that pass through L3 (Markram et al., 1997; Petreanu et al., 2009). Thus, if the experience-dependent changes in synaptic density were restricted to only a particular population of synapses, our synapse density measurements would be underestimating the magnitude of the change.

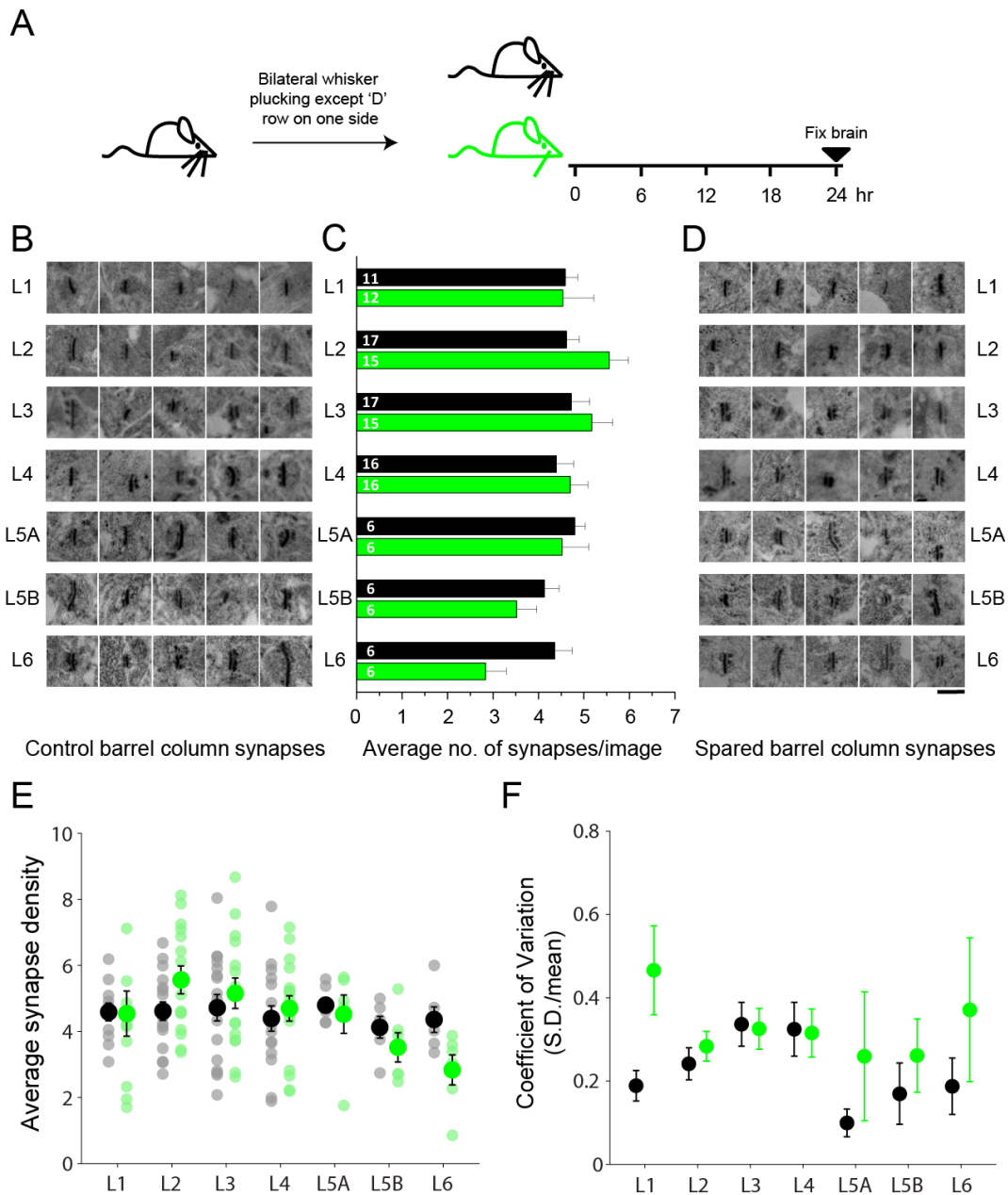


**Fig. 3.1 Layer-specific changes in synapse density**

- A. Schematic showing the experimental paradigm and timeline of altered sensory experience
- B. Example images of synapses from each cortical layer from control barrel column
- C. Average synapse density measured in control (black) and spared (green) barrel columns. Numbers indicate number of animals, Error bars indicate SEM.
- D. Example images of synapses from each cortical layer from spared barrel column. Scale bar – 200nm.
- E. Scatter plot showing distribution of average synapse densities measured in each individual animal
- F. C.V. of average synapse densities in each cortical layer from control and spared barrel columns.

There was substantial amount of inter-animal variability in both control animals and those that underwent altered whisker experience (Fig. 3.1 E). Quantifying the CV for the two groups, we observed that, in certain cortical layers, animals with the spared whisker tended to exhibit higher variability than control animals (Fig. 3.1 F). The CV for synapse density in spared whisker animals in infragranular layers, L5A, L5B and L6 ranged from 0.25 to 0.4 while those for control animals ranged from 0.1 to 0.2. This amount of variation in synapse density measurement between animals, did not allow the 20-30% differences in synapse density in L2 and L6 to reach statistical significance.

### **Global distribution of synapses across the cortical layers undergoes change following 24h SRE**

While small apparent differences in synapse density in individual layers may not reach statistical significance, it is the sum total of changes across the entire circuit that would enable the system to process the new stimulus appropriately. To determine whether the control and spared whisker barrel columns differ in this manner, we used linear regression to test if the global distribution of synapses across the cortical layers was different after 24h SRE.

Firstly, we had to address the inter-animal variability. To be able to compare between control and spared whisker animals, any normalization procedure used would have to be identical to both groups. Our experimental design was such that each litter was divided into control and spared whisker animals and cortical tissue from animals belonging to a single litter were processed together as a single batch. Thus, we reasoned that, normalization to a within-litter parameter would address any batch-to-batch variation in tissue processing and also litter-to-

litter variation that may exist due to differences in developmental or sensory experience in the home cage (Fig 3.2 A). It has been well established that synapses in L4 do not exhibit experience-dependent plasticity at the developmental time point we had chosen for this study, namely PND 13 (Glazewski and Fox, 1996). Thus, synapse density in layer 4 would be most representative of the state of the cortical circuit of an animal given its sensory experiences since birth and normalizing to synapse densities of layer 4 should abolish animal-to-animal variability arising due to differential sensory experiences the individual animals have had during their lifetime. Thus, we calculated the mean synapse density in L4 for the control animals from each litter and used that to normalize synapse densities in all layers for all the animals belonging to the corresponding litter.

Next, we fitted the linear regression model,  $Y = \beta_0 + \beta_1 X_1 + \beta_2 X_2 + \beta_3 (X_1 * X_2)$ , where  $Y$  represented the synapse density measurements,  $X_1$  represented the cortical layers ( $X_1 = 1$  through 7 for layers 1, 2, 3, 4, 5A, 5B and 6 respectively) and  $X_2$  represented the state of whisker experience with control animals signified by  $X_2 = 0$ , and spared whisker animals signified by  $X_2 = 1$ . The term  $(X_1 * X_2)$  signified interaction between layers and the nature of sensory experience. If 24h SRE significantly shifted the global distribution of synapses across the layers, then the addition of the interaction term to the above model would significantly improve the amount of variability explained by the model. The adjusted  $R^2$  parameter of a linear regression model shows an increase upon the addition of an extra term to the model only if the addition leads to a significant increase in the amount of variability explained. To determine the adj.  $R^2$  value in a rigorous fashion, we carried out a bootstrapping procedure, wherein we fitted the models on randomly chosen 90% of all synapse density measurements. This procedure was iterated 500 times and the mean adj.  $R^2$  was determined from all these iterations.

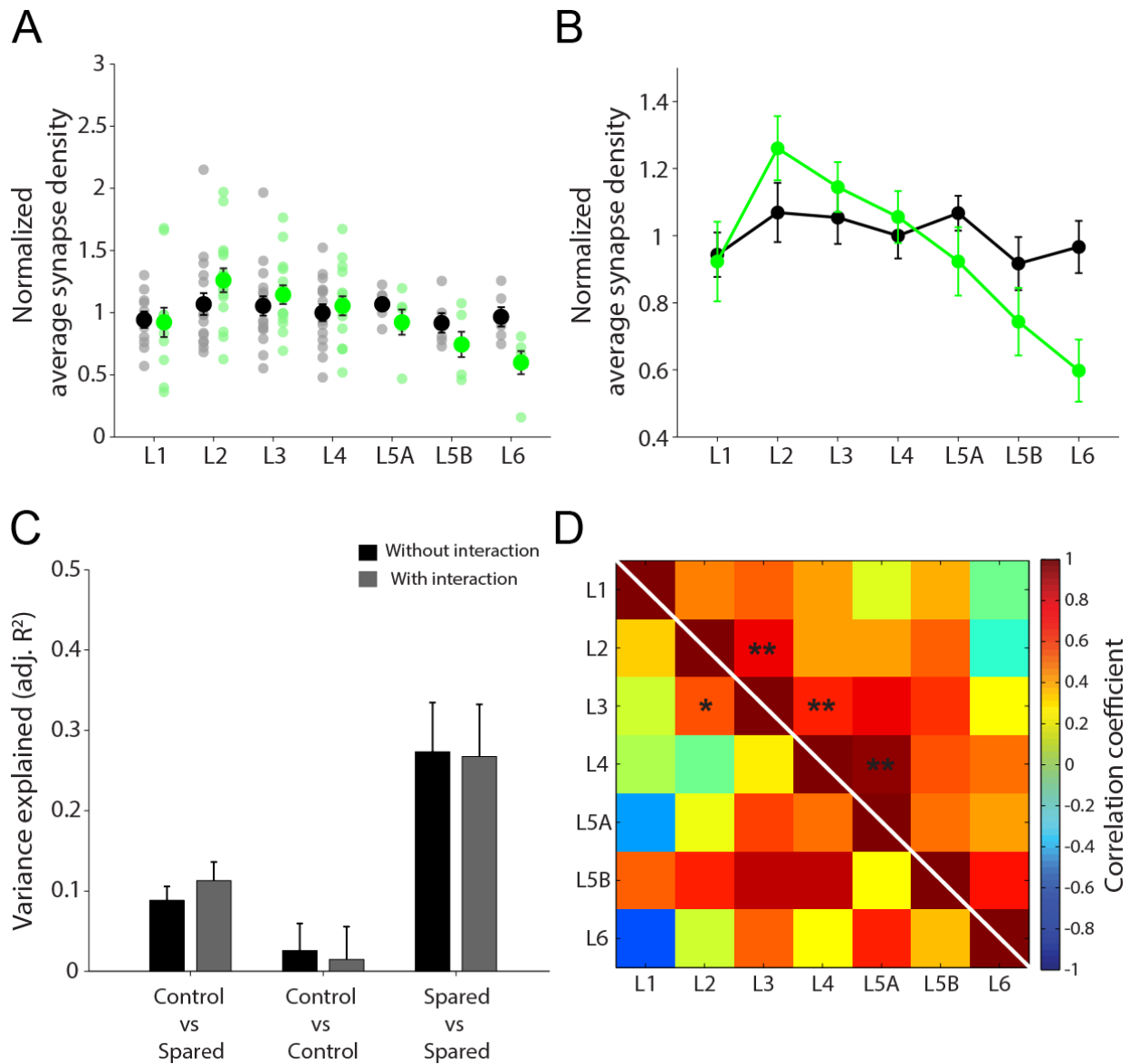


**Fig. 3.2 Distribution of synapses across cortical layers significantly different in spared barrel column**

- A. Scatter plot of average synapse density measured in control (black) and spared (green) barrel columns normalized to litter-wise mean L4 synapse density in control animals.
- B. Trend of normalized mean synapse density across cortical layers in control and spared barrel column.
- C. Adjusted  $R^2$  for linear models fitting synapse density measurements from control and spared animals (Control vs Spared), from only control animals randomly split into two groups (Control vs Control) or from only spared whisker animals split into two groups (Spared vs Spared), with interaction between layers and whisker experience (gray) or without interaction (black).
- D. Bottom left half: Pairwise correlation coefficient of average synapse densities across layers in control barrel column. \* indicates  $p < 0.05$ . Top right half: Pairwise correlation coefficient of average synapse densities across layers in spared barrel column. \*\* indicates  $p < 0.01$ .

We found that there was an increase in the adjusted  $R^2$  parameter upon adding the interaction term to the model (adj.  $R^2$  without the interaction term = 0.09; adj.  $R^2$  with the interaction term = 0.11). Also, the overall model was significantly different from a constant intercept model ( $p = 0.03$ ). This suggests that, 24h SRE significantly changes the overall distribution of synapses across the cortical layers as compared to control animals (Fig. 3.2 B).

We noted that the increase in adj.  $R^2$  is quite small. In the linear model, the contribution of layers ( $X_2$ ) is computed over observations averaged over the nature of whisker experience ( $X_1$ ). Thus, if the synapse density measurements from the spared whisker column exhibit high amount of laminar-specific differences, then the contribution of the layers ( $X_2$ ) in explaining the overall variability will be quite high, leading to a high adj.  $R^2$  even without the interaction term. To determine that the increase observed in adj.  $R^2$  is indeed robust, we generated two populations that comprised of synapse density measurements entirely from either control or spared whisker columns. Subsequently, the population was split in half randomly.

We expected to find that in the simulation where we compare two randomly generated populations of control synapse density measurements, we expected neither layers nor the interaction term to be able to explain the variability, that is, an adj.  $R^2$  of zero or a negative value. On the other hand, in the case of comparing two randomly generated populations of spared whisker synapse density measurements, we expected layers to be able to explain a lot of the variability but the addition of the interaction term would not increase the adj.  $R^2$ . This was exactly what we observed (Fig. 3.2 C). In case of the control animals being split into two groups, the linear model could not explain the variability any more than a constant intercept model. Thus, layers, when taken alone or the interaction of layers and whisker experience did not contribute significantly to explaining the variability (mean adj.  $R^2$  without interaction = 0.026;

mean adj.  $R^2$  without interaction = 0.015). In case of the spared whisker animals being split into two groups, the adj.  $R^2$  was high for the model without the interaction term, as layers could explain a substantial amount of the spread of the synapse density measurements (mean adj.  $R^2$  = 0.27). Including the interaction between layers and whisker experience did not increase adj.  $R^2$  (mean adj.  $R^2$  = 0.27). This clearly shows that it is the specific interaction of 24h SRE and cortical layers that sets apart the spared whisker synapse density population from the control synapse density population.

### **Correlation in synapse density between adjacent layers is stronger after 24h SRE**

The correlation in synapse density between the different cortical layers was low in case of the control barrel column (Fig. 3.2 D, bottom left half). Layers 2 and 3 were the only layers to exhibit substantial correlation ( $r = 0.57$ ;  $p = 0.02$ ). We reasoned that the weak correlation between layers is due to the fact that the synapse densities measured in the different layers were similar in magnitude. But, since we observed, layer specific changes in synapse density after 24h SRE, we hypothesized that the correlation between layers would also change. After 24h SRE, there was increased correlation in synapse density measurements between adjacent layers (Fig. 3.2 D; top right half). The strongest correlation was observed in L2 vs L3 ( $r = 0.75$ ;  $p < 0.01$ ), L3 vs L4 ( $r = 0.68$ ;  $p < 0.01$ ) and L4 vs L5A ( $r = 0.96$ ,  $p < 0.01$ ). This again points to minor changes in synaptic density occurring throughout the cortical column rather than a specific hotspot of change following 24h SRE.

### **Synapses in L3 are significantly longer following 24h SRE**

Previous electrophysiological work from the lab has shown that L4-L2/3 synapses are potentiated after 24h SRE at PND 14 (Wen and Barth, 2011; Wen et al., 2013). We were interested in observing morphological changes that corroborated with this functional change. It has been well-established that the length of synapses as observed in ultrastructural studies is highly correlated with the strength of the synapse (Cheetham et al., 2014). Thus, an experience-dependent increase in lengths of the synapses detected would be expected with the increase in synaptic strength. We observed that there was a significant increase in mean synapse length among L3 synapses (Fig. 3.3 A) after 24h SRE (by 2-way ANOVA,  $F(1,6) = 3.14$ ;  $p < 0.01$ ).

We were interested in exploring how the population of L3 synapses changed to bring about this increase in average synapse length. We generated cumulative histogram distributions of synapse lengths for synapses in L3. We ensured that the synaptic population constituted of synapses from every animal in an unbiased fashion. For this, we computed the total number of synapses detected by adding up the number of synapses detected in each animal. Then, we divided this by the total number of animals used to obtain the number of synapses that would ensure equal representation for synapses from each animal. Next, we generated a weighting factor for each animal that was the ratio between the number of synapses detected in that sample and the number of synapses required for equal representation in the overall population of synapses. Finally, we generated a simulated population by choosing synapses from each animal randomly based on the weighting factor.

For layer 3 synapses, we observed that the cumulative distribution histograms from control and 24h SRE animal deviated from each other only for synapses whose length was

around 0.25-0.35 $\mu$ m (Fig 3.3 D). The slight rightward shift of the 24h SRE histogram ( $p < 0.01$ , 2 sample KS test) suggests that the population of synapses has a higher proportion of synapses of these lengths.

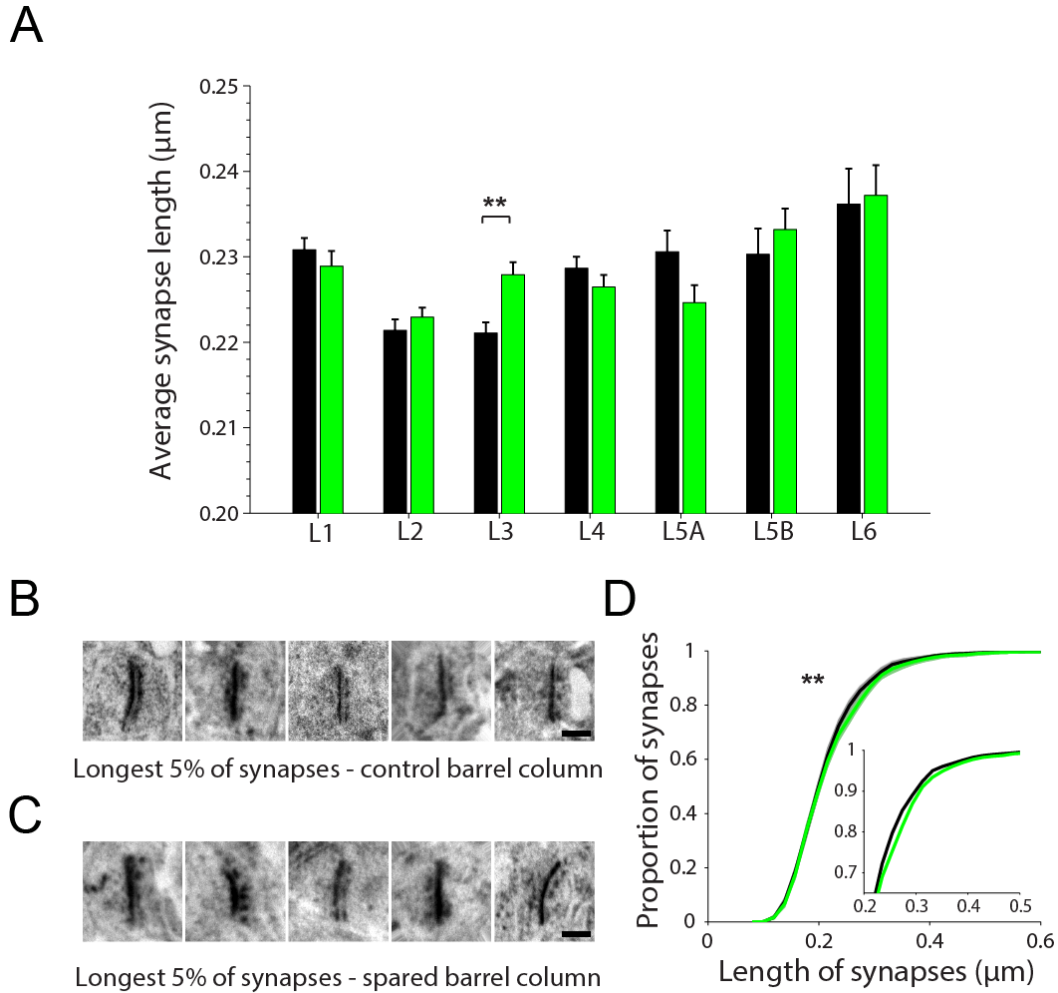


**Fig. 3.3 Significant increase in synapse lengths in L3 after 24h SRE**

- A. Average synapse length measured in each cortical layer in control (black) and spared (green) barrel columns. \*\* indicates  $p < 0.01$  by 2-way ANOVA –  $F(1,6) = 3.14$  and post-hoc Tukey HSD test. Number of synapses detected in each layer in the ‘D’ barrel column of control animals were as follows, L1 – 2753 synapses from 10 animals, L2 – 2937 synapses from 10 animals, L3 – 3206 synapses from 11 animals and L4 – 2942 synapses from 10 animals, L5A – 1151 synapses from 4 animals, L5B – 531 synapses from 2 animals and L6 – 424 synapses from 2 animals. Number of synapses detected in each layer in the spared barrel column of animals that underwent 24h SRE were as follows, L1 – 2307 synapses from 7 animals, L2 – 4076 synapses from 11 animals, L3 – 2799 synapses from 9 animals and L4 – 2669 synapses from 9 animals, L5A – 1119 synapses from 4 animals, L5B – 1040 synapses from 5 animals and L6 – 539 synapses from 3 animals.
- B. Example images of longest 5% of synapses in L3 in control animals. Scale bar – 200nm
- C. Example images of longest 5% of synapses in L3 in spared animals. Scale bar – 200nm
- D. Cumulative histogram of synapse length in L3 from control (black) and spared (green) animals. \*\* indicates  $p < 0.01$ , 2-sample K-S test with Bonferroni correction for multiple comparison.

### **3.4 Discussion**

In this study, we utilized selective staining and subsequent automated detection of synapses to quantify changes in synaptic density and length following 24h SRE. We observed that there were only modest differences in synaptic density within individual layers following 24h SRE as compared to control animals. But, the overall distribution of synapses across the different cortical layers was significantly different from control animals. Finally, we observed a L3 specific increase in synaptic length following 24h SRE.

#### **Global change in synapse density after 24h SRE**

The lack of a strong experience-dependent change in synapse density in any individual cortical layer is mostly attributable to the fact that our technique identifies synapses irrespective of the source or target of the synapses. The synapses localized in any cortical layer can be a highly mixed population of synapses. For example, the synaptic population found in L3 comprises of L4-L3 synapses (Feldmeyer et al., 2002), within-column (Feldmeyer et al., 2006) and inter-column L3-L3 synapses and synapses that are made onto L5 apical dendrites that pass through L3 (Markram et al., 1997; Petreanu et al., 2009). Numerous studies have shown that the axons of L2/3 and L5 neurons arborize extensively into adjacent barrel columns (Broser et al., 2008; Bruno et al., 2009). Inter-column L2/3-L5B axonal projections onto intrinsic bursting (IB) cells have been shown to increase in connectivity when the principle whisker of the target barrel has been removed (Jacob et al., 2012) while within-column L2-L5B axonal projections onto regular spiking (RS) cells undergo reduction in connectivity. Such opposing changes in specific pathways could be masked in our approach.

## **Experience-dependent decrease in synapse density in L6**

We were surprised to observe that our strongest effect on synapse density, a 35% reduction, occurred in L6. Our imaging was centered on the topmost section of L6 (900 $\mu$ m from the pia) which is the depth at which TC axons arborize (Crocker-Buque et al., 2014). But, recent experiments have shown that TC connectivity to L6 cells do not undergo experience-dependent changes in response to sensory deprivation during early development (Wang et al., 2013; Crocker-Buque et al., 2014). Thus, TC synapses are unlikely to be the candidate synapses responsible for the observed change.

The excitatory neurons of L6 are primarily classified into two classes based on their axonal projections, corticothalamic (CT) projecting and corticocortical (CC) projecting neurons (Briggs, 2010; Thomson, 2010). Extensive studies involving cell labeling and reconstructions have shown that the axons of CC neurons arborize extensively both within the barrel and in neighboring barrels (Zhang and Deschenes, 1997; Pichon et al., 2012). Paired with the observation that neurons in other layers in the barrel column connect to L6 neurons at substantially low rates (Lefort et al., 2009), it could be that these inter-barrel L6-L6 synapses are responsible for our observation of experience-dependent reduction in synapse density in L6.

The reduction in synapse density in L6 of the spared barrel column could be due to weakening of connections from the surrounding deprived barrel columns. It would be interesting to observe whether the projections from the L6 neurons of the spared barrel column into the surrounding deprived columns strengthen and subsequently lead to an increase in synapse density. This would be consistent with previous observations of broadening of the spared whisker receptive field observed in supragranular layers (Glazewski and Fox, 1996).

Alternatively, the synapses on L6 could be long-range connections from other areas of the brain as is the case in the visual cortex for CC neurons (Velez-Fort et al., 2014).

It is possible that inhibitory synapses could be undergoing experience-dependent changes in L6. But, given that they just constitute just 15-20% of all synapses in all layers (Micheva and Beaulieu, 1996; De Felipe et al., 1997), they are unlikely to be solely responsible for the 35% reduction in synapse density.

### **L3-specific increase in synapse length**

Following 24h SRE, we observed an increase in the mean length of L3 synapses and also observed an enrichment of longer synapses in the synaptic population. It has been previously established that the area of the postsynaptic density is highly correlated to the number of AMPA receptors at the synapse (Nusser et al., 1998) and the spine volume (Harris and Stevens, 1989; Schikorski and Stevens, 1999; Cheetham et al., 2014) which, in turn, dictates the strength of the synapse. Thus, our data suggests that L4-L3 synapses are getting strengthened. This is in accordance with previous work from our lab that found strengthened L4-L2/3 synapses following 24h SRE at the age (Wen and Barth, 2011).

The actual difference in the mean synapse length is small because we are counting synapses identified only from a single ~100nm section. This results in the majority of the synapses being cut and observed as a smaller synapse than their actual length. Thus, it would require a large number of synapses to observe a shift in the size of the population of synapses. The high throughput nature of our technique enabled us to identify and characterize hundreds of

synapses in each cortical layer and thereby uncover this experience-dependent increase in synapse length.

It is quite interesting to note that the cortical circuit can modify synapse number and synapse strength in an independent and layer-specific manner. More targeted experiments like electrophysiological recordings will be needed to ascertain which pathways are responsible for slight increase in synapse density in L2 and the 35% reduction in L6.

In conclusion, using a high throughout unbiased synapse detection and characterization technique we uncovered global changes in synapse density and L3-specific increase in synapse length across all cortical layers after 24h altered sensory experience in the mouse somatosensory cortex.

## **Chapter 4**

# **Layer-specific critical periods for synaptic plasticity in the infragranular layers**

### **4.1 Introduction**

#### **Layer-specific critical periods**

Previous work from our lab has characterized a critical period for rapid experience-dependent strengthening of synapses targeting L2/3 pyramidal neurons in the mouse barrel cortex (Clem and Barth, 2006; Wen and Barth, 2011). After 24h of single whisker experience (SWE), L4-L2/3 and L2/3-L2/3 show increase in strength. While the CP for this L4-L2/3 strengthening spans the ages P12-14, the CP of L2/3-L2/3 synaptic strengthening spans the ages P13-16 (Wen and Barth, 2011).

## **Progression of critical period onsets through cortical layers**

Interestingly, the progression of critical periods for each cortical layer closely follows the developmental timeline of cortical circuits. For instance, thalamocortical circuits exhibit critical period very early in postnatal development (Crair and Malenka, 1995; Kirkwood et al., 1995), followed by L4-L2/3 synapses and then the recurrent excitatory connections in L2/3 (Wen and Barth, 2011) which matches the timeline of maturation of receptive fields of neurons in S1 (Stern et al., 2001). Layer 4 cells of the rat barrel cortex respond to whisker stimulation reliably at P12, compared with layer 2/3 cells that respond to whisker stimulation only at P14 (Stern et al., 2001). Thus, the earlier maturation of L4 neuronal responses to sensory stimulation may facilitate an earlier CP for L4-L2/3 synapses. Although a similar trend of the timeline of maturation of visual-evoked responses in rodent V1 (Fagiolini et al., 1994), matching the critical periods is observed in the visual cortex, layer-specific CPs have not been reported.

While layer-specific critical periods have been well-characterized in L4 and L2/3, little is known if other cortical layers exhibit a critical period for synaptic plasticity. Following MD around the critical period in mice, L5 apical dendrites show extensive spine motility (Oray et al., 2004) but only localized to the supragranular and infragranular layers. But, L5 apical dendritic spines were observed to be motile even in adult animals with short periods of MD (Hofer et al., 2009) or whisker deprivation (Holtmaat A. et al., 2006). Also, L2/3-L5B synapses can undergo plasticity after prolonged whisker deprivation (Jacob et al., 2012) in P30 mice. The ability to shift their responsiveness to the undeprived eye has been observed to linger in L5 and L6 neurons to a much later developmental time point (Daw et al., 1992), though these were longer (3 month) deprivations. This raises the question – does the sequential progression of critical period onsets reach L5 synapses after L2/3 synapses? A systematic exploration of whether a

critical period, as characterized by rapid changes, exists for L2/3-L5 or recurrent L5-L5 synapses has not been carried out. Even less is known about synapses targeting L6 neurons. Although, several studies have established that TC synapses in L6 do not undergo plasticity (Wang et al., 2013; Crocker-Buque et al., 2014), the development, maturation and plasticity of L6-L6 synapses is largely uncharacterized.

We employed our automated synapse detection technique to test, in an unbiased fashion, whether infragranular cortical layers exhibit a critical period, possibly at a slightly later developmental time point. Our analysis revealed that L5A synapses in the spared barrel column do show a rapid increase in size, and thus, strength of synapses, in response to just 24hrs of SRE starting at age PND 17. Since this change was not observed when the same manipulation was carried out an earlier age, it suggests that the L5A synapses do exhibit a critical period for synaptic plasticity and that its onset is later than that for L2/3 synapses. Also, L6 synapses in the spared barrel column showed an increase in synaptic density. This shows that cortical circuits can modify synaptic strengths and numbers independently in response to altered sensory experience.

## 4.2 Methods

**Whisker experience and animal preparation:** Litters of wildtype C57bl6 (Harlan) mice aged PND 13 or 17 were divided into two groups, namely the control group and the single row experience (SRE) group. For the SRE group, all the whiskers were plucked gently from the snout of the animal except the 'D' row on the right side. After 24hrs, the animals were euthanized, their brains dissected out and drop-fixed in 2.5% Glutaraldehyde (Electron Microscopy Sciences; EMS) in 0.1M Phosphate Buffer. After 24h of glutaraldehyde fixations, brains were transferred to 30% sucrose solution. The brains were kept in this solution until they were sectioned.

**Tissue preparation:** Brains stored in 30% sucrose solution were cut at 45° to the midline (Fig. 2.1A) and mounted on the cryostat (Finnerty et al., 1999). 50µm-thick sections were cut and stored in 0.1M phosphate buffer. The presence of barrels was verified by mitochondrial (cytochrome oxidase) staining. The slices in which the 'D' barrel could be identified unambiguously (Fig. 2.1 B) were selected for dissecting out the column (Fig. 2.1 C).

**Electron Microscopy tissue preparation:** Tissue was prepared for transmission electron microscopy (TEM, Hitachi H7100) in a series of steps.

For EPTA staining of synapses, the 50µm thick slice, chosen in the previous step, was washed with three changes (5 minutes each) of distilled water, followed by incubation in 0.02% NaOH for 10 minutes. Second, the tissue was dehydrated with an ascending series of EtOH (25%, 50%, 70%, 80%, 90%, and 100%), followed by fixation with 1% phosphotungstic acid (PTA) (Ladd) in 100% EtOH. Third, a small amount, 7µl, of 95% ethanol, was added to each 1000µl of PTA stain used, and the PTA was washed from the sample with two changes of 100% ethanol. Fourth, propylene oxide (PO) (EMS) was used as a transitional solvent (the first change

of PO was on ice), and then the specimen was infiltrated with Spurr (Ted Pella) embedding resin, which was polymerized at 60° C for 48h. Finally, 100nm sections were cut using a diamond knife (Delaware Diamond Knife) on an Ultracut-E ultramicrotome (Riechert-Jung), and were picked up using single slot copper grids (EMS).

For conventional EM imaging, the 50µm thick slice was initially exposed to osmium tetroxide (OsO<sub>4</sub>) and lead citrate. Then, the tissue was taken through same procedure as described above with the exception of the exposure to EPTA.

**Tissue shrinkage:** We found that, there was substantial amount of shrinkage of the tissue after it was cut from the resin block and mounted onto the copper grid for imaging. The amount of shrinkage was determined by comparing the separation between fiduciary landmarks, namely the pia and an angular cut manually made underneath layer 6, under the TEM versus when the tissue is in the resin. Once cut and mounted, the sections measured only 70-80% of their length as when embedded in the resin. This was remarkably consistent across all our samples. Subsequently, we adjusted the previously reported depths of each layer as measured from the pia (Lefort et al., 2009) with the shrinkage factor we determined.

**Image Acquisition:** The specimen was observed using a TEM and images were taken digitally using a Kodak Megaplug 1.6i camera. The electron beam was scanned across each cortical layer parallel to the pial surface and images were obtained in a continuous fashion (Fig. 2.1 C). The electron beam was positioned for each image such that there was no overlap between images of adjacent areas of the cortex. In order to ensure that the images were indeed obtained from the designated cortical layer, the acquisition of images was done at the following depths, as measured from the pia, for the respective cortical layers, L1 - 50µm, L2 - 125µm, L3 - 325µm, L4 - 500µm, L5A - 600µm, L5B - 725µm and L6 - 900µm. Depending upon the shrinkage

determined for each individual tissue section, these depths were adjusted accordingly. We obtained about 100 images (an example image from layer 2 is shown in Fig. 2.1 D) per cortical layer with each image capturing  $4.31\mu\text{m} \times 4.31\mu\text{m}$  region of the cortex.

**Image Analysis:** The analysis of all the images was carried out using custom-written software in MATLAB. Firstly, the contrast of each image was enhanced and then subsequently, each image was binarized based on a manually determined threshold. Following this, connected segments were computed in each image and were filtered based on their size (min. area -  $5.5 \times 10^3 \text{ nm}^2$  and max. area -  $66 \times 10^3 \text{ nm}^2$ ). Each connected segment and its surrounding area as bounded by a square patch of side 125 pixels ( $\sim 500\text{nm}$ ) is used for subsequent classification. A machine learning algorithm that employs support vector machines (SVM) was used to classify the connected segments as synapses based on texture- and shape-based features (Navlakha et al., 2013). The classifier was first trained using 1,665 positive (synapses; Fig. 2.1 E) and 10,441 negative (non-synapses) examples. In order to provide a quantitative estimate for sample variability, a testing dataset that included both synapses as well as non-synapses was generated from 10% of images for each layer in each animal. All synapses within this image subset were identified manually. The performance of the classifier was evaluated on the testing image set. A classification threshold of 50% correct recall (where exactly 50% of manually-identified synapses were labeled correctly by the classifier) was chosen for the subsequent analysis of all images obtained for that particular layer in a given animal. In cases where the classifier performed at very high levels (correctly identifying 95% of synapses), we found an unacceptably high level of false positives, i.e., objects that were not synapses; thus, a threshold of 50% recall was established to compromise between accurate detection of synapses without inaccurate classification of non-synapses.

For synapse density, we scaled the measured density by the precision that the classifier exhibited at 50% recall. For all other measurements, we used only samples that had >75% precision. The lengths of synapses were obtained when the connected segments were calculated for each image.

### 4.3 Results

In order to explore the existence of a critical period for L5 and L6 that might occur later in development, we used animals of the age PND 18. This age was chosen as the critical periods for L4-L2/3 and L2/3-L2/3 synapses have closed by now (Wen and Barth, 2011). Thus, we do not expect any synaptic changes in L2/3. This will act as a negative control for our technique and any change in L5 or L6 might be indicative of another layer-specific critical period.

#### **Synapse density increases in superficial layers from P14 to P18**

As expected from numerous studies (Micheva and Beaulieu, 1996; De Felipe et al., 1997; White E. L. et al., 1997), synaptic density increased substantially in the superficial layers of the whisker barrel cortex in mice from PND 14 to PND 18. Cortical layer 1 showed the highest increase in synaptic density with 6.60 synapses per image in older animals as compared to 4.59 synapses per image at PND 14, an increase of about 44%. Among the infragranular layers, the increase is much smaller for L5A (P18 – 5.73 synapses/image, P14 – 4.80 synapses/image; 19% increase) and L5B (P18 – 5.12 synapses/image, P14 – 4.13 synapses/image; 24% increase) and completely absent for L6 (Fig. 4.1 A). Although, the changes in synaptic density observed by us are smaller than previously reported, the trend of supragranular and granular layers exhibiting greater increase in synapse density as compared to infragranular layers is consistent with what has been previously reported in the mouse barrel cortex (De Felipe et al., 1997).

We determined the CV for each cortical layer for the two ages. The CV for cortical layers 2, 3 and 4 were much lower in older animals. This aligns well with our hypothesis that the high

CV or inter-animal variability we observed in P14 animals was due to developmental factors and not a result of the automated synapse detection technique having issues of irreproducibility.

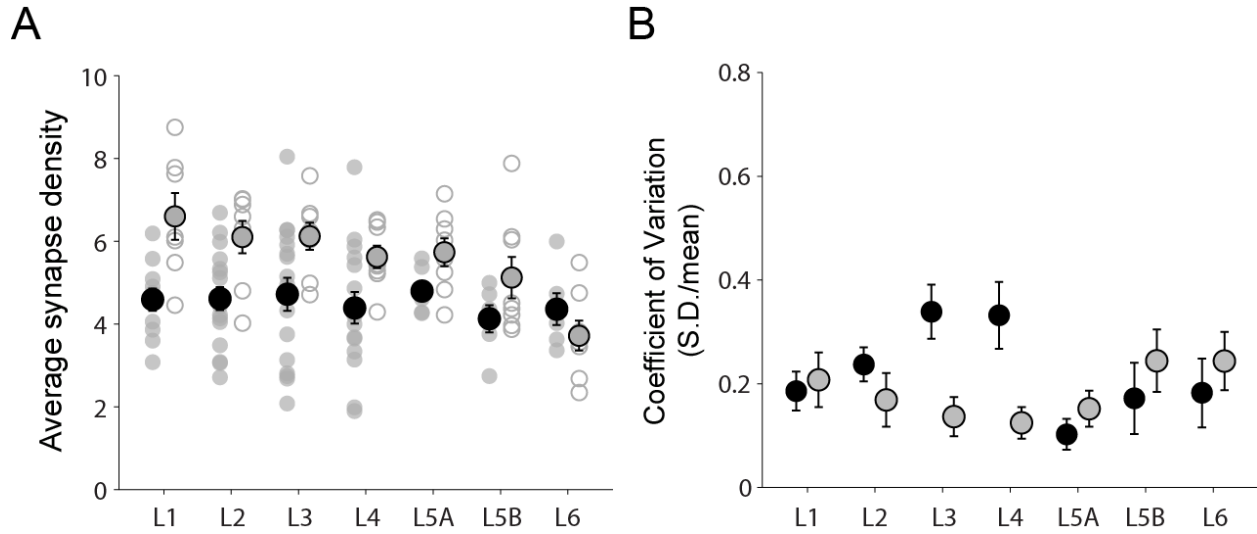


**Fig. 4.1: Increase in synapse density preferentially in the superficial layers from PND 14 to PND 18**

- A. Scatter plot showing the average synapse density of control animals aged PND 14 (grey filled circles, mean – black filled circle) as reported in the previous chapter and PND 18 (grey open circles, mean – grey filled circle with black border)
- B. Plot showing the CV of synapse density for each layer in both sets of animals, PND 14 (black circles) and PND 18 (grey circles).

## **24hr single row experience at PND 17 results in changes in synapse density in L6**

Similar to the earlier experiments involving younger animals, we subjected C57 mice aged PND 17 to bilateral whisker deprivation sparing the 'D' row on the right side. Each litter was divided into animals that underwent SRE and others that underwent sham deprivation. Following 24hrs of SRE, the mice were euthanized and the brains were fixed in 2.5% glutaraldehyde (Fig. 4.2 A).

With the exception of L6, none of the layers underwent any change in synapse density following 24h SRE in these older animals. L6, on the other hand, showed a 30% increase in synapse density (Fig. 4.2 C). Given that synapse density underwent a reduction of similar magnitude at PND 14, it appears that synapses onto L6 neurons can undergo bidirectional plasticity depending upon the developmental state of the cortical circuit. Thus, L6 synapses do not exhibit a critical period restricted to a particular time point and are able to exhibit rapid experience-dependent changes in synapse density during much of the third postnatal week of development of the circuit.

An interesting observation was that the inter-animal variability for PND 18 animals was quite low for both control and SRE animals (Fig. 4.2 E). Of all the layers, only L5B and L6 exhibit a slightly elevated CV but still less than 0.3 (Fig. 4.2 F). This again shows that our technique can indeed generate highly reproducible data across animals.

We used linear regression to further test whether the distribution of synapses across the cortical layers is different after altered whisker experience in these older animals as well. Firstly, we normalized the density measurements to the mean density measurement for L4 obtained for each litter that the animal belonged to. We found that there was an increase in the

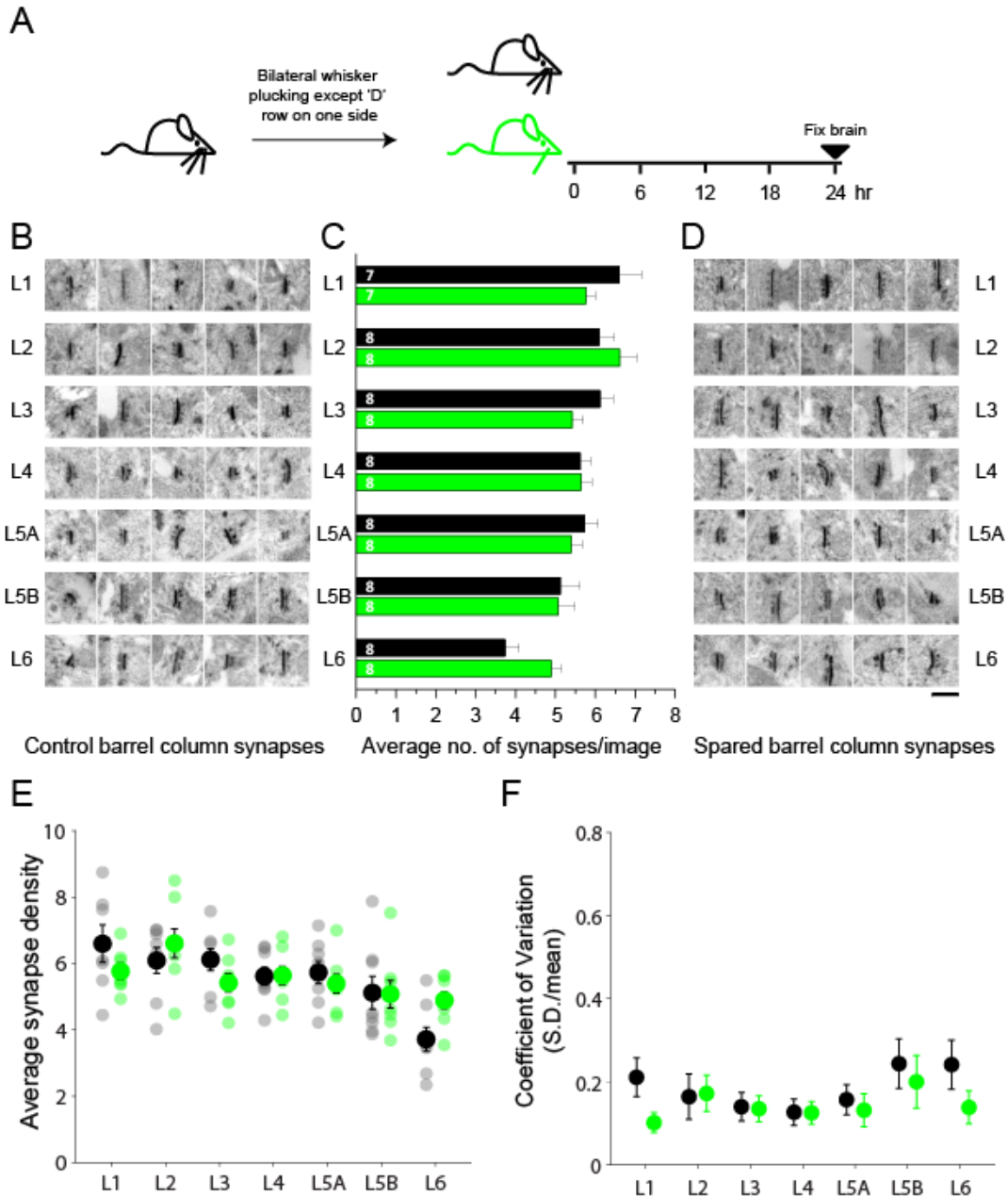


**Fig. 4.2 Layer-specific changes in synapse density in PND 18 animals**

- A. Schematic showing the experimental paradigm and timeline of altered sensory experience.
- B. Example images of synapses from each cortical layer from control barrel column
- C. Average synapse density measured in control (black) and spared (green) barrel columns. Numbers indicate number of animals, Error bars indicate SEM.
- D. Example images of synapses from each cortical layer from spared barrel column. Scale bar – 200nm.
- E. Scatter plot showing distribution of average synapse densities measured in each individual animal
- F. C.V. of average synapse densities in each cortical layer from control and spared barrel columns.

adjusted  $R^2$  parameter upon adding the term that signified an interaction between whisker experience and cortical layer to the model (adj.  $R^2$  without the interaction term = 0.22; adj.  $R^2$  with the interaction term = 0.24). Also, the overall model was significantly different from a constant intercept model ( $p < 0.01$ ). This suggests that, 24h SRE significantly changes the overall distribution of synapses across the cortical layers as compared to control animals (data not shown) in older animals as well.

### **Synapses in L5A are significantly longer after 24h SRE in PND 18 animals**

In addition to synapse density, we explored if there was any increase in synapse size in any of the layers. An increase of synapse size would be indicative of increase in synaptic strength. Comparing mean lengths of synapses from all animals pooled together, we were surprised to observe that following 24h SRE in PND 18 animals, synapses in L5A were significantly longer than in control animals (by 2-way ANOVA,  $F(1,6) = 4.25$ ;  $p < 0.01$ ; Fig. 4.3 A). The population of synapses compared consisted of 1973 synapses from 5 animals for the control group (mean = 394.6 synapses, S.D. = 72.08 synapses) and 1417 synapses from 5 animals for the SRE group (mean = 283.4 synapses, S.D. = 41.82 synapses). This suggests that synapses targeting L5A neurons are undergoing rapid strengthening in response to SRE. We also observed a strong decrease in synapse size in L1 but, it was not statistically significant as we could not obtain highly reliable synapse length measurements in more than one animal in the control group. None of the other layers, showed any difference including L3 which had exhibited an increase in synapse size when 24h SRE was subjected to animals at PND 13. Thus, our

experiments reproduced accurately the closure of the critical period as established previously (Wen and Barth, 2011).

To further determine the nature of the increase in the synapse size among the L5A synapse population, we generated cumulative distribution histograms as described previously. We noticed that the entire population distribution in animals that underwent 24h SRE was shifted to the right as compared to that from control animals ( $p < 0.01$ , 2 sample KS test). This was unlike the synapse population of L3 in PND 14 animals, which showed a deviation in the distribution of synapses that were longer than  $0.2\mu\text{m}$ . This suggests that this increase in length is occurring across a large population of synapses, irrespective of initial synapse strength.

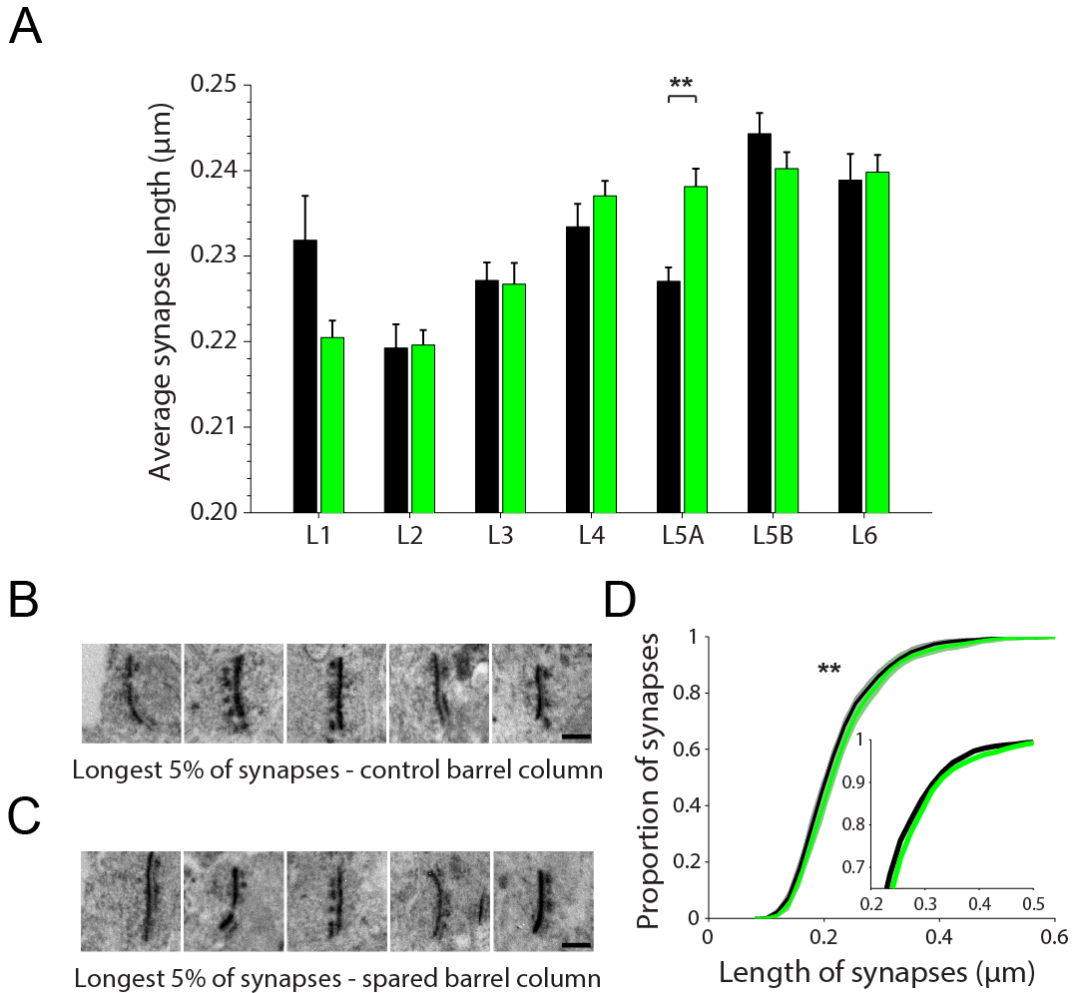


**Fig. 4.3 Significant increase in synapse lengths in L3 after 24h SRE**

- A. Average synapse length measured in each cortical layer in control (black) and spared (green) barrel columns. \*\* indicates  $p < 0.01$  by 2-way ANOVA –  $F(1,6) = 4.25$  and post-hoc Tukey HSD test. Numbers of synapses detected in each layer in the ‘D’ barrel column of control animals were as follows, L1 – 393 synapses from 1 animal, L2 – 652 synapses from 2 animals, L3 – 1429 synapses from 4 animals and L4 – 956 synapses from 3 animals, L5A – 1973 synapses from 5 animals, L5B – 1120 synapses from 4 animals and L6 – 725 synapses from 3 animals. Numbers of synapses detected in each layer in the spared barrel column of animals that underwent 24h SRE were as follows, L1 – 1373 synapses from 4 animals, L2 – 1683 synapses from 4 animals, L3 – 849 synapses from 3 animals and L4 – 2063 synapses from 6 animals, L5A – 1417 synapses from 5 animals, L5B – 1745 synapses from 6 animals and L6 – 1329 synapses from 5 animals.
- B. Example images of longest 5% of synapses in L5A in control animals. Scale bar – 200nm
- C. Example images of longest 5% of synapses in L5A in spared animals. Scale bar – 200nm
- D. Cumulative histogram of synapse length in L5A from control (black) and spared (green) animals. \*\* indicates  $p < 0.01$ , 2-sample K-S test with Bonferroni correction for multiple comparison.

## 4.4 Discussion

In this section, we utilized the unbiased nature of our technique to test the hypothesis that infragranular layers may exhibit a critical period that has an onset later than that reported for L2/3 synapses. Previous studies of critical periods in the mouse whisker barrel cortex have uncovered multiple critical periods, with each class of synapses having a unique onset and offset for its CP. TC synapses targeting L4 neurons show rapid experience-dependent plasticity in terms of both functional (Fox, 1992; Crair and Malenka, 1995) and structural aspects (Coleman et al., 2010), very early in development. Following the closure of this critical period, L4-L2/3 synapses and then, subsequently L2/3-L2/3 synapses, exhibit a critical period in the second postnatal week for experience-dependent synaptic strengthening (Wen and Barth, 2011). This rolling progression of critical periods strikingly matched the progression of development of maturation of the cortical circuit (Stern et al., 2001) and the progression of sensory information in the cortex. We hypothesized that after the CP of L2/3, there would be an onset of a short-developmental epoch wherein synapses in the infragranular layers would exhibit rapid experience-dependent synaptic changes. Thus, we subjected mice to 24hrs of single row experience at the age of PND 17 and characterized synaptic changes in the spared barrel column.

### **Increase in synaptic density in the supragranular layers**

We observed that synapse density measurements obtained at PND 18 were significantly higher than those obtained at PND 14 for the supragranular layers. This is in accordance with previous reports that have characterized synapse density across development in rodents (Micheva and Beaulieu, 1996; De Felipe et al., 1997). But, the infragranular layers showed very little

change in synapse density in contrast to the previously reported numbers in mice (De Felipe et al., 1997). The magnitude of increase in synapse density in our measurements are more in accordance with what has been previously reported for rats at around the same developmental age (Micheva and Beaulieu, 1996). The previous work done in mice (De Felipe et al., 1997) reported that the peak in synapse density is reached only at PND 32 following which synaptic pruning is initiated. But, both the study in rats (Micheva and Beaulieu, 1996) and previous work in our lab focused on L4 in mice (Navlakha et al., under review), have established that the peak synaptic density is attained at around PND 20. The fact that the previous work (De Felipe et al., 1997) report synapse density with respect to the neuropil only and not the entire cortex, could be a cause for the discrepancy between the synapse densities reported by us and them. Thus, we conclude that while L1-4 exhibit large increases in synapse density from PND 14 to PND 18, L5A and L5B show less of an increase with L6 showing no increase at all.

### **Experience-dependent changes in synapse density in L6**

Following 24h SRE, there was a strong increase in synapse density in L6. This was in stark contrast to the effect of a similar whisker experience at PND 14 which leads to a decrease in synapse density in L6. This is indeed remarkable as L6 connectivity can undergo rapid bidirectional modulation depending on the developmental state of the circuit. Such a developmental switch in direction of plasticity has been reported previously in the mouse visual cortex for L6 neurons (Petrus et al., 2011). In this study, the mean amplitude of mEPSCs received by L6 neurons increased after 2 days of dark exposure at P14 whereas the mean

amplitude decreased after a 7d dark exposure at P21. However, this study did not observe any change in frequency of mEPSCs, functional analog of synapse density, at either time point.

Another study established that *in vitro* stimulation of TC input to L6 neurons, using a theta burst to generate LTP, lead to strengthening of the TC synapses but simultaneously weakened of the synapses made by upper layer inputs to L6 neurons. Stimulation of the upper layer input generated the opposite effect (Arami et al., 2013). Thus, L6 synapses can and do exhibit bidirectional plasticity in response to altered sensory experience or the consequent altered circuit state.

One of the most significant findings made using this technique was that the synapses in L6 were highly plastic and switched their direction of plasticity as the circuit matured. Following 24hr SRE, synapse density in L6 increased by 35% in PND 14 animals whereas it fell by 30% in PND animals for the same altered whisker experience. We imaged synapses in L6 at a depth of ~900 $\mu$ m from the pia which corresponds to the upper half of L6 (Lefort et al., 2009). TC axons arborize preferentially in the upper half of L6 (Zhang and Deschenes, 1998; Wang et al., 2013). The upper half is populated by those CT neurons that project to the VPM, while CC neurons are uniformly distributed throughout L6 (Zhang and Deschenes, 1997)

The absence of substantial amount of connectivity from the other layers to L6 (Lefort et al., 2009) suggests that most of the synapses within L6 represent L6-L6 recurrent connections. The CC projecting neurons of L6 have been shown to arborize extensively within the barrel field, with 60% of the boutons in L6 and the rest in L4 (Pichon et al., 2012). Thus, these L6-L6 connections could be undergoing rapid plasticity in response to 24h SRE.

Interestingly, our results differ from the previous report of bidirectional plasticity in two major ways (Petrus et al., 2011). Firstly, we never observed a change in synapse length suggesting that synapse strengths did not undergo a substantial change while their bidirectional plasticity involved only synaptic strength and no change in synaptic frequency was observed. Secondly, we observed rapid change in synapse density in both PND 14 and PND 18 animals whereas in they had to use a prolonged the sensory deprivation in the older animals to bring about the reported plasticity. This suggests the L6 synapses in the somatosensory cortex do not seem to exhibit a critical period for synaptic plasticity at least till PND 18 whereas those in the visual cortex do.

What is the functional implication of the bidirectional plasticity? It is unclear what the bidirectional plasticity might entail in terms of how the circuit responds to the same altered sensory experience at two different time points. One possibility can be that the targets of these newly formed synapses may be different. That is, the recipients of these additional synapses or those pruned could be either excitatory pyramidal neurons at one time point and inhibitory interneurons at the next or vice versa. Studies with altered sensory experience (Kuhlman et al., 2013) and fear association learning (Letzkus et al., 2011), have shown that cortical circuits reduce the excitation provided to parvalbumin (PV)-containing interneurons first, which in turn enables the plasticity of excitatory neurons. This could be the reason for reduction of synaptic density in L6 of younger animals, that is, the reduction of excitation to inhibitory interneurons of L6. Simple electrophysiological experiments that measure the change in the frequency of spontaneous synaptic inputs received by PV-interneurons and CC neurons in L6 following 24h SRE would determine if this is indeed the case.

## **Experience-dependent increase in synapse length in L5A**

In accordance with our hypothesis of a CP for L5A synapses that has an onset slightly delayed as compared to that of L2/3, we found rapid experience-dependent increase in synapse length in L5A in the spared barrel column at PND 18 animals following 24hr SRE. This suggests that some set of synapses localized to L5A show rapid experience-dependent strengthening within 24hrs of onset of SRE.

Numerous studies have characterized the experience-dependent plasticity of spines on the dendrites of L5 neurons but, using two-photon *in vivo* imaging, they were restricted to the superficial layers and adult animals (Trachtenberg et al., 2002; Holtmaat A. et al., 2006; Hofer et al., 2009; Wilbrecht et al., 2010). Spines of L5 apical dendrites that are located in L5 do show experience-dependent plasticity (Oray et al., 2004). L5A neurons receive inputs from three major sources – POm, L5A and L4. The strengthening observed could be due to any of these set of inputs or a combination of them.

For this to be truly an onset of a critical period, we would have to determine its time of closure as well. L5 neurons, like L2/3 neurons, retain the ability to exhibit plasticity well into adulthood but, they require prolonged periods of experience and the resultant plasticity is not as strong and extensive. L4-L2/3 and L2/3-L2/3 synapses have been shown to exhibit a 3-4 day CP. A quick study of slightly older animals, like PND 21, targeted at L5A can help determine if there is indeed a CP even for infragranular layers.

L5A consists of cells that can be classified as regular-spiking (RS) and intrinsic-bursting (IB) cells based on their electrophysiological properties (Schubert et al., 2006) but, unlike L5B pyramidal neurons, on the basis of morphology and sources of inputs, these neurons seem to

form a homogeneous group. It is in L5A, in addition to L1, that the axonal projections from the posteromedial nucleus (POm) of the thalamus arborize (Lu and Lin, 1993; Bureau et al., 2006; Wimmer et al., 2010b). Recently it was shown that a subset of L2 neurons expressing the activity-dependent marker *fos*-GFP, were preferentially innervated by POm inputs (Jouhanneau et al., 2014) which enabled them to possess broad receptive fields.

Moreover, L5A neurons receive prominent input from other L5A neurons both within the home barrel (Lefort et al., 2009) and neighboring barrels (Schubert et al., 2007). The next major source of input for L5A neurons is L4 (Feldmeyer et al., 2005; Schubert et al., 2007; Lefort et al., 2009) leading to the idea that L5A neurons constitute yet another locus of integration of the inputs of the lemniscal and the paralemniscal pathways (Schubert et al., 2007; Wimmer et al., 2010b) along with the *fos*-expressing subset of L2 neurons (Jouhanneau et al., 2014). The increase in synaptic size observed, which functionally corresponds to an increase in the strength of the synapses, could be occurring in any of these major classes of synapses that populate L5A.

The onset of CP for rapid experience-dependent plasticity in L4-L2/3 and L2/3-L2/3 synapses (Wen and Barth, 2011) has been observed to coincide with the maturation of whisker-evoked responses in the source neurons (Stern et al., 2001). The timeline of maturation of whisker-evoked responses in L5A neurons is unclear. Since, L2/3 neurons do not extensively innervate L5A, the plasticity observed here does not appear to be part of the canonical cortical column circuit that conveys information through the TC → L4 → L2/3 → L5B pathway (Douglas and Martin, 2004; Feldmeyer, 2012). Thus, the experience-dependent plasticity observed here seems to belong to the parallel thalamic pathway involving POm-L5A synapses or a parallel cortical pathway involving L5A-L5A and/or L4-L5A synapses.

TC-L4 connections show rapid experience-dependent plasticity only for a short period of time early in development (Fox, 1992; Crair and Malenka, 1995). Even though, they have been shown to exhibit plasticity well into adulthood, it requires prolonged exposure to altered sensory experience (Wimmer et al., 2010a; Oberlaender et al., 2012b). Given that, P<sub>Om</sub> axons are observed to have already innervated the cortex at birth (Kichula and Huntley, 2008), it is likely that P<sub>Om</sub>-L5A synapses would exhibit rapid experience-dependent plasticity early in development. Thus, it is more likely that intracortical synapses, namely L4-L5A and/or L5A-L5A, are undergoing rapid experience-dependent plasticity in these older animals.

In conclusion, using our unbiased, automated synapse detection technique we have uncovered a bidirectional, age-dependent synaptic plasticity in L6 and the potential onset of a CP for L5A synapses.

# Chapter 5

## Discussion

### **Unbiased high-throughput analysis of synaptic plasticity**

Synaptic changes can occur at different connections in a cortical circuit simultaneously. It is by the combination of all those synaptic changes that the cortical circuit achieves the desired output. While a typical cortical circuit spans a few hundred microns (Helmstaedter, 2013), the synapses in the circuit are about a few hundred nanometers in size (Bourgeois and Rakic, 1993; De Felipe et al., 1997; White E. L. et al., 1997). This difference of a few orders of magnitude makes it extremely difficult to characterize the changes occurring in the multitude of synaptic pathways that exist within a circuit.

*In vivo* imaging of dynamics of dendritic spines has given us insight into how circuits rewire in response to development (Holtmaat A. J. et al., 2005), altered sensory (Trachtenberg et al., 2002; Holtmaat A. et al., 2006; Hofer et al., 2009) or a learning experience (Xu et al., 2009; Yang et al., 2009). Similarly dynamics of axons and their boutons have also been studied *in vivo* during development (Portera-Cailliau et al., 2005) and altered sensory experience (Yamahachi et al., 2009)

But, all these studies have been restricted to certain parts of the cortical circuit, either the superficial layers due to the fact that synaptic structures in deeper cortical layers are inaccessible to imaging techniques in a living animal or the axons of a particular set of neurons for labeling studies. By characterizing specific synaptic pathways in isolation using electrophysiological recordings, it has been shown that the synapses in the infragranular layers also exhibit experience-dependent plasticity (Petrus et al., 2011; Jacob et al., 2012; Arami et al., 2013).

Attempts to evaluate the synaptic changes occurring throughout the cortical column by analyzing each cortical layer have been carried out previously. Traditional electron microscopy studies for developmental changes (De Felipe et al., 1997; Huttenlocher and Dabholkar, 1997; Peters et al., 2008) uncovered that different cortical layers, though following the same broad trends, varied slightly in their development with supragranular layers exhibiting high rates of synapse growth and their subsequent pruning as compared to infragranular layers. Layer specific differences were more evident with experience-dependent plasticity. Prolonged whisker deprivation resulted in higher density of inhibitory synapses specifically in L4 of rats (Micheva and Beaulieu, 1995). Recently, by using *in vitro* imaging of dendritic spine motility, it was established that spines of L5 apical dendrites showed plasticity only if they were located outside L4 (Oray et al., 2004). L6 synapses exhibit synaptic strengthening or weakening depending in response to same sensory experience based on the developmental state of circuit (Petrus et al., 2011). These location-specific synaptic changes draw attention to the different inputs that form the synapses in these cortical layers.

Thus, we developed a technique that could identify synapses and analyze their properties in an unbiased and high-throughput fashion. This allows the study of synaptic changes over an entire circuit, say a cortical column as in this study and can be compared across various conditions like age, sensory or learning experience, and disease. Using this technique, we made two novel discoveries. We discovered bidirectional changes in synaptic density in L6 depending upon the developmental state of the circuit, in response to the same altered whisker experience. We also uncovered an onset of a phase wherein L5A synapses undergo rapid (within 24hr) strengthening in response to SRE. In addition to these novel findings, the technique faithfully reproduced the closure of the CP of L2/3 synapses in P18 animals and also the pattern of synapse density changes in the different cortical layers during development.

### **Future endeavours**

The rich dataset of synaptic properties from each cortical layer opens up a number of avenues to further explore the effect of altered sensory experience.

#### *Excitatory vs Inhibitory synapses*

Numerous studies have made it clear that experience-dependent changes are not restricted to excitatory synapses (Micheva and Beaulieu, 1995; Gaiarsa et al., 2002; Knott et al., 2002; Katzel and Miesenbock, 2014). Thus, one of the major steps would be to use morphological features to identify excitatory and inhibitory synapses from the EPTA images of synapses. It has long been established in the field of conventional EM that excitatory synapses are characterized by an asymmetrical appearance while inhibitory synapses appear more symmetrical in EM images. In fact, the seminal work describing the two types of synapses, namely Gray Type I

synapse and Gray Type II synapse, in neuronal circuits for the first time used EPTA to highlight the differences between these synapses (Gray, 1959). Given that, the tissue preparation protocol we used was slightly different, it needs to be established if this relation between morphological features and functional identity of synapses holds in our tissue as well. This could be achieved by performing immunogold labeling using gold-tagged antibodies targeting markers of excitatory synapses, namely glutamate and those of inhibitory synapses, like gephyrin. This would identify excitatory and inhibitory synapses in the EPTA images and help isolate the morphological features that distinguish them from each other. Following this, the machine-learning algorithm could be trained to classify synapses based on these features thereby providing information about synaptic changes occurring in both excitatory and inhibitory synapses in a high-throughput fashion.

#### *Critical period plasticity*

In this study, we primarily analyzed rapid experience-dependent synaptic changes at specific time points during development. While L2/3 and L5 synapses have been known to exhibit plasticity well into adulthood (Cheetham et al., 2007; Bruno et al., 2009; Jacob et al., 2012), synaptic changes to short durations of altered sensory experience have been observed to be restricted to specific ages, called CP plasticity (Clem and Barth, 2006; Wen and Barth, 2011). Our data successfully recapitulates the CP plasticity and the subsequent closure of CP of L2/3 synapses as reported by electrophysiological experiments. Our results regarding L5A synapses point towards a potential CP for these synapses with an onset around PND 18. Further experiments would be necessary to determine if there is a developmental time point after which this plasticity ceases to occur.

Moreover, the apparent serial progression of CP starting from L4, moving to L2/3 and then potentially L5A raises intriguing questions. The current theory is that maturation of sensory responses in the specific set of neurons marks the onset of the CP for those synapses (Wen and Barth, 2011). It would be interesting to test this hypothesis by determining if the maturation of sensory responses in L5A neurons coincide with the CP we discovered.

The bidirectional plasticity in L6 raises intriguing questions as well. Do the same synapses undergo plasticity at the two time points? Are the target cells different or the same at the two time points? Finally, how does this plasticity affect the processing of incoming sensory input by the cortical circuit? Previous work has revealed that L6 neurons function modulate the orientation tuning selectivity of L2/3 neurons in the visual cortex (Olsen et al., 2012), acting as a gain control to the responses of these neurons. It is possible that L6 neurons in barrel cortex have a similar function which might necessitate bidirectional plasticity based on the developmental state of the circuit. It would be interesting to compare the effect on L2/3 and L5 neuronal responses to whisker stimulation in control and 24h SRE animals, with and without stimulation, say by optogenetic approaches, of L6 neurons. Such an experiment could test the hypothesis that the plasticity in the two directions enables L6 neurons to maintain homeostasis in the cortical circuit in the barrel column.

### **Potential applications of the technique**

Our results clearly show that a high-throughput analysis of synaptic changes can uncover novel loci of synaptic plasticity and can help guide subsequent targeted experiments like electrophysiological recordings to further characterize the observed changes. Due to the unbiased

and high-throughput nature, the technique could be employed to characterize synaptic properties across various conditions like genetic background as in the case of transgenic animals, in disease conditions as in the case of Alzheimer's disease or autism spectrum disorders (ASD) and to characterize the effects of potential pharmacological interventions for such diseases.

A recent study discovered that both increased and decreased functional connectivity could be observed in the brains of high-functioning autistic adults (Hahamy et al., 2015). Morphological correlates of connectivity, namely spine or synapse density, might be affected in the same way. Thus, it would be necessary to utilize a high-throughput technique to assess changes in connectivity in ASD, characterize animal models for ASD and subsequently test efficacy of therapeutical interventions for these disorders.

## Appendix A. Average synapse density in unit volume of cortex

Various papers have addressed the issue of estimating synaptic density in a unit volume of tissue from synapse density obtained from electron microscopy images which are inherently two-dimensional in nature (Mayhew, 1979; Sterio, 1984; Colonnier and Beaulieu, 1985). One of the most commonly used methods is the disector method. This method requires serial sections of the tissue. One of the sections is used as the reference section and the subsequent adjacent section is used as the look-up section. This method uses the formula,  $N_V = \Sigma Q/a \times h$ , where  $\Sigma Q$  is the number of synapses that appear in the reference section but not in the look-up section,  $a$  is the sampled area and  $h$  is the thickness of the sections (Sterio, 1984). The other most prevalent method is the size-frequency method which utilizes the formula,  $N_V = N_A/d$ , where  $N_A$  is the number of synapses in a unit area and  $d$  is the average length of these synapses (Colonnier and Beaulieu, 1985). The advantage of the latter method is that it does not require imaging serial sections of the tissue. A systematic comparison of the synaptic density estimates provided by these two techniques revealed that they were quite comparable and that the latter method generated more reliable estimates with low variability (DeFelipe et al., 1999a).

Using the size-frequency method for our dataset of synapse densities obtain per image, we estimated the synapse density in a unit volume of cortex (Table A1). We obtained an estimated synapse density of about 1 synapse per  $\mu\text{m}^3$ . This is in accordance with measurements obtained by other studies that have either used synapse detection ( $0.94 \pm 0.12$  synapses per  $\mu\text{m}^3$ ) in volumetric reconstructions of cortical tissue using EM tomography (Merchan-Perez et al., 2014) or employed statistical estimates of dense connectome in the rat barrel cortex (Egger et al., 2014).

**Table A1: Synapse density per unit volume of cortex estimated by size-frequency method**

<b>Layers</b>	<b>Mean synapse density (per <math>\mu\text{m}^2</math>)</b>	<b>Mean synapse length (<math>\mu\text{m}</math>)</b>	<b>Mean synapse density (per <math>\mu\text{m}^3</math>)</b>	<b>Laminar heights (<math>\mu\text{m}</math>)</b>	<b>Laminar volumes (<math>\times 10^6 \mu\text{m}^3</math>)</b>	<b>Number of synapses (<math>\times 10^6</math>)</b>
L1	0.2470	0.2308	1.070	100	7.1	7.60
L2	0.2484	0.2214	1.122	150	10.6	11.89
L3	0.2542	0.2211	1.150	150	10.6	12.19
L4	0.2364	0.2287	1.034	200	14.1	14.58
L5A	0.2583	0.2306	1.120	100	7.1	7.96
L5B	0.2222	0.2303	0.965	200	14.1	13.61
L6	0.2347	0.2362	0.994	250	17.7	17.59

## Appendix B. Inter-animal variability

Individual animals can differ in their synapse densities due to various factors. Gender differences have been shown to result in higher synapse density in male humans (Alonso-Nanclares et al., 2008). In addition to gender differences, there could be substantial differences in the development of individual animals. Even within the same litter, wherein all the pups are born within minutes of each other, a few individual animals could lag behind in overall development (Fig. B1). This could be the result of prenatal litter size which contributes most to variation in bod size of the pups (Leamy and Zhang, 1993), intrauterine variations in access to nutrients or hormones (Lathe, 2004) or subsequent postnatal effects of litter size on development (Wainwright et al., 1989). Such differences between individual animals could result in developmentally regulated processes like synapse density while generating no discernible differences in behavior (Wainwright et al., 1989).



**Figure B1. Differences in body size, a correlate of overall development of animals from the same litter.**

## **Appendix C. Increase in mEPSC frequency in L2 pyramidal neurons following 24h SRE**

Given that we observed a 25% increase in synapse density in L2 in the spared barrel column following 24h SRE, we carried out targeted electrophysiological recordings in L2 pyramidal neurons to determine whether we observe a corresponding functional change, i.e., an increase in the frequency of spontaneous synaptic events. Other groups have observed a direct correlation between spine (MacAskill et al., 2014) or excitatory synapse (Spiegel et al., 2014) density with frequency of excitatory synaptic events. We analyzed both spontaneous excitatory and inhibitory post synaptic currents (mEPSCs and mIPSCs; Audette NJ, unpublished data).

We found that there was a significant increase in the frequency of spontaneous excitatory synaptic events in L2 pyramidal neurons in the spared barrel column (mean mEPSC frequency = 2.36 Hz, SD = 0.65 Hz) as compared to those in the control barrel column (mean mEPSC frequency = 1.16 Hz, SD = 0.19 Hz; Student t-test,  $p = 0.008$ ) but not in the case of the frequency of inhibitory events (mIPSC frequency in control barrel columns, mean = 1.47 Hz, SD = 0.24 Hz; mIPSC frequency in spared barrel column, mean = 1.62 Hz, SD = 0.57 Hz; Fig C1). Thus, targeted electrophysiological experiments revealed an increase in frequency of synaptic events in line with the EM observations. But, the change in frequency of synaptic events is restricted to excitatory synapses and the magnitude of the increase is much larger than that predicted by the increase in synapse density.

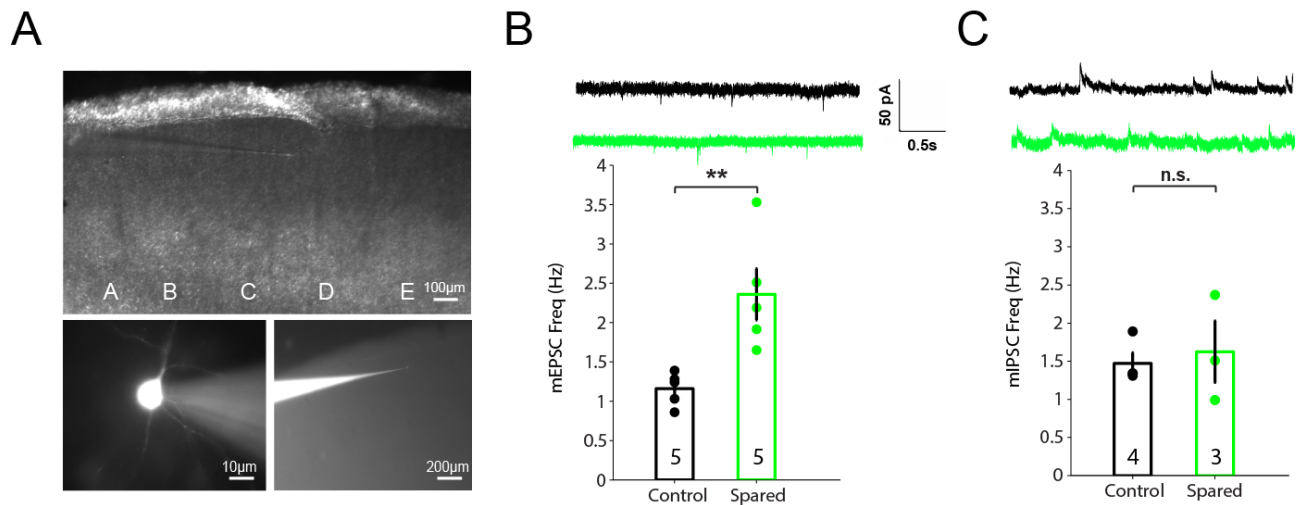


**Figure C1. mEPSC frequency shows a significant increase in L2 pyramidal neurons in the spared barrel column**

- A. Top panel shows an example cortical tissue with the 5 barrel rows identified. Bottom left panel shows an example L2 pyramidal neuron filled with the fluorescent dye, Alexa 594. Bottom right panel shows the recording electrode with the fluorescent dye targeting an L2 pyramidal neuron.
- B. Top panels show example traces with spontaneous excitatory synaptic events in a L2 pyramidal neuron from control (black) and spared (green) barrel column. Bottom panel shows the mean frequency of excitatory synaptic events in L2 pyramidal neurons from control and spared barrel columns. Error bars indicate SEM. \*\* $p < 0.01$ , Student t-test.
- C. Top panels show example traces with spontaneous inhibitory synaptic events in a L2 pyramidal neuron from control (black) and spared (green) barrel column. Bottom panel shows the mean frequency of inhibitory synaptic events in L2 pyramidal neurons from control and spared barrel columns. Error bars indicate SEM. n.s. – not significant, Student t-test.

A number of factors could be contributing to result in the discrepancy in the magnitude of the change. Firstly, the synapse density measurements provide only a morphological correlate of synaptic change. But, functional changes like an increase in the release probability of synapses could also occur. Such a change would contribute to the observed increase in synaptic event frequency without a corresponding increase in synapse density. Secondly, the increase in synapse density observed was restricted to L2. Thus, they include only the synapses that exist on the basal dendrites of L2 pyramidal neurons. On the other hand, the electrophysiological recordings

include the changes that might be occurring in the synapses that target the apical dendrites of these neurons. Finally, the EM images cannot determine the target neurons of the L2 synapses. For instance, a correlated decrease in synapse density targeting another specific class of neurons, say PV interneurons, could be occurring. This would result in a lower net increase in synapse density as compared to the increase in density synapses targeting L2 pyramidal neurons.

In spite of these caveats, we can definitely conclude that our technique of high-throughput analysis of synaptic changes could uncover new loci of synaptic plasticity and could subsequently guide targeted experiments for further characterization of these changes.

## Appendix D. Time course of synaptic plasticity

Previous work from the lab has shown that there exist two distinct phases to the synaptic plasticity exhibited by L4-L2/3 synapses in the spared barrel column following SRE. Although L4-L2/3 synapses exhibit strengthening after 24h SRE, it was observed that these synapses were significantly stronger at 12h after onset of SRE than at 24h (Wen et al., 2013). Thus, synaptic plasticity at L4-L2/3 had two distinct phases, a rapid initiation phase spanning the first 12h after SRE onset and a labile phase wherein further experience reduced prior gains in synapse strength. We were interested in determining whether our technique is sensitive enough to capture these changes that targeted a specific class of synapses, namely L4-L2/3 synapses. From the electrophysiological observations, we expected that after 12h SRE, the population of synapses in L2 or L3 would be longer than those after 24h SRE. But, it was unclear whether synapse density, which showed a 20% increase in L2 after 24h SRE, would also exhibit such distinct initiation and labile phases. We restricted our analysis to cortical layers 1 through 4.

We found that while there were no significant differences in synapse density in any of the cortical layers analyzed, L2 and L3, after 12h SRE, showed intermediate levels of synapse density to control and animals that underwent 24h SRE (Fig. D1 B). This suggests that synapse density increases gradually throughout the 24h period of SRE in a monotonic fashion. When we analyzed the length of synapses after 12h SRE, we surprisingly discovered that L2 synapses were significantly shorter in length (Fig. D2 A and B) than control animals. We hypothesized that this might be due to the addition of synapses in L2 as newer synapses are known to be smaller in length and grow in size as they mature functionally (Knott et al., 2006).

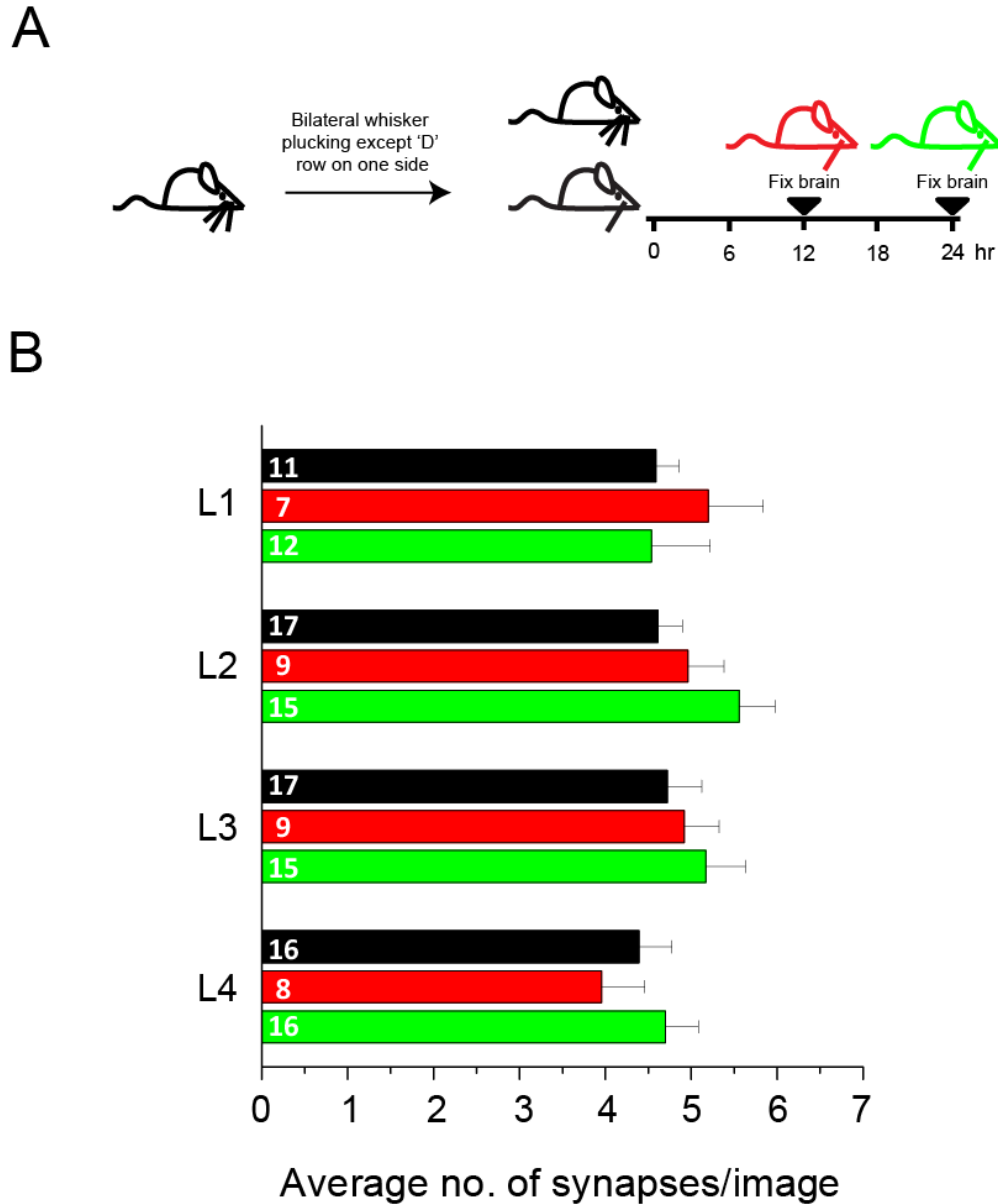


**Figure D1. No significant differences in synapse density in any layer with L2 and L3 showing intermediate levels of synapse density between Control and 24h SRE**

G. Schematic showing the experimental paradigm and timeline of altered sensory experience

H. Average synapse density measured in barrel columns in control animals (black), spared barrel columns from animals after 12h SRE (red) and 24h SRE (green). Numbers indicate number of animals. Error bars indicate SEM.

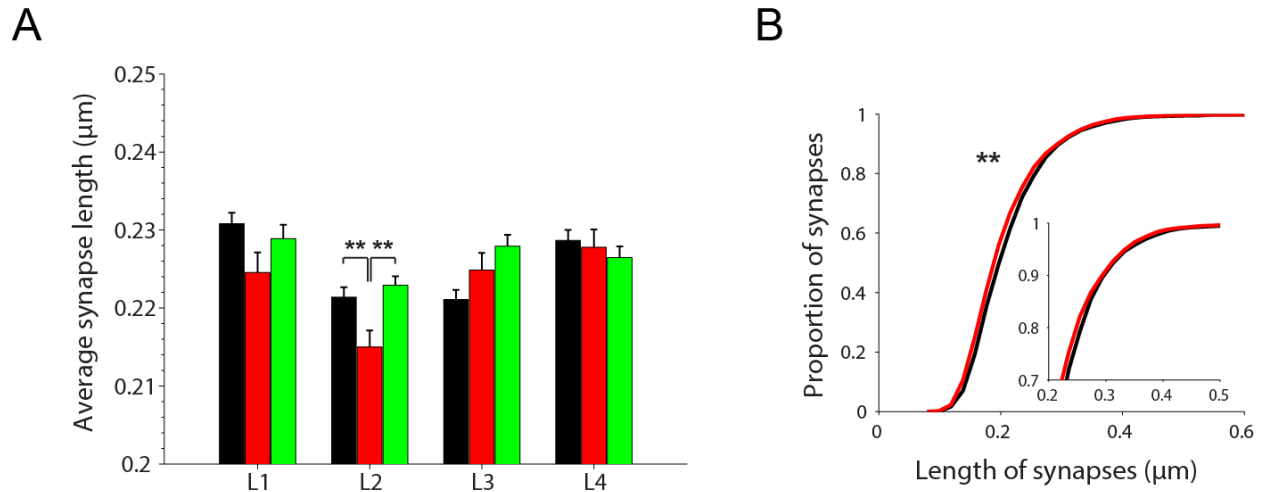


**Figure D2. Synapse length in L2 decreases significantly after 12h SRE**

- E. Average synapse length measured in each cortical layer in control (black) and spared (green) barrel columns. \*\* indicates  $p < 0.01$  by 2-way ANOVA –  $F(1,6) = 4.07$  and post-hoc Tukey HSD test. Numbers of synapses detected in each layer in the spared barrel column of animals that underwent 12h SRE were as follows, L1 – 1909 synapses from 5 animals, L2 – 2106 synapses from 7 animals, L3 – 2108 synapses from 7 animals and L4 – 1449 synapses from 6 animals.
- F. Cumulative histogram of synapse length in L3 from control (black) and spared (red) animals after 12h SRE. \*\* indicates  $p < 0.01$ , 2-sample K-S test with Bonferroni correction for multiple comparison.

Further characterization of the distinct phases of synaptic plasticity revealed that the weakening of synapses during the labile phase was dependent on N-methyl-D-aspartate (NMDA) receptors. This was ascertained by blocking these receptors by administering, by intra-peritoneal injection, 3-(2-Carboxypiperazin-4-yl)propyl-1-phosphonic acid (CPP), an NMDAR antagonist, after 12h of SRE onset which prevented the reduction in synaptic strength that was observed in the labile phase (Wen et al., 2013). Again, we used to our technique to study the effect of NMDAR antagonist on the synaptic changes occurring in the L1-4. We were particularly interested in how synaptic density and synaptic strength were regulated during SRE and the role of NMDARs in this regulation. We hypothesized that synapses in L2 or L3 in CPP-administered

animals would be on average longer than those in animals that underwent SRE but without CPP injection.

CPP injection at 12h after SRE onset did not affect the change in synapse density in any cortical layers and were similar to those observed in animals undergoing SRE and did not receive CPP, especially in L2 and L3 (Fig. D3 B). Since at 12h after SRE, synapse density values are at intermediate levels between control and 24h SRE values, it suggests that NMDAR activity after the 12h time point since SRE onset is not necessary for the generation of new synapses in response to altered sensory experience.

When we analyzed the length of synapses after CPP administration, we found that synapse lengths were indistinguishable from those in animals that did not receive CPP and underwent 24h SRE (Fig. D4 A). Surprisingly we observed a significant decrease in synapse lengths in L4 upon CPP administration as compared to control animals (Fig. D4 B).

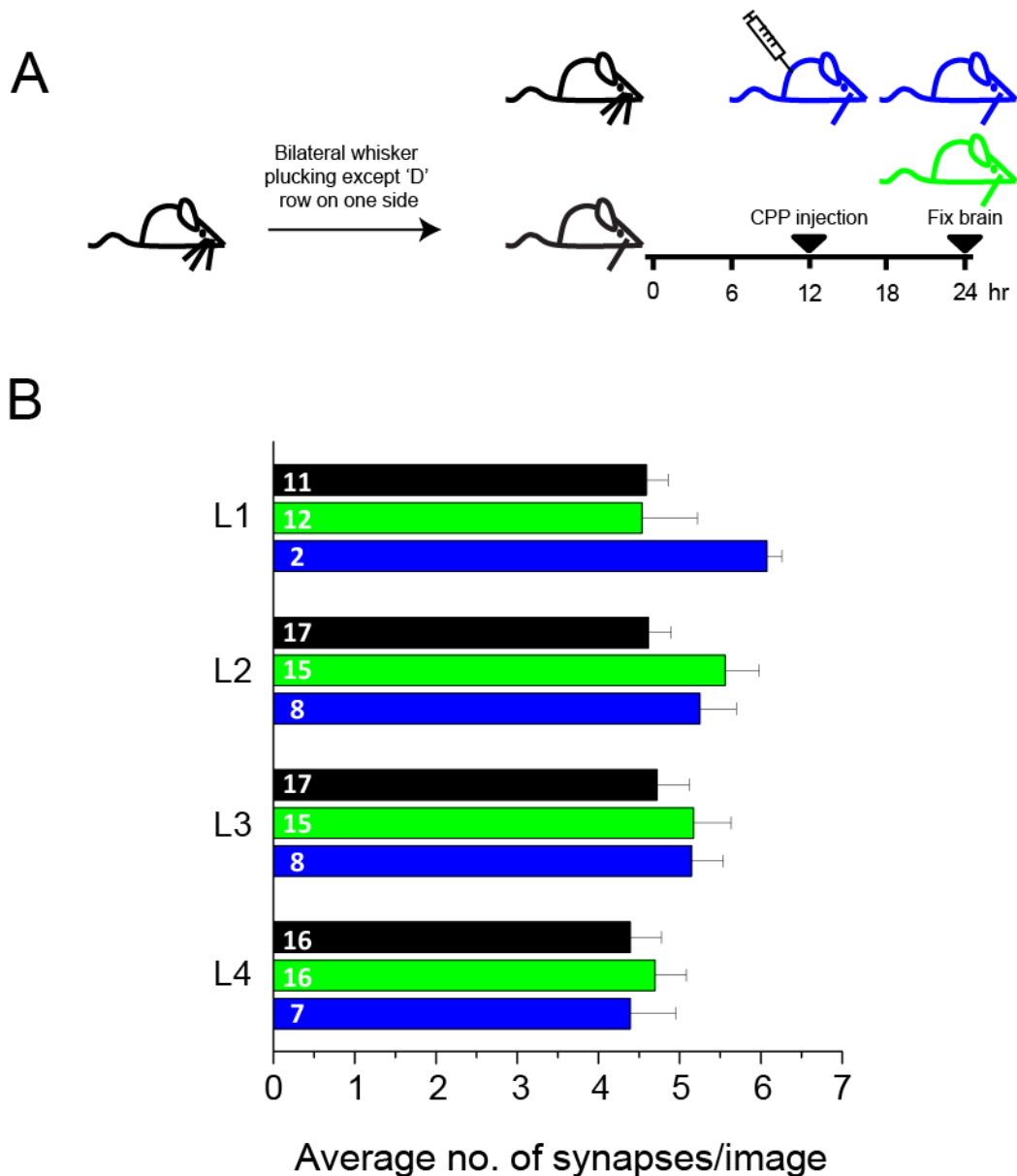


**Figure D3. No significant differences in synapse density in any layer with L2 and L3 showing intermediate levels of synapse density between Control and 24h SRE**

- A. Schematic showing the experimental paradigm and timeline of altered sensory experience. CPP was administered at 12h after SRE onset and all animals were sacrificed at 24h after SRE onset.
- B. Average synapse density measured in barrel columns from control animals (black), spared barrel columns from 24h SRE animals (green) and animals that received CPP administration at 12h after onset of SRE (blue). Numbers indicate number of animals, Error bars indicate SEM.

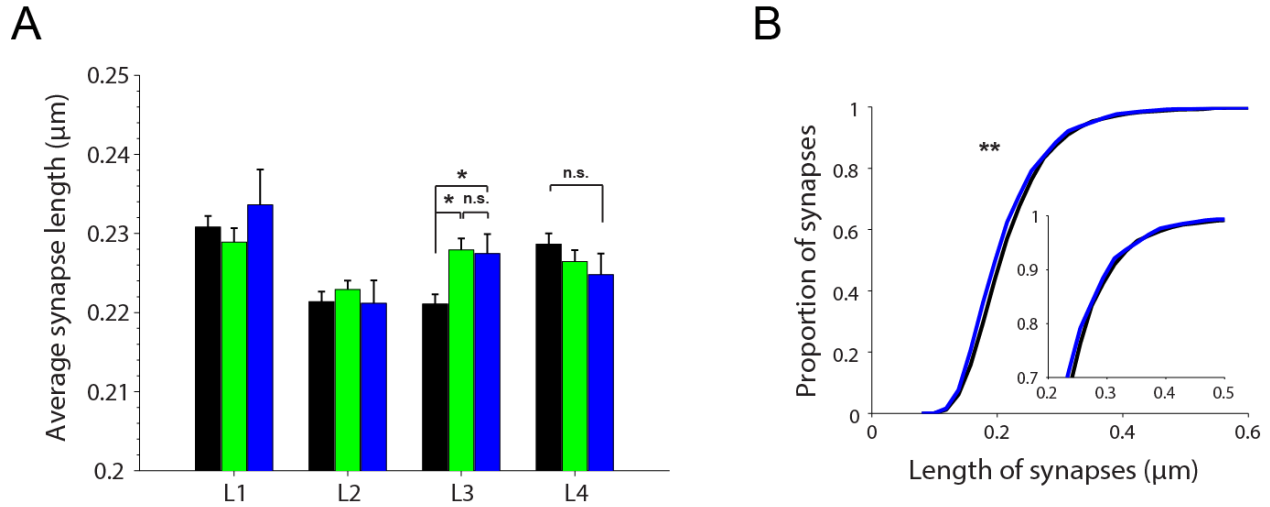


**Figure D4. Synapse length in L4 decreases significantly after CPP administration at 12h after SRE onset**

- A. Average synapse length measured in each cortical layer in control (black) and spared barrel columns with (blue) and without (green) administration of CPP at 12h after SRE onset. \* indicates  $p < 0.05$  by 2-way ANOVA –  $F(1,6) = 4.12$  and post-hoc Tukey HSD test. Numbers of synapses detected in each layer in the spared barrel column of animals that underwent 12h SRE were as follows, L1 – 713 synapses from 2 animals, L2 – 1849 synapses from 6 animals, L3 – 2000 synapses from 7 animals and L4 – 1551 synapses from 7 animals.
- B. Cumulative histogram of synapse length in L4 from control (black) and spared (blue) animals that received CPP administration at 12h after onset of SRE. \*\* indicates  $p < 0.01$ , 2-sample K-S test with Bonferroni correction for multiple comparison

## Appendix E. Synapse density measurements

Table E1. Synapse density measurements in 'D' barrel column for control animals at P14

Controls (P14)		L1			L2			L3			L4			L5A			L5B			L6		
		Precision	Mean	Mean x Prec x 2	Precision	Mean	Mean x Prec x 2	Precision	Mean	Mean x Prec x 2	Precision	Mean	Mean x Prec x 2	Precision	Mean	Mean x Prec x 2	Precision	Mean	Mean x Prec x 2	Precision	Mean	Mean x Prec x 2
4/3/2013	P-1796-2d				0.52	2.62	2.71	0.71	2.21	3.13	0.50	6.04	6.04									
	P-1796-4d				0.77	2.76	4.22	0.60	4.69	5.62	0.91	1.04	1.90									
4/24/2013	P-1808-1d				0.62	5.38	6.68	0.46	6.67	6.11	0.73	2.49	3.65									
	P-1808-2d				0.81	2.51	4.05	0.76	1.76	2.68	0.44	4.15	3.68									
	P-1808-3d				0.32	4.74	3.06	0.63	2.20	2.75	0.33	2.98	1.99									
5/16/2013	P-1809-1d	0.91	2.59	4.70	0.92	2.90	5.33	0.95	1.98	3.75	0.81	2.58	4.19									
	P-1809-2d	0.77	3.60	5.58	0.93	2.42	4.49	0.90	1.56	2.81	0.80	2.50	3.99									
	P-1809-3d				0.39	3.98	3.08	0.88	2.68	4.71	0.78	3.61	5.61									
	P-1809-4d	0.76	3.33	5.09	0.78	3.99	6.21	0.88	2.94	5.15	0.86	1.95	3.34									
6/9/2013	P-1820-1d	0.93	3.35	6.19	0.72	3.56	5.11	0.90	3.47	6.27												
	P-1820-2d	0.87	2.68	4.66	0.84	3.57	5.99	0.97	4.15	8.04	0.88	2.52	4.42									
	P-1820-3d	0.87	2.83	4.91	0.96	2.42	4.63	0.95	3.00	5.70	0.90	4.33	7.79									
11/28/2013	P-1839-1d	0.89	1.72	3.08	0.61	3.40	4.14	0.71	4.14	5.91	0.64	3.79	4.86	0.85	3.29	5.59	0.57	3.69	4.19	0.33	9.00	6.00
	P-1839-2d	1.00	1.93	3.87	0.95	2.93	5.56	0.79	3.15	4.96	0.83	3.29	5.42	0.69	3.90	5.38	0.80	2.73	4.36	0.83	2.67	4.41
	P-1839-3d	0.88	2.71	4.75	0.89	2.50	4.44	0.81	3.89	6.27	0.77	3.79	5.87	0.61	3.83	4.67	0.54	4.64	5.00	0.46	4.34	4.02
2/24/2014	P-1851-1d	0.69	2.61	3.60	0.82	2.12	3.49	0.11	9.75	2.08	0.41	3.82	3.14	0.86	2.50	4.29	0.43	3.20	2.74	0.51	3.53	3.64
	P-1851-2d	0.93	2.17	4.06	0.40	6.56	5.25	0.93	2.34	4.33	0.88	2.50	4.38	0.80	2.66	4.26	0.67	3.54	4.72	0.69	3.43	4.73
	P-1851-3d													0.81	2.85	4.61	0.75	2.51	3.76	0.93	1.81	3.36
<b>Mean</b>		3.06	4.59		3.43	4.61		3.56	4.72		3.21	4.39		3.17	4.80		3.38	4.13		4.13	4.36	
<b>SD</b>		0.41	0.59		1.20	1.15		2.04	1.65		1.16	1.53		0.60	0.56		0.77	0.80		2.53	0.94	

Table E2. Synapse density measurements in ‘D’ barrel column for animals at P14 after 24h SRE

24h SRE Spared (P14)	L1			L2			L3			L4			L5A			L5B			L6			
	Precision	Mean	Mean x Prec x 2	Precision	Mean	Mean x Prec x 2	Precision	Mean	Mean x Prec x 2	Precision	Mean	Mean x Prec x 2	Precision	Mean	Mean x Prec x 2	Precision	Mean	Mean x Prec x 2	Precision	Mean	Mean x Prec x 2	
4/3/2013 P-1796-3d																						
P-1796-5d				0.70	3.25	4.55	0.69	1.99	2.75	0.78	1.81	2.81										
4/24/2013 P-1808-4d				0.63	3.69	4.62	0.79	2.35	3.71	0.72	1.53	2.20										
P-1808-5d				0.86	3.56	6.12	0.77	2.75	4.26	0.66	3.41	4.49										
P-1808-6d				0.93	2.18	4.05	0.79	1.66	2.62	0.89	2.93	5.20										
5/16/2013 P-1809-5d	0.53	3.92	4.18	0.70	2.46	3.45	0.74	2.66	3.92	0.70	3.10	4.32										
P-1809-6d	0.22	3.87	1.70	0.83	3.07	5.11	0.82	2.58	4.25	0.64	1.73	2.23										
P-1809-7d	0.62	3.39	4.20	0.78	5.22	8.12				0.60	4.14	4.97										
P-1809-8d	0.95	3.73	7.12	0.96	3.35	6.43	0.92	4.11	7.56	0.83	2.70	4.49										
6/9/2013 P-1820-4d	0.84	6.08	10.25	0.94	3.84	7.24	0.51	6.76	6.91	0.67	5.10	6.81										
P-1820-6d	0.87	3.17	5.53	0.94	3.66	6.88	0.68	4.27	5.82	0.94	2.82	5.32										
11/28/2013 P-1839-4d	0.75	2.99	4.49	1.00	2.28	4.55	0.91	3.38	6.17	0.82	3.60	5.93	0.96	2.89	5.56	0.96	2.02	3.88	0.93	1.93	3.59	
P-1839-5d	0.96	2.53	4.86	0.76	5.19	7.87	0.68	6.40	8.67	0.85	4.21	7.15	0.59	4.78	5.64	0.78	3.37	5.28	0.68	2.83	3.87	
P-1839-6d	0.55	1.77	1.95	0.84	2.00	3.37	0.88	3.06	5.35	0.89	3.46	6.19	0.76	3.25	4.93	0.83	1.62	2.70	0.89	1.91	3.39	
P-1839-7d	0.81	2.55	4.15	0.62	5.71	7.08	0.80	4.21	6.73	0.43	6.07	5.23	0.88	2.71	4.74	0.78	1.59	2.47	0.19	2.20	0.85	
2/24/2014 P-1851-4d																						
P-1851-5d	0.69	1.68	2.33				0.65	3.93	5.08	0.81	3.20	5.16	0.96	2.35	4.50	0.50	4.04	4.04	1.00	1.52	3.04	
P-1851-6d	0.80	2.31	3.70	0.92	2.13	3.92	0.84	2.23	3.74	1.00	1.33	2.65	0.71	1.23	1.76	0.80	1.70	2.72	0.63	1.82	2.27	
<b>Mean</b>		3.17	4.54		3.44	5.56		3.49	5.17		3.20	4.70		2.87	4.52		2.39	3.52		2.03	2.84	
<b>SD</b>		1.19	2.36		1.18	1.63		1.50	1.79		1.29	1.54		1.16	1.43		1.05	1.09		0.45	1.12	

Table E3. Synapse density measurements in 'D' barrel column for animals after 12h SRE

12h SRE Spared		L1			L2			L3			L4		
		Precision	Mean	Mean x Prec x 2	Precision	Mean	Mean x Prec x 2	Precision	Mean	Mean x Prec x 2	Precision	Mean	Mean x Prec x 2
6/20/2013	P-1822-6d	0.83	3.10	5.13	0.95	1.78	3.37	0.87	1.99	3.46	0.93	1.15	2.14
	P-1822-7d	0.76	2.95	4.47	0.93	2.33	4.34	0.73	2.94	4.29	0.59	2.61	3.09
	P-1822-8d	0.95	1.87	3.58	0.85	3.87	6.57	0.90	2.91	5.24	0.75	2.81	4.21
8/9/2013	P-1833-4d				0.62	3.41	4.23	1.00	1.72	3.45	0.75	1.55	2.32
	P-1833-5d	0.27	5.12	2.77	0.74	2.97	4.41	0.68	3.23	4.37			
	P-1833-6d				0.77	2.36	3.65	0.94	2.36	4.46	0.67	3.09	4.12
12/5/2013	P-1841-1d												
	P-1841-2d												
	P-1841-3d	0.97	3.49	6.77	0.97	3.45	6.67	0.78	3.65	5.71	0.96	2.33	4.45
	P-1841-4d	0.86	3.78	6.51	0.94	2.69	5.08	0.92	3.56	6.58	0.86	2.76	4.73
	P-1841-5d	0.85	4.19	7.16	0.97	3.24	6.31	0.84	4.01	6.71	0.97	3.38	6.55
<b>Mean</b>			3.50	5.20		2.90	4.96		2.93	4.92		2.46	3.95
<b>SD</b>			1.02	1.69		0.67	1.26		0.78	1.22		0.76	1.43

Table E4. Synapse density measurements in 'D' barrel column for control animals at P14 after 24h SRE and CPP injection at 12h after SRE onset

24h SRE Spared + CPP Injection		L1			L2			L3			L4		
		Precision	Mean	Mean x Prec x 2	Precision	Mean	Mean x Prec x 2	Precision	Mean	Mean x Prec x 2	Precision	Mean	Mean x Prec x 2
6/20/2013	P-1822-3d				0.90	2.73	4.89	0.94	3.36	6.32	0.85	2.32	3.94
	P-1822-4d				1.00	1.75	3.50	0.95	2.25	4.28	0.88	3.61	6.37
	P-1822-5d				0.85	4.35	7.42	0.93	2.87	5.36			
8/9/2013	P-1833-1d				0.95	2.56	4.84	0.82	2.14	3.51	0.34	3.88	2.67
	P-1833-2d				0.88	2.55	4.46	0.96	2.78	5.33	0.55	2.95	3.22
	P-1833-3d				0.83	3.24	5.35	0.84	2.80	4.71	0.91	1.92	3.49
4/3/2014	P-1855-3d	0.85	3.45	5.89	0.65	5.18	6.78	0.96	2.42	4.65	0.76	3.07	4.70
	P-1855-5d	0.89	3.51	6.26	0.71	3.32	4.74	0.64	5.45	6.98	0.87	3.66	6.37
<b>Mean</b>						3.21	5.25		3.01	5.14		3.06	4.39
<b>SD</b>						1.10	1.27		1.06	1.12		0.73	1.49

Table E5. Synapse density measurements in 'D' barrel column for control animals at P18

Controls (P18)		L1			L2			L3			L4			L5A			L5B			L6		
		Precision	Mean	Mean x Prec x 2	Precision	Mean	Mean x Prec x 2	Precision	Mean	Mean x Prec x 2	Precision	Mean	Mean x Prec x 2	Precision	Mean	Mean x Prec x 2	Precision	Mean	Mean x Prec x 2	Precision	Mean	Mean x Prec x 2
2/5/2014	P-1846-1d				0.50	6.31	6.31	0.73	4.51	6.60	0.95	3.39	6.46	0.92	2.86	5.25	0.89	2.54	4.51	0.52	2.38	2.49
	P-1846-2d	0.74	5.26	7.78	0.69	4.81	6.59	0.86	2.75	4.71	0.65	4.14	5.41	0.54	5.14	5.58	0.86	2.30	3.96	0.86	2.00	3.45
5/22/2014	P-1866-1d	0.36	8.46	6.02	0.71	4.92	7.00	0.73	3.42	4.99	0.45	5.79	5.22	0.91	3.32	6.03	0.79	2.67	4.22	0.65	2.75	3.55
	P-1866-2d	0.71	5.39	7.63	0.68	5.05	6.89	0.66	4.65	6.14	0.67	4.89	6.51	0.83	3.92	6.54	0.52	7.54	7.88	0.42	6.57	5.49
	P-1866-3d	0.55	4.99	5.49	0.47	5.16	4.80	0.78	3.98	6.24	0.78	3.51	5.45	0.45	5.39	4.83	0.70	4.30	6.04	0.75	3.17	4.75
	P-1866-4d	0.38	5.87	4.45	0.40	5.03	4.02	0.58	5.23	6.03	0.62	3.45	4.29	0.45	4.73	4.22	0.49	3.95	3.87	0.41	3.30	2.68
7/11/2014	P-1891-1d	0.70	6.28	8.75	0.90	3.88	7.02	0.80	4.17	6.67	0.72	4.41	6.34	0.80	3.93	6.29	0.91	3.35	6.11	0.81	2.35	3.81
	P-1891-2d																					
	P-1891-3d	0.78	3.89	6.10	0.97	3.19	6.16	1.00	3.79	7.58	0.88	3.02	5.29	0.81	4.44	7.15	0.63	3.50	4.38	0.30	6.16	3.67
<b>Mean</b>			5.74	6.60		4.79	6.10		4.06	6.12		4.07	5.62		4.22	5.74		3.77	5.12		3.58	3.74
<b>SD</b>			1.42	1.50		0.92	1.11		0.77	0.92		0.93	0.77		0.87	0.96		1.68	1.42		1.77	0.99

Table E6. Synapse density measurements in 'D' barrel column for animals at P18 after 24h SRE

24h SRE Spared (P18)	L1			L2			L3			L4			L5A			L5B			L6		
	Precision	Mean	Mean x Prec x 2	Precision	Mean	Mean x Prec x 2	Precision	Mean	Mean x Prec x 2	Precision	Mean	Mean x Prec x 2	Precision	Mean	Mean x Prec x 2	Precision	Mean	Mean x Prec x 2	Precision	Mean	Mean x Prec x 2
2/5/2014 P-1846-3d	0.52	5.84	6.12	0.60	4.83	5.84	0.57	3.68	4.21	0.81	3.54	5.72	0.97	2.28	4.41	0.87	2.56	4.46	0.96	2.55	4.90
P-1846-4d				0.63	4.99	6.24	0.73	3.70	5.43	0.89	3.16	5.62	0.93	2.91	5.41	0.85	2.98	5.08	0.94	3.01	5.64
P-1846-5d																					
5/22/2014 P-1866-5d	0.58	4.68	5.41	0.51	6.49	6.58	0.64	4.40	5.65	0.60	4.57	5.44	0.62	4.65	5.78	0.42	6.68	5.55	0.53	5.27	5.63
P-1866-6d	0.80	3.33	5.36	0.76	2.96	4.48	0.61	4.97	6.10	0.76	3.24	4.91	0.46	6.01	5.52	0.86	2.46	4.24	0.71	3.08	4.34
P-1866-7d	0.83	4.14	6.89	0.89	3.72	6.63	0.88	3.17	5.57	0.94	3.45	6.51	0.88	3.02	5.31	0.79	4.75	7.52	0.78	2.98	4.64
P-1866-8d	0.55	5.04	5.50	0.72	4.61	6.61	0.65	5.17	6.72	0.55	4.04	4.44	0.67	5.21	7.00	0.68	3.98	5.44	0.55	4.96	5.48
7/11/2014 P-1891-4d	0.80	3.81	6.10	0.85	4.71	8.00	0.88	2.73	4.80	0.94	3.01	5.68	0.82	3.19	5.22	1.00	2.31	4.61	1.00	1.77	3.54
P-1891-5d	0.94	2.62	4.94	0.82	5.18	8.50	0.97	2.51	4.85	0.81	4.23	6.81	0.91	2.48	4.52	0.95	1.93	3.69	0.93	2.66	4.97
P-1891-6d																					
<b>Mean</b>		4.21	5.76		4.69	6.61		3.79	5.42		3.65	5.64		3.72	5.40		3.46	5.07		3.29	4.89
<b>SD</b>		0.95	0.65		1.04	1.24		0.99	0.79		0.56	0.77		1.38	0.80		1.60	1.17		1.21	0.72

## References

- Adesnik H, Scanziani M. 2010. Lateral competition for cortical space by layer-specific horizontal circuits. *Nature* 464:1155-1160.
- Allen CB, Celikel T, Feldman DE. 2003. Long-term depression induced by sensory deprivation during cortical map plasticity in vivo. *Nature neuroscience* 6:291-299.
- Alonso-Nanclares L, Gonzalez-Soriano J, Rodriguez JR, DeFelipe J. 2008. Gender differences in human cortical synaptic density. *Proceedings of the National Academy of Sciences of the United States of America* 105:14615-14619.
- Antonini A, Fagiolini M, Stryker MP. 1999. Anatomical correlates of functional plasticity in mouse visual cortex. *The Journal of neuroscience : the official journal of the Society for Neuroscience* 19:4388-4406.
- Antonini A, Stryker MP. 1993. Rapid remodeling of axonal arbors in the visual cortex. *Science* 260:1819-1821.
- Arami MK, Sohya K, Sarihi A, Jiang B, Yanagawa Y, Tsumoto T. 2013. Reciprocal Homosynaptic and heterosynaptic long-term plasticity of corticogeniculate projection neurons in layer VI of the mouse visual cortex. *The Journal of neuroscience : the official journal of the Society for Neuroscience* 33:7787-7798.
- Arendt T. 2009. Synaptic degeneration in Alzheimer's disease. *Acta neuropathologica* 118:167-179.

- Aronoff R, Matyas F, Mateo C, Ciron C, Schneider B, Petersen CC. 2010. Long-range connectivity of mouse primary somatosensory barrel cortex. *The European journal of neuroscience* 31:2221-2233.
- Bates CA, Killackey HP. 1985. The organization of the neonatal rat's brainstem trigeminal complex and its role in the formation of central trigeminal patterns. *The Journal of comparative neurology* 240:265-287.
- Bender KJ, Allen CB, Bender VA, Feldman DE. 2006. Synaptic basis for whisker deprivation-induced synaptic depression in rat somatosensory cortex. *The Journal of neuroscience : the official journal of the Society for Neuroscience* 26:4155-4165.
- Benedetti BL, Glazewski S, Barth AL. 2009. Reliable and precise neuronal firing during sensory plasticity in superficial layers of primary somatosensory cortex. *The Journal of neuroscience : the official journal of the Society for Neuroscience* 29:11817-11827.
- Bloom FE, Aghajanian GK. 1966. Cytochemistry of synapses: selective staining for electron microscopy. *Science* 154:1575-1577.
- Bloom FE, Aghajanian GK. 1968. Fine structural and cytochemical analysis of the staining of synaptic junctions with phosphotungstic acid. *Journal of ultrastructure research* 22:361-375.
- Bourgeois JP, Rakic P. 1993. Changes of synaptic density in the primary visual cortex of the macaque monkey from fetal to adult stage. *The Journal of neuroscience : the official journal of the Society for Neuroscience* 13:2801-2820.
- Briggman KL, Bock DD. 2012. Volume electron microscopy for neuronal circuit reconstruction. *Current opinion in neurobiology* 22:154-161.
- Briggs F. 2010. Organizing principles of cortical layer 6. *Frontiers in neural circuits* 4:3.

- Broser P, Grinevich V, Osten P, Sakmann B, Wallace DJ. 2008. Critical period plasticity of axonal arbors of layer 2/3 pyramidal neurons in rat somatosensory cortex: layer-specific reduction of projections into deprived cortical columns. *Cereb Cortex* 18:1588-1603.
- Bruno RM, Hahn TT, Wallace DJ, de Kock CP, Sakmann B. 2009. Sensory experience alters specific branches of individual corticocortical axons during development. *The Journal of neuroscience : the official journal of the Society for Neuroscience* 29:3172-3181.
- Bureau I, von Saint Paul F, Svoboda K. 2006. Interdigitated paralemniscal and lemniscal pathways in the mouse barrel cortex. *PLoS biology* 4:e382.
- Cahill ME, Xie Z, Day M, Photowala H, Barbolina MV, Miller CA, Weiss C, Radulovic J, Sweatt JD, Disterhoft JF, Surmeier DJ, Penzes P. 2009. Kalirin regulates cortical spine morphogenesis and disease-related behavioral phenotypes. *Proceedings of the National Academy of Sciences of the United States of America* 106:13058-13063.
- Caroni P, Donato F, Muller D. 2012. Structural plasticity upon learning: regulation and functions. *Nature reviews Neuroscience* 13:478-490.
- Chao HT, Zoghbi HY, Rosenmund C. 2007. MeCP2 controls excitatory synaptic strength by regulating glutamatergic synapse number. *Neuron* 56:58-65.
- Cheetham CE, Barnes SJ, Albieri G, Knott GW, Finnerty GT. 2014. Pansynaptic enlargement at adult cortical connections strengthened by experience. *Cereb Cortex* 24:521-531.
- Cheetham CE, Hammond MS, Edwards CE, Finnerty GT. 2007. Sensory experience alters cortical connectivity and synaptic function site specifically. *The Journal of neuroscience : the official journal of the Society for Neuroscience* 27:3456-3465.
- Chen CC, Lu J, Zuo Y. 2014. Spatiotemporal dynamics of dendritic spines in the living brain. *Frontiers in neuroanatomy* 8:28.

- Chen JL, Villa KL, Cha JW, So PT, Kubota Y, Nedivi E. 2012. Clustered dynamics of inhibitory synapses and dendritic spines in the adult neocortex. *Neuron* 74:361-373.
- Chklovskii DB, Vitaladevuni S, Scheffer LK. 2010. Semi-automated reconstruction of neural circuits using electron microscopy. *Current opinion in neurobiology* 20:667-675.
- Clem RL, Barth A. 2006. Pathway-specific trafficking of native AMPARs by in vivo experience. *Neuron* 49:663-670.
- Clem RL, Celikel T, Barth AL. 2008. Ongoing in vivo experience triggers synaptic metaplasticity in the neocortex. *Science* 319:101-104.
- Coleman JE, Nahmani M, Gavornik JP, Haslinger R, Heynen AJ, Erisir A, Bear MF. 2010. Rapid structural remodeling of thalamocortical synapses parallels experience-dependent functional plasticity in mouse primary visual cortex. *The Journal of neuroscience : the official journal of the Society for Neuroscience* 30:9670-9682.
- Colonnier M, Beaulieu C. 1985. An empirical assessment of stereological formulae applied to the counting of synaptic disks in the cerebral cortex. *J Comp Neurol* 231:175-179.
- Crair MC, Malenka RC. 1995. A critical period for long-term potentiation at thalamocortical synapses. *Nature* 375:325-328.
- Crocker-Buque A, Brown SM, Kind PC, Isaac JT, Daw MI. 2014. Experience-Dependent, Layer-Specific Development of Divergent Thalamocortical Connectivity. *Cereb Cortex*.
- Daw NW, Fox K, Sato H, Czepita D. 1992. Critical period for monocular deprivation in the cat visual cortex. *Journal of neurophysiology* 67:197-202.
- De Felipe J, Marco P, Fairen A, Jones EG. 1997. Inhibitory synaptogenesis in mouse somatosensory cortex. *Cereb Cortex* 7:619-634.

- de Villers-Sidani E, Chang EF, Bao S, Merzenich MM. 2007. Critical period window for spectral tuning defined in the primary auditory cortex (A1) in the rat. *The Journal of neuroscience : the official journal of the Society for Neuroscience* 27:180-189.
- DeFelipe J, Marco P, Busturia I, Merchan-Perez A. 1999a. Estimation of the number of synapses in the cerebral cortex: methodological considerations. *Cerebral cortex* 9:722-732.
- DeFelipe J, Marco P, Busturia I, Merchan-Perez A. 1999b. Estimation of the number of synapses in the cerebral cortex: methodological considerations. *Cereb Cortex* 9:722-732.
- Diamond ME, Armstrong-James M, Budway MJ, Ebner FF. 1992. Somatic sensory responses in the rostral sector of the posterior group (POm) and in the ventral posterior medial nucleus (VPM) of the rat thalamus: dependence on the barrel field cortex. *The Journal of comparative neurology* 319:66-84.
- Diamond ME, Huang W, Ebner FF. 1994. Laminar comparison of somatosensory cortical plasticity. *Science* 265:1885-1888.
- Dobbing J. 1964. The Influence of Early Nutrition on the Development and Myelination of the Brain. *Proceedings of the Royal Society of London Series B, Containing papers of a Biological character Royal Society* 159:503-509.
- Douglas RJ, Martin KA. 2004. Neuronal circuits of the neocortex. *Annual review of neuroscience* 27:419-451.
- Durbin RM. 1987. Studies on the development and organisation of the nervous system of *Caenorhabditis elegans*. In: Citeseer.
- Egger R, Dercksen VJ, Udvary D, Hege HC, Oberlaender M. 2014. Generation of dense statistical connectomes from sparse morphological data. *Front Neuroanat* 8:129.

- Espinosa JS, Stryker MP. 2012. Development and plasticity of the primary visual cortex. *Neuron* 75:230-249.
- Fagiolini M, Fritschy JM, Low K, Mohler H, Rudolph U, Hensch TK. 2004. Specific GABA<sub>A</sub> circuits for visual cortical plasticity. *Science* 303:1681-1683.
- Fagiolini M, Hensch TK. 2000. Inhibitory threshold for critical-period activation in primary visual cortex. *Nature* 404:183-186.
- Fagiolini M, Pizzorusso T, Berardi N, Domenici L, Maffei L. 1994. Functional postnatal development of the rat primary visual cortex and the role of visual experience: dark rearing and monocular deprivation. *Vision research* 34:709-720.
- Feldman DE. 2009. Synaptic mechanisms for plasticity in neocortex. *Annual review of neuroscience* 32:33-55.
- Feldman DE, Nicoll RA, Malenka RC, Isaac JT. 1998. Long-term depression at thalamocortical synapses in developing rat somatosensory cortex. *Neuron* 21:347-357.
- Feldmeyer D. 2012. Excitatory neuronal connectivity in the barrel cortex. *Frontiers in neuroanatomy* 6:24.
- Feldmeyer D, Egger V, Lubke J, Sakmann B. 1999. Reliable synaptic connections between pairs of excitatory layer 4 neurones within a single 'barrel' of developing rat somatosensory cortex. *The Journal of physiology* 521 Pt 1:169-190.
- Feldmeyer D, Lubke J, Sakmann B. 2006. Efficacy and connectivity of intracolumnar pairs of layer 2/3 pyramidal cells in the barrel cortex of juvenile rats. *The Journal of physiology* 575:583-602.
- Feldmeyer D, Lubke J, Silver RA, Sakmann B. 2002. Synaptic connections between layer 4 spiny neurone-layer 2/3 pyramidal cell pairs in juvenile rat barrel cortex: physiology and

- anatomy of interlaminar signalling within a cortical column. *The Journal of physiology* 538:803-822.
- Feldmeyer D, Roth A, Sakmann B. 2005. Monosynaptic connections between pairs of spiny stellate cells in layer 4 and pyramidal cells in layer 5A indicate that lemniscal and paralemniscal afferent pathways converge in the infragranular somatosensory cortex. *The Journal of neuroscience : the official journal of the Society for Neuroscience* 25:3423-3431.
- Finnerty GT, Roberts LS, Connors BW. 1999. Sensory experience modifies the short-term dynamics of neocortical synapses. *Nature* 400:367-371.
- Fox K. 1992. A critical period for experience-dependent synaptic plasticity in rat barrel cortex. *The Journal of neuroscience : the official journal of the Society for Neuroscience* 12:1826-1838.
- Fu M, Zuo Y. 2011. Experience-dependent structural plasticity in the cortex. *Trends in neurosciences* 34:177-187.
- Gaiarsa JL, Caillard O, Ben-Ari Y. 2002. Long-term plasticity at GABAergic and glycinergic synapses: mechanisms and functional significance. *Trends in neurosciences* 25:564-570.
- Galvez R, Greenough WT. 2005. Sequence of abnormal dendritic spine development in primary somatosensory cortex of a mouse model of the fragile X mental retardation syndrome. *American journal of medical genetics Part A* 135:155-160.
- Gambino F, Holtmaat A. 2012. Spike-timing-dependent potentiation of sensory surround in the somatosensory cortex is facilitated by deprivation-mediated disinhibition. *Neuron* 75:490-502.

- Glantz LA, Lewis DA. 2000. Decreased dendritic spine density on prefrontal cortical pyramidal neurons in schizophrenia. *Archives of general psychiatry* 57:65-73.
- Glazewski S, Benedetti BL, Barth AL. 2007. Ipsilateral whiskers suppress experience-dependent plasticity in the barrel cortex. *The Journal of neuroscience : the official journal of the Society for Neuroscience* 27:3910-3920.
- Glazewski S, Fox K. 1996. Time course of experience-dependent synaptic potentiation and depression in barrel cortex of adolescent rats. *Journal of neurophysiology* 75:1714-1729.
- Goaillard JM, Taylor AL, Schulz DJ, Marder E. 2009. Functional consequences of animal-to-animal variation in circuit parameters. *Nature neuroscience* 12:1424-1430.
- Gordon JA, Stryker MP. 1996. Experience-dependent plasticity of binocular responses in the primary visual cortex of the mouse. *The Journal of neuroscience : the official journal of the Society for Neuroscience* 16:3274-3286.
- Granger B, Tekaia F, Le Sourd AM, Rakic P, Bourgeois JP. 1995. Tempo of neurogenesis and synaptogenesis in the primate cingulate mesocortex: comparison with the neocortex. *The Journal of comparative neurology* 360:363-376.
- Grashow R, Brookings T, Marder E. 2010. Compensation for variable intrinsic neuronal excitability by circuit-synaptic interactions. *The Journal of neuroscience : the official journal of the Society for Neuroscience* 30:9145-9156.
- Gray EG. 1959. Axo-somatic and axo-dendritic synapses of the cerebral cortex: an electron microscope study. *Journal of anatomy* 93:420-433.
- Hahamy A, Behrmann M, Malach R. 2015. The idiosyncratic brain: distortion of spontaneous connectivity patterns in autism spectrum disorder. *Nature neuroscience* 18:302-309.

- Harris KM, Stevens JK. 1989. Dendritic spines of CA 1 pyramidal cells in the rat hippocampus: serial electron microscopy with reference to their biophysical characteristics. *The Journal of neuroscience : the official journal of the Society for Neuroscience* 9:2982-2997.
- Helmstaedter M. 2013. Cellular-resolution connectomics: challenges of dense neural circuit reconstruction. *Nat Methods* 10:501-507.
- Hensch TK. 2005. Critical period plasticity in local cortical circuits. *Nature reviews Neuroscience* 6:877-888.
- Hensch TK, Fagiolini M, Mataga N, Stryker MP, Baekkeskov S, Kash SF. 1998. Local GABA circuit control of experience-dependent plasticity in developing visual cortex. *Science* 282:1504-1508.
- Heynen AJ, Yoon BJ, Liu CH, Chung HJ, Haganir RL, Bear MF. 2003. Molecular mechanism for loss of visual cortical responsiveness following brief monocular deprivation. *Nature neuroscience* 6:854-862.
- Hildebrandt H, Hoffmann NA, Illing RB. 2011. Synaptic reorganization in the adult rat's ventral cochlear nucleus following its total sensory deafferentation. *PloS one* 6:e23686.
- Hofer SB, Mrsic-Flogel TD, Bonhoeffer T, Hubener M. 2009. Experience leaves a lasting structural trace in cortical circuits. *Nature* 457:313-317.
- Holtmaat A, Svoboda K. 2009. Experience-dependent structural synaptic plasticity in the mammalian brain. *Nature reviews Neuroscience* 10:647-658.
- Holtmaat A, Wilbrecht L, Knott GW, Welker E, Svoboda K. 2006. Experience-dependent and cell-type-specific spine growth in the neocortex. *Nature* 441:979-983.

- Holtmaat AJ, Trachtenberg JT, Wilbrecht L, Shepherd GM, Zhang X, Knott GW, Svoboda K. 2005. Transient and persistent dendritic spines in the neocortex in vivo. *Neuron* 45:279-291.
- Horton J. 1997. Disruption of orientation tuning in visual cortex by artificially correlated neuronal activity. *Survey of ophthalmology* 42:291-292.
- Huang ZJ, Kirkwood A, Pizzorusso T, Porciatti V, Morales B, Bear MF, Maffei L, Tonegawa S. 1999. BDNF regulates the maturation of inhibition and the critical period of plasticity in mouse visual cortex. *Cell* 98:739-755.
- Hubel DH, Wiesel TN. 1970. The period of susceptibility to the physiological effects of unilateral eye closure in kittens. *The Journal of physiology* 206:419-436.
- Hutsler JJ, Zhang H. 2010. Increased dendritic spine densities on cortical projection neurons in autism spectrum disorders. *Brain research* 1309:83-94.
- Huttenlocher PR, Dabholkar AS. 1997. Regional differences in synaptogenesis in human cerebral cortex. *The Journal of comparative neurology* 387:167-178.
- Huttenlocher PR, de Courten C. 1987. The development of synapses in striate cortex of man. *Human neurobiology* 6:1-9.
- Irwin SA, Patel B, Idupulapati M, Harris JB, Crisostomo RA, Larsen BP, Kooy F, Willems PJ, Cras P, Kozlowski PB, Swain RA, Weiler IJ, Greenough WT. 2001. Abnormal dendritic spine characteristics in the temporal and visual cortices of patients with fragile-X syndrome: a quantitative examination. *American journal of medical genetics* 98:161-167.
- Issa NP, Trachtenberg JT, Chapman B, Zahs KR, Stryker MP. 1999. The critical period for ocular dominance plasticity in the Ferret's visual cortex. *The Journal of neuroscience : the official journal of the Society for Neuroscience* 19:6965-6978.

- Jacob V, Petreanu L, Wright N, Svoboda K, Fox K. 2012. Regular spiking and intrinsic bursting pyramidal cells show orthogonal forms of experience-dependent plasticity in layer V of barrel cortex. *Neuron* 73:391-404.
- Jiao Y, Zhang C, Yanagawa Y, Sun QQ. 2006. Major effects of sensory experiences on the neocortical inhibitory circuits. *The Journal of neuroscience : the official journal of the Society for Neuroscience* 26:8691-8701.
- Jouhanneau JS, Ferrarese L, Estebanez L, Audette NJ, Brecht M, Barth AL, Poulet JF. 2014. Cortical fosGFP Expression Reveals Broad Receptive Field Excitatory Neurons Targeted by P<sub>OM</sub>. *Neuron* 84:1065-1078.
- Katzel D, Miesenbock G. 2014. Experience-dependent rewiring of specific inhibitory connections in adult neocortex. *PLoS biology* 12:e1001798.
- Kay KR, Smith C, Wright AK, Serrano-Pozo A, Pooler AM, Koffie R, Bastin ME, Bak TH, Abrahams S, Kopeikina KJ, McGuone D, Frosch MP, Gillingwater TH, Hyman BT, Spires-Jones TL. 2013. Studying synapses in human brain with array tomography and electron microscopy. *Nature protocols* 8:1366-1380.
- Kichula EA, Huntley GW. 2008. Developmental and comparative aspects of posterior medial thalamocortical innervation of the barrel cortex in mice and rats. *The Journal of comparative neurology* 509:239-258.
- Killackey HP, Fleming K. 1985. The role of the principal sensory nucleus in central trigeminal pattern formation. *Brain research* 354:141-145.
- Kim JJ, Diamond DM. 2002. The stressed hippocampus, synaptic plasticity and lost memories. *Nature reviews Neuroscience* 3:453-462.

- Kirkwood A, Lee HK, Bear MF. 1995. Co-regulation of long-term potentiation and experience-dependent synaptic plasticity in visual cortex by age and experience. *Nature* 375:328-331.
- Knott GW, Holtmaat A, Wilbrecht L, Welker E, Svoboda K. 2006. Spine growth precedes synapse formation in the adult neocortex in vivo. *Nature neuroscience* 9:1117-1124.
- Knott GW, Quairiaux C, Genoud C, Welker E. 2002. Formation of dendritic spines with GABAergic synapses induced by whisker stimulation in adult mice. *Neuron* 34:265-273.
- Kolluri N, Sun Z, Sampson AR, Lewis DA. 2005. Lamina-specific reductions in dendritic spine density in the prefrontal cortex of subjects with schizophrenia. *The American journal of psychiatry* 162:1200-1202.
- Kreshuk A, Koethe U, Pax E, Bock DD, Hamprecht FA. 2014. Automated Detection of Synapses in Serial Section Transmission Electron Microscopy Image Stacks. *PloS one* 9.
- Kreshuk A, Straehle CN, Sommer C, Koethe U, Cantoni M, Knott G, Hamprecht FA. 2011. Automated Detection and Segmentation of Synaptic Contacts in Nearly Isotropic Serial Electron Microscopy Images. *PloS one* 6.
- Kuhlman SJ, O'Connor DH, Fox K, Svoboda K. 2014. Structural Plasticity within the Barrel Cortex during Initial Phases of Whisker-Dependent Learning. *The Journal of neuroscience : the official journal of the Society for Neuroscience* 34:6078-6083.
- Kuhlman SJ, Olivas ND, Tring E, Ikrar T, Xu X, Trachtenberg JT. 2013. A disinhibitory microcircuit initiates critical-period plasticity in the visual cortex. *Nature* 501:543-546.
- Lai CS, Franke TF, Gan WB. 2012. Opposite effects of fear conditioning and extinction on dendritic spine remodelling. *Nature* 483:87-91.

- Land PW, Simons DJ. 1985. Cytochrome oxidase staining in the rat SmI barrel cortex. *The Journal of comparative neurology* 238:225-235.
- Landers MS, Knott GW, Lipp HP, Poletaeva I, Welker E. 2011. Synapse formation in adult barrel cortex following naturalistic environmental enrichment. *Neuroscience* 199:143-152.
- Lathe R. 2004. The individuality of mice. *Genes, brain, and behavior* 3:317-327.
- Leamy L, Zhang Z. 1993. Effects of prenatal litter size in inbred mice on morphometric characters with different developmental patterns. *Growth, development, and aging : GDA* 57:13-23.
- Lefort S, Tómm C, Floyd Sarria JC, Petersen CC. 2009. The excitatory neuronal network of the C2 barrel column in mouse primary somatosensory cortex. *Neuron* 61:301-316.
- Lendvai B, Stern EA, Chen B, Svoboda K. 2000. Experience-dependent plasticity of dendritic spines in the developing rat barrel cortex in vivo. *Nature* 404:876-881.
- Letzkus JJ, Wolff SB, Meyer EM, Tovote P, Courtin J, Herry C, Luthi A. 2011. A disinhibitory microcircuit for associative fear learning in the auditory cortex. *Nature* 480:331-335.
- LeVay S, Wiesel TN, Hubel DH. 1980. The development of ocular dominance columns in normal and visually deprived monkeys. *The Journal of comparative neurology* 191:1-51.
- Linkenhoker BA, von der Ohe CG, Knudsen EI. 2005. Anatomical traces of juvenile learning in the auditory system of adult barn owls. *Nature neuroscience* 8:93-98.
- Liu D, Diorio J, Day JC, Francis DD, Meaney MJ. 2000. Maternal care, hippocampal synaptogenesis and cognitive development in rats. *Nature neuroscience* 3:799-806.

- Lu SM, Lin RC. 1993. Thalamic afferents of the rat barrel cortex: a light- and electron-microscopic study using Phaseolus vulgaris leucoagglutinin as an anterograde tracer. *Somatosensory & motor research* 10:1-16.
- MacAskill AF, Cassel JM, Carter AG. 2014. Cocaine exposure reorganizes cell type- and input-specific connectivity in the nucleus accumbens. *Nature neuroscience* 17:1198-1207.
- Markram H, Lubke J, Frotscher M, Roth A, Sakmann B. 1997. Physiology and anatomy of synaptic connections between thick tufted pyramidal neurones in the developing rat neocortex. *The Journal of physiology* 500 ( Pt 2):409-440.
- Mayhew TM. 1979. Stereological approach to the study of synapse morphometry with particular regard to estimating number in a volume and on a surface. *J Neurocytol* 8:121-138.
- McKinney BC, Grossman AW, Elisseou NM, Greenough WT. 2005. Dendritic spine abnormalities in the occipital cortex of C57BL/6 Fmr1 knockout mice. *American journal of medical genetics Part B, Neuropsychiatric genetics : the official publication of the International Society of Psychiatric Genetics* 136B:98-102.
- Merchan-Perez A, Rodriguez JR, Gonzalez S, Robles V, Defelipe J, Larranaga P, Bielza C. 2014. Three-dimensional spatial distribution of synapses in the neocortex: a dual-beam electron microscopy study. *Cerebral cortex* 24:1579-1588.
- Meyer HS, Egger R, Guest JM, Foerster R, Reissl S, Oberlaender M. 2013. Cellular organization of cortical barrel columns is whisker-specific. *Proceedings of the National Academy of Sciences of the United States of America* 110:19113-19118.
- Meyer HS, Wimmer VC, Oberlaender M, de Kock CP, Sakmann B, Helmstaedter M. 2010. Number and laminar distribution of neurons in a thalamocortical projection column of rat vibrissal cortex. *Cereb Cortex* 20:2277-2286.

- Micheva KD, Beaulieu C. 1995. An anatomical substrate for experience-dependent plasticity of the rat barrel field cortex. *Proceedings of the National Academy of Sciences of the United States of America* 92:11834-11838.
- Micheva KD, Beaulieu C. 1996. Quantitative aspects of synaptogenesis in the rat barrel field cortex with special reference to GABA circuitry. *The Journal of comparative neurology* 373:340-354.
- Micheva KD, Smith SJ. 2007. Array tomography: a new tool for imaging the molecular architecture and ultrastructure of neural circuits. *Neuron* 55:25-36.
- Mishchenko Y, Hu T, Spacek J, Mendenhall J, Harris KM, Chklovskii DB. 2010. Ultrastructural analysis of hippocampal neuropil from the connectomics perspective. *Neuron* 67:1009-1020.
- Moczulska KE, Tinter-Thiede J, Peter M, Ushakova L, Wernle T, Bathellier B, Rumpel S. 2013. Dynamics of dendritic spines in the mouse auditory cortex during memory formation and memory recall. *Proceedings of the National Academy of Sciences of the United States of America* 110:18315-18320.
- Morales J, Alonso-Nanclares L, Rodriguez JR, DeFelipe J, Rodriguez A, Merchán-Pérez A. 2011. ESPINA: a tool for the automated segmentation and counting of synapses in large stacks of electron microscopy images. *Frontiers in neuroanatomy* 5.
- Navlakha S, Suhan J, Barth AL, Bar-Joseph Z. 2013. A high-throughput framework to detect synapses in electron microscopy images. *Bioinformatics* 29:i9-17.
- Nusser Z, Lujan R, Laube G, Roberts JD, Molnar E, Somogyi P. 1998. Cell type and pathway dependence of synaptic AMPA receptor number and variability in the hippocampus. *Neuron* 21:545-559.

- Oberlaender M, Boudewijns ZS, Kleele T, Mansvelder HD, Sakmann B, de Kock CP. 2011. Three-dimensional axon morphologies of individual layer 5 neurons indicate cell type-specific intracortical pathways for whisker motion and touch. *Proceedings of the National Academy of Sciences of the United States of America* 108:4188-4193.
- Oberlaender M, de Kock CP, Bruno RM, Ramirez A, Meyer HS, Dercksen VJ, Helmstaedter M, Sakmann B. 2012a. Cell type-specific three-dimensional structure of thalamocortical circuits in a column of rat vibrissal cortex. *Cereb Cortex* 22:2375-2391.
- Oberlaender M, Ramirez A, Bruno RM. 2012b. Sensory experience restructures thalamocortical axons during adulthood. *Neuron* 74:648-655.
- Olsen SR, Bortone DS, Adesnik H, Scanziani M. 2012. Gain control by layer six in cortical circuits of vision. *Nature* 483:47-52.
- Oray S, Majewska A, Sur M. 2004. Dendritic spine dynamics are regulated by monocular deprivation and extracellular matrix degradation. *Neuron* 44:1021-1030.
- Osten P, Margrie TW. 2013. Mapping brain circuitry with a light microscope. *Nat Methods* 10:515-523.
- Penzes P, Cahill ME, Jones KA, VanLeeuwen JE, Woolfrey KM. 2011. Dendritic spine pathology in neuropsychiatric disorders. *Nature neuroscience* 14:285-293.
- Peters A, Sethares C, Luebke JI. 2008. Synapses are lost during aging in the primate prefrontal cortex. *Neuroscience* 152:970-981.
- Petreaanu L, Mao T, Sternson SM, Svoboda K. 2009. The subcellular organization of neocortical excitatory connections. *Nature* 457:1142-1145.

- Petrus E, Anguh TT, Pho H, Lee A, Gammon N, Lee HK. 2011. Developmental switch in the polarity of experience-dependent synaptic changes in layer 6 of mouse visual cortex. *Journal of neurophysiology* 106:2499-2505.
- Pichon F, Nikonenko I, Kraftsik R, Welker E. 2012. Intracortical connectivity of layer VI pyramidal neurons in the somatosensory cortex of normal and barreless mice. *The European journal of neuroscience* 35:855-869.
- Portera-Cailliau C, Weimer RM, De Paola V, Caroni P, Svoboda K. 2005. Diverse modes of axon elaboration in the developing neocortex. *PLoS biology* 3:e272.
- Prinz AA, Bucher D, Marder E. 2004. Similar network activity from disparate circuit parameters. *Nature neuroscience* 7:1345-1352.
- Prusky GT, Douglas RM. 2003. Developmental plasticity of mouse visual acuity. *The European journal of neuroscience* 17:167-173.
- Quintarelli G, Cifonelli JA, Zito R. 1971a. On phosphotungstic acid staining. II. *The journal of histochemistry and cytochemistry : official journal of the Histochemistry Society* 19:648-653.
- Quintarelli G, Zito R, Cifonelli JA. 1971b. On phosphotungstic acid staining. I. *The journal of histochemistry and cytochemistry : official journal of the Histochemistry Society* 19:641-647.
- Rakic P, Bourgeois JP, Eckenhoff MF, Zecevic N, Goldman-Rakic PS. 1986. Concurrent overproduction of synapses in diverse regions of the primate cerebral cortex. *Science* 232:232-235.
- Rapin I. 1997. Autism. *The New England journal of medicine* 337:97-104.

- Riolt-Pedotti MS, Donoghue JP, Dunaevsky A. 2007. Plasticity of the synaptic modification range. *Journal of neurophysiology* 98:3688-3695.
- Riolt-Pedotti MS, Friedman D, Donoghue JP. 2000. Learning-induced LTP in neocortex. *Science* 290:533-536.
- Rocha-de-Melo AP, Cavalcanti Jde B, Barros AS, Guedes RC. 2006. Manipulation of rat litter size during suckling influences cortical spreading depression after weaning and at adulthood. *Nutritional neuroscience* 9:155-160.
- Rodel HG, Prager G, Stefanski V, von Holst D, Hudson R. 2008. Separating maternal and litter-size effects on early postnatal growth in two species of altricial small mammals. *Physiology & behavior* 93:826-834.
- Sato M, Stryker MP. 2008. Distinctive features of adult ocular dominance plasticity. *The Journal of neuroscience : the official journal of the Society for Neuroscience* 28:10278-10286.
- Sawtell NB, Frenkel MY, Philpot BD, Nakazawa K, Tonegawa S, Bear MF. 2003. NMDA receptor-dependent ocular dominance plasticity in adult visual cortex. *Neuron* 38:977-985.
- Schikorski T, Stevens CF. 1999. Quantitative fine-structural analysis of olfactory cortical synapses. *Proceedings of the National Academy of Sciences of the United States of America* 96:4107-4112.
- Schubert D, Kotter R, Luhmann HJ, Staiger JF. 2006. Morphology, electrophysiology and functional input connectivity of pyramidal neurons characterizes a genuine layer va in the primary somatosensory cortex. *Cereb Cortex* 16:223-236.

- Schubert D, Kotter R, Staiger JF. 2007. Mapping functional connectivity in barrel-related columns reveals layer- and cell type-specific microcircuits. *Brain structure & function* 212:107-119.
- Selkoe DJ. 2002. Alzheimer's disease is a synaptic failure. *Science* 298:789-791.
- Simons DJ. 1978. Response properties of vibrissa units in rat SI somatosensory neocortex. *Journal of neurophysiology* 41:798-820.
- Simons DJ. 1985. Temporal and spatial integration in the rat SI vibrissa cortex. *Journal of neurophysiology* 54:615-635.
- Simons DJ, Land PW. 1987. Early experience of tactile stimulation influences organization of somatic sensory cortex. *Nature* 326:694-697.
- Spiegel I, Mardinly AR, Gabel HW, Bazinet JE, Couch CH, Tzeng CP, Harmin DA, Greenberg ME. 2014. Npas4 regulates excitatory-inhibitory balance within neural circuits through cell-type-specific gene programs. *Cell* 157:1216-1229.
- Sterio DC. 1984. The unbiased estimation of number and sizes of arbitrary particles using the disector. *J Microsc* 134:127-136.
- Stern EA, Maravall M, Svoboda K. 2001. Rapid development and plasticity of layer 2/3 maps in rat barrel cortex in vivo. *Neuron* 31:305-315.
- Sweet RA, Hentleff RA, Zhang W, Sampson AR, Lewis DA. 2009. Reduced dendritic spine density in auditory cortex of subjects with schizophrenia. *Neuropsychopharmacology : official publication of the American College of Neuropsychopharmacology* 34:374-389.
- Tabuchi K, Blundell J, Etherton MR, Hammer RE, Liu X, Powell CM, Sudhof TC. 2007. A neuroligin-3 mutation implicated in autism increases inhibitory synaptic transmission in mice. *Science* 318:71-76.

- Thomson AM. 2010. Neocortical layer 6, a review. *Frontiers in neuroanatomy* 4:13.
- Trachtenberg JT, Chen BE, Knott GW, Feng G, Sanes JR, Welker E, Svoboda K. 2002. Long-term in vivo imaging of experience-dependent synaptic plasticity in adult cortex. *Nature* 420:788-794.
- Trachtenberg JT, Trepel C, Stryker MP. 2000. Rapid extragranular plasticity in the absence of thalamocortical plasticity in the developing primary visual cortex. *Science* 287:2029-2032.
- Uemura E. 1980. Age-related changes in prefrontal cortex of *Macaca mulatta*: synaptic density. *Experimental neurology* 69:164-172.
- van Versendaal D, Rajendran R, Saiepour MH, Klooster J, Smit-Rigter L, Sommeijer JP, De Zeeuw CI, Hofer SB, Heimel JA, Levelt CN. 2012. Elimination of inhibitory synapses is a major component of adult ocular dominance plasticity. *Neuron* 74:374-383.
- Veinante P, Deschenes M. 1999. Single- and multi-whisker channels in the ascending projections from the principal trigeminal nucleus in the rat. *The Journal of neuroscience : the official journal of the Society for Neuroscience* 19:5085-5095.
- Veinante P, Jacquin MF, Deschenes M. 2000. Thalamic projections from the whisker-sensitive regions of the spinal trigeminal complex in the rat. *The Journal of comparative neurology* 420:233-243.
- Velez-Fort M, Rousseau CV, Niedworok CJ, Wickersham IR, Rancz EA, Brown AP, Strom M, Margrie TW. 2014. The stimulus selectivity and connectivity of layer six principal cells reveals cortical microcircuits underlying visual processing. *Neuron* 83:1431-1443.

- Wainwright P, Pelkman C, Wahlsten D. 1989. The quantitative relationship between nutritional effects on preweaning growth and behavioral development in mice. *Developmental psychobiology* 22:183-195.
- Wallace DJ, Sakmann B. 2008. Plasticity of representational maps in somatosensory cortex observed by in vivo voltage-sensitive dye imaging. *Cereb Cortex* 18:1361-1373.
- Wallace H, Fox K. 1999a. The effect of vibrissa deprivation pattern on the form of plasticity induced in rat barrel cortex. *Somatosensory & motor research* 16:122-138.
- Wallace H, Fox K. 1999b. Local cortical interactions determine the form of cortical plasticity. *Journal of neurobiology* 41:58-63.
- Wang L, Kloc M, Gu Y, Ge S, Maffei A. 2013. Layer-specific experience-dependent rewiring of thalamocortical circuits. *The Journal of neuroscience : the official journal of the Society for Neuroscience* 33:4181-4191.
- Wen JA, Barth AL. 2011. Input-specific critical periods for experience-dependent plasticity in layer 2/3 pyramidal neurons. *The Journal of neuroscience : the official journal of the Society for Neuroscience* 31:4456-4465.
- Wen JA, DeBlois MC, Barth AL. 2013. Initiation, labile, and stabilization phases of experience-dependent plasticity at neocortical synapses. *The Journal of neuroscience : the official journal of the Society for Neuroscience* 33:8483-8493.
- White EL, Weinfeld L, Lev DL. 1997. A survey of morphogenesis during the early postnatal period in PMBSF barrels of mouse SmI cortex with emphasis on barrel D4. *Somatosensory & motor research* 14:34-55.
- White JG, Southgate E, Thomson JN, Brenner S. 1986. The Structure of the Nervous-System of the Nematode *Caenorhabditis-Elegans*. *Philos T Roy Soc B* 314:1-340.

- Wilbrecht L, Holtmaat A, Wright N, Fox K, Svoboda K. 2010. Structural plasticity underlies experience-dependent functional plasticity of cortical circuits. *The Journal of neuroscience : the official journal of the Society for Neuroscience* 30:4927-4932.
- Wimmer VC, Broser PJ, Kuner T, Bruno RM. 2010a. Experience-induced plasticity of thalamocortical axons in both juveniles and adults. *The Journal of comparative neurology* 518:4629-4648.
- Wimmer VC, Bruno RM, de Kock CP, Kuner T, Sakmann B. 2010b. Dimensions of a projection column and architecture of VPM and POm axons in rat vibrissal cortex. *Cereb Cortex* 20:2265-2276.
- Woolsey TA, Van der Loos H. 1970. The structural organization of layer IV in the somatosensory region (SI) of mouse cerebral cortex. The description of a cortical field composed of discrete cytoarchitectonic units. *Brain research* 17:205-242.
- Xu T, Yu X, Perlik AJ, Tobin WF, Zweig JA, Tennant K, Jones T, Zuo Y. 2009. Rapid formation and selective stabilization of synapses for enduring motor memories. *Nature* 462:915-919.
- Yamahachi H, Marik SA, McManus JN, Denk W, Gilbert CD. 2009. Rapid axonal sprouting and pruning accompany functional reorganization in primary visual cortex. *Neuron* 64:719-729.
- Yang G, Pan F, Gan WB. 2009. Stably maintained dendritic spines are associated with lifelong memories. *Nature* 462:920-924.
- Yashiro K, Riday TT, Condon KH, Roberts AC, Bernardo DR, Prakash R, Weinberg RJ, Ehlers MD, Philpot BD. 2009. Ube3a is required for experience-dependent maturation of the neocortex. *Nature neuroscience* 12:777-783.

- Yoo J, Bakes J, Bradley C, Collingridge GL, Kaang BK. 2014. Shank mutant mice as an animal model of autism. *Philosophical transactions of the Royal Society of London Series B, Biological sciences* 369:20130143.
- Yu X, Chung S, Chen DY, Wang S, Dodd SJ, Walters JR, Isaac JT, Koretsky AP. 2012. Thalamocortical inputs show post-critical-period plasticity. *Neuron* 74:731-742.
- Yuste R, Denk W. 1995. Dendritic spines as basic functional units of neuronal integration. *Nature* 375:682-684.
- Zhang ZW, Deschenes M. 1997. Intracortical axonal projections of lamina VI cells of the primary somatosensory cortex in the rat: a single-cell labeling study. *The Journal of neuroscience : the official journal of the Society for Neuroscience* 17:6365-6379.
- Zhang ZW, Deschenes M. 1998. Projections to layer VI of the posteromedial barrel field in the rat: a reappraisal of the role of corticothalamic pathways. *Cereb Cortex* 8:428-436.
- Zuo Y, Yang G, Kwon E, Gan WB. 2005. Long-term sensory deprivation prevents dendritic spine loss in primary somatosensory cortex. *Nature* 436:261-265.